UNIVERSITÉ DE MONTRÉAL

FIRST EMTP-RV BENCHMARK FOR OFF-LINE SIMULATION OF RAPID TRANSIT TRAIN DC AUXILIARY SYSTEMS

MAXIME BERGER

DÉPARTEMENT DE GÉNIE ÉLECTRIQUE

ÉCOLE POLYTECHNIQUE DE MONTRÉAL

MÉMOIRE PRÉSENTÉ EN VUE DE L'OBTENTION

DU DIPLÔME DE MAÎTRISE ÈS SCIENCES APPLIQUÉES

(GÉNIE ÉLECTRIQUE)

DÉCEMBRE 2015

UNIVERSITÉ DE MONTRÉAL

ÉCOLE POLYTECHNIQUE DE MONTRÉAL

Ce mémoire intitulé :

FIRST EMTP-RV BENCHMARK FOR OFF-LINE SIMULATION OF RAPID TRANSIT TRAIN DC AUXILIARY SYSTEMS

présenté par : BERGER Maxime

en vue de l'obtention du diplôme de : Maîtrise ès sciences appliquées

a été dûment accepté par le jury d'examen constitué de :

M. KARIMI Houshang, Ph. D., président

M. KOCAR Ilhan, Ph. D., membre et directeur de recherche

M. MAHSEREDJIAN Jean, Ph. D., membre et codirecteur de recherche

M. LAVERTU Carl, B. Ing., membre

DEDICATION

To my parents who always believed in me and…

…will probably not read this thesis.

ACKNOWLEDGEMENTS

First, I would like to thank M. Jacques Belley and Mme. Isabelle Provost from Bombardier Transportation who believed in me from the first day I announced my wish to pursue a master research project with them. I will never forget the amazing opportunity they gave me.

I would also like to thank M. Carl Lavertu from Bombardier Transportation for all his support and technical advices. I consider myself very privileged to learn from him every day. Carl has been more than available for me anytime I needed him. It was an honour to share this experience with him.

A special thanks also to M. Stéphane Goulet, M. Dany Lévesque, M. Herman Lévesque, M. Pierre Miclette and M. Jean-Pierre Magalhaes Grave from Bombardier Transportation for all their help and support in different ways.

I will also always be grateful to my advisor Prof. Ilhan Kocar who believed in me the first time I came in his office to expose him my plan to apply for graduate studies at Polytechnique Montreal. From our first discussion regarding the definition of the research project at Bombardier's office to the writing of a scientific paper and this master thesis, he has been very supportive, available and provided me all the guidance and advices I needed within the best of his knowledge and experience.

Moreover, I can't pass over the unbelievable collaboration with Prof. Jean Mahseredjian. He gave me the opportunity to enter the EMTP-RV family and I consider myself very fortunate of being a small part of this amazing story.

Despite the distance, I will always be thankful to my parents, Céline and Sylvain, for their unconditional support and encouragement that allowed me to chase my dreams. They are an important part of what I became and I could never thank them enough for what they have been and still are for me.

Last but not least, I would like to thank my lovely Brigitte for all her encouragement during the best and harder moments of this adventure. She has been and still is more than understanding being also my best confidant. It will be difficult for me to give her back everything she have done for me during her own master. I wish you all the best. I am proud of you.

This project has been financially supported by Bombardier Transportation, FRQNT, and CRSNG through the Industrial Innovation Scholarship Program.

RÉSUMÉ

Les exigences de performance opérationnelle optimale dans l'industrie ferroviaire du transport de passagers nécessitent le développement continu de solutions innovatrices. Le défi principal des manufacturiers est de fournir des véhicules toujours plus efficaces, plus légers et à un coût moindre tout en offrant de bonnes performances en matière de fiabilité, disponibilité, maintenabilité et sécurité. La distribution auxiliaire DC est ciblée dans ce projet de recherche en raison de son haut potentiel d'améliorations majeures. Le niveau de tension est un enjeu majeur. Les distributions actuelles sont généralement à des tensions très basses variant entre 24 V et 110 V. Les récents développements dans les distributions DC à 380 V sont prometteurs et intéressants pour les manufacturiers de matériel roulant; la distribution auxiliaire DC d'une rame de métro n'étant ni plus ni moins qu'un micro-réseau DC intelligent. Toutefois, le passage à des tensions plus élevées mène inévitablement à de nouveaux enjeux techniques et soulève des questionnements sur les aspects de sécurité.

Par ailleurs, le développement de nouvelles architectures ainsi que l'intégration de nouvelles technologies doivent nécessairement se faire en considérant l'environnement ferroviaire dans son ensemble et les pratiques et normes actuelles de l'industrie. L'analyse par simulation combinée aux pratiques, aux normes et à l'expérience de l'industrie peut s'avérer un outil efficace pour réduire les risques inhérents associés aux changements majeurs.

Dans ce projet, un modèle complet de distribution auxiliaire DC typique d'une rame de métro est développé dans le logiciel de simulation EMTP-RV en se basant sur les données de Bombardier Transport. Chaque composante du réseau est modélisée et validée individuellement. Le modèle est orienté vers les besoins et les objectifs d'analyse de l'industrie. Il permet de faire des études complètes et détaillées dans le but de développer de nouvelles architectures et valider différents concepts qui ne peuvent être expérimentés à la phase de conception. Le modèle permet également d'étudier plusieurs scénarios rapidement.

Les possibilités et les performances du modèle de simulation sont finalement démontrées par la réalisation de différentes études de réseaux électriques : protection de court-circuit, mise à la terre et protection de défaut à la terre, étude de surtension transitoire et protection contre les surtensions, dimensionnement des batteries d'urgence, stabilité de tension et courant d'appel. Les analyses sont basées sur des observations expérimentales ainsi que sur des études de cas réelles présentées dans la littérature.

ABSTRACT

In the rapid transit industry, market interest toward optimal operational performance requires innovative solutions. The main challenge for vehicle manufacturers is to increase the efficiency and reduce the weight and the cost of its vehicles while keeping high levels of reliability, availability, maintainability, and safety. Vehicle DC auxiliary systems are targeted in this master thesis because they offer a high potential of major improvements. Voltage level is a major challenge. Actual distribution are at very low voltages ranging between 24 V to 110 V. Recent developments in 380 V DC systems are promising and interesting for vehicle manufacturers. DC auxiliary systems in railway vehicles are in fact no other than rolling smart DC microgrids. The shift toward higher voltage DC auxiliary systems inherently leads to new technical challenges and safety concerns.

Moreover, the development of new architectures and the integration of new technologies must be done with an appropriate knowledge of the rail environment and the actual practices and standards. Analysis using simulation models combined with established industry practices, standards and past experiences is an efficient tool to reduce the inherent risk exposure with major changes.

In this project, a complete generic rapid transit train DC auxiliary system model is developed in EMTP-RV based on Bombardier Transportation data. Models of the network components are developed and validated individually based on the available information. The developed train model is highly oriented toward the industry specific needs and provides sufficient level of details for design purpose and architecture development of railway vehicle DC auxiliary systems. The simulation model can be a useful tool at the design phase to investigate design concerns which cannot be tested at early project stage.

The capabilities of the simulation model are finally demonstrated for different power system studies such as: overcurrent protection, grounding and ground fault analysis, transient overvoltage and insulation coordination, emergency battery sizing, voltage stability, and inrush current. Phenomena, and events observed during field testing and presented in the literature are reproduced using the developed model and the influence of network parameters is investigated.

TABLE OF CONTENTS

LIST OF TABLES

LIST OF FIGURES

LIST OF SYMBOLS AND ABBREVIATIONS

AC	Alternative Current
AFCI	Arc Fault Circuit Interrupter
AWG	American Wire Gauge
BC	Bypass Contactor
CC	Charging Contactor
CPL	Constant Power Load
CSC	Current Source Converter
DC	Direct Current
DPS	Distributed Power System
EMT	Electromagnetic Transient
EMTP-RV	Electromagnetic Transient Program – Restructured Version
ESL	Equivalent Series Inductance
ESR	Equivalent Series Resistance
ETSI	European Telecommunications Standards Institute
FFT	Fast Fourier Transform
FMEA	Failure Mode and Effects Analysis
FMECA	Failure Mode and Effects Criticality Analysis
FTA	Fault Tree Analysis
GFD	Ground Fault Detector
GMR	Geometric Mean Radius
HSCB	High Speed Circuit Breaker
HVDC	High Voltage Direct Current
LVDC	Low Voltage Direct Current

MCCB	Molded-Case Circuit Breaker
MOV	Metal Oxide Varistor
MTDC	Multi-Terminal Direct Current
MVDC	Medium Voltage Direct Current
NEC	National Electrical Code
NTC	Negative Temperature Coefficient
PEC	Power Electronic Converter
RF	Radio Frequency
RMS	Root Mean Square
SOC	State-of-Charge
SPICE	Simulation Program with Integrated Circuit Emphasis
TCC	Time-Current Curve
TOV	Transient Overvoltage
TRV	Transient Recovery Voltage
TVS	Transient Voltage Suppressor
UAV	Unmanned Aerial Vehicle
VFD	Variable Frequency Drive
VSC	Voltage Source Converter

LIST OF APPENDICES

CHAPTER 1 INTRODUCTION

1.1 Context

Heavy Rail (e.g. subway, metro, rapid transit or rapid rail) operating on DC electric railway systems are widely used in North America for high volume and rapid passenger transportation. Heavy Rail systems are composed of passenger vehicles operating generally as multi-vehicle trains on a separate rights-of-way rail system which is supplied by a dedicated electric traction system (Figure 1.1) [1].

Modern DC traction systems are equipped with 6- and 12- pulse diode rectifiers but the trend is now to use 12-pulse parallel rectifiers [2]. The DC output voltage varies between 600 V to 1500 V with 600 V and 750 V being widely used in North America [3]. A typical DC traction power system using a 12-pulse uncontrolled parallel bridge rectifier is shown in Figure 1.2.

Bombardier Transportation is a world leader in rail vehicles manufacturing, maintenance and fleet management. As a vehicle manufacturer, the main objective is to provide vehicles with optimal operational performance. It is defined by high levels of reliability, availability, maintainability, safety, environmental performance, and by cost-efficiency solutions [4]. Market appetite for optimal operational performance requires innovative solutions. Vehicle power systems are targeted in this master thesis because they offer a high potential of major improvements, the main objectives being to increase the efficiency and reduce the weight and the cost of the manufactured vehicles.

A single line diagram of a typical railway car on-board power system is shown in Figure 1.3. Vehicle power system can be divided into three (3) subsystems: the vehicle primary power, the propulsion system, and the auxiliary system.

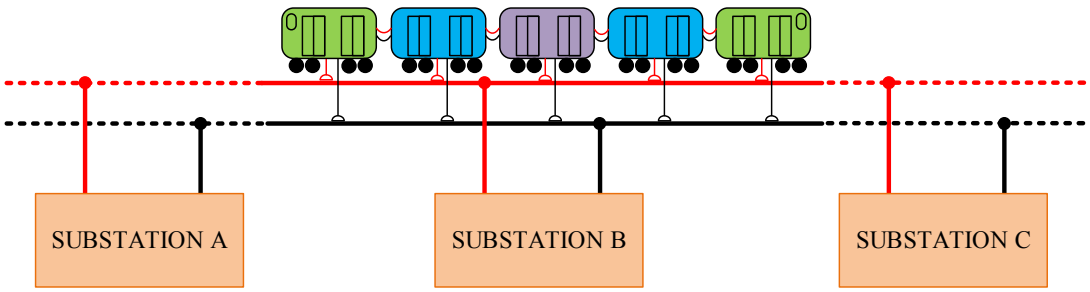

Figure 1.1: Train Supplied by Multiple Substations

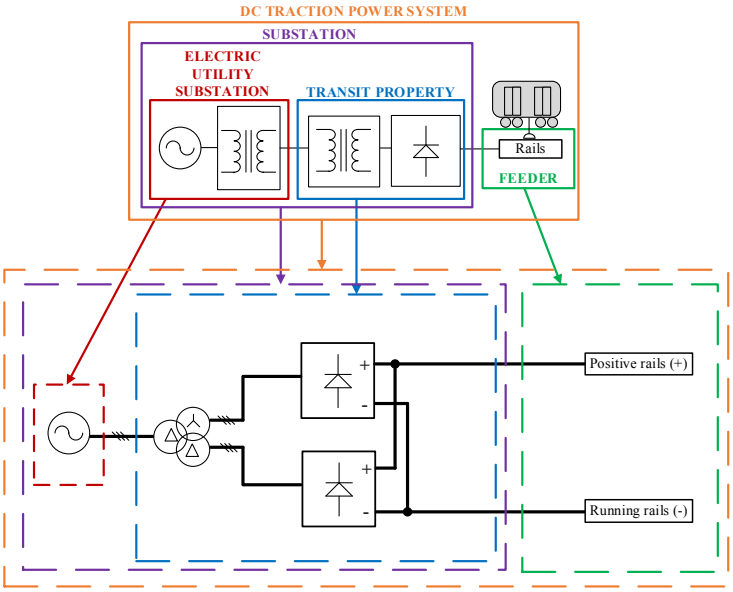

Figure 1.2: DC Traction Power System

The power from the traction system substations is first delivered to the moving train by third-rail, fourth-rail or catenary systems [5][6]. In the primary power, collector shoe fuses are used to protect the primary power cables and equipment. The propulsion High Speed Circuit Breaker (HSCB) is used to protect the propulsion system equipment while the auxiliary fuse is used to protect the auxiliary converter [7].

The propulsion system of each vehicle is generally composed of one (1) or two (2) traction inverters connected each to one (1) or two (2) AC traction motors. A rheostatic braking system based on a buck converter topology is also generally added to dissipate extra braking energy in case of non-receptivity of the DC traction system during dynamic braking operation [8].

The train auxiliary subsystems are supplied by an auxiliary converter which converts the DC traction power system supply into lower galvanically isolated DC and three-phase AC supplies. Examples of train auxiliary subsystems are: lighting, communication, automatic control systems, surveillance systems, doors, propulsion/brake control, and heating ventilation air conditioning (HVAC) systems. The DC auxiliary system also includes backup batteries to support essential loads under degraded or emergency operation. A load shedding scheme is also present to improve the train survivability. In this master thesis, only the DC auxiliary systems will be covered. DC primary power protection analysis has also been performed during this master thesis project but the results are presented in a dedicated paper [7].

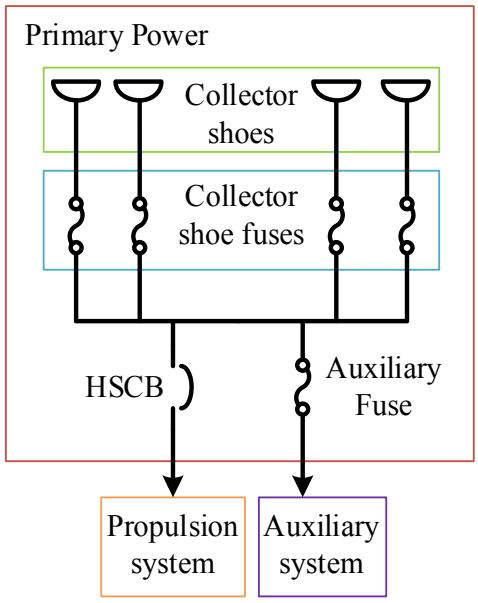

Figure 1.3: Overview of a Railway Vehicle Power System

DC auxiliary systems voltage varies between 24 V to 110 V with 37.5 V being widely used in North America and 110 V being popular in Europe [9][10]. One of today's main advantage of using DC over AC for auxiliary systems is the ease to distribute variable frequency drives (VFD) near the loads directly connected on a single DC bus without any AC to DC conversion stage [11]. The reduction of conversion stages increases the overall efficiency and reliability of the system. The use of DC over AC also offers a direct connection of the energy storage systems being mainly backup batteries in the railway industry.

Standardization of power system architectures and technologies is also necessary to stay competitive. In their effort to standardize railway vehicle on-board auxiliary system architecture, the European R&D Working Group MODTRAIN defines several system and operational requirements in the design of auxiliary systems: the train type, the architecture of the propulsion system, and specific customer requirements such as primary power voltage, the performance, the level of redundancy, and the interface between various sources [12].

Transit authorities and vehicle manufacturers are generally conservative in integrating new technologies. Train power systems are complex and it may be difficult to evaluate the benefits of new architectures and new technologies while predicting with precision the impact on the power system operational performance.

The development of new architectures and the integration of new technologies in train power systems must also be done with an appropriate understanding of the rail environment and the actual standards. Analysis using simulation models combined with established industry practices and standards can significantly reduce the risks in applying new technologies [13]. For example, behavioral analysis using simulation models as part of academic research projects have been done in the last few years to study new architectures for aircraft [14],[15], shipboard [16], and DC microgrid [17].

1.2 Objectives

The main objective of this project is to develop a complete train DC auxiliary systems simulation model with sufficient details for design purpose, architecture development and standardization of railway vehicle power systems. The model should be highly oriented toward the industry specific needs. The targeted power systems studies and their associated time frame are presented in Table 1.1.

From this main objective, three (3) specific objectives are then defined:

1. Develop and validate a complete train DC auxiliary systems simulation model based on existing designs.
2. Identify important design considerations for new DC distribution systems.
3. Demonstrate the capabilities of the simulation model for various power systems studies based on railway industry experiences with DC systems and a literature survey.

Table 1.1: Targeted Power System Analysis

Power System Study	Time Frame
Network Stability	(ms) to (s)
Component Sizing	(ms) to (h)
Transient Phenomenon	
• Overload Current	(s) to (min)
• Inrush Current	(ms)
• Fault Current	(ms) to (s)
• Overvoltage	(ms)
Automatic Control Operation	(ms) to (s)

1.3 Simulation Tool Selection

The selection of the simulation tool must be done by taking into account the targeted power system studies, the frequency range of the transient events and the characteristics of the available simulation tools on the market. This section presents an overview of the characteristics of the available simulation tools which will lead to the final choice.

1.3.1 Off-Line vs On-Line Simulation

EMT-type (Electromagnetic Transient - type) simulation tools are widely used for load flow, electromechanical and electromagnetic transient phenomenon studies in large power systems such as electric utility generating plant and transmission and distribution networks. Simulation can be *Off-Line* or *On-Line*.

Simulations are said to be Off-Line when there is no physical link between the simulation tool and the power systems. Off-Line simulation tools have no time constraints and can be very precise. On-Line simulation tools are synchronized with a real-time clock and can be interfaced with physical devices. The main drawback is the precision constraints due to the synchronism required with the real-time clock [18].

On-Line simulation requires important initial investment. It is useful for testing hardware equipment during testing phases. For design analysis during early project phases, Off-Line simulation is better suited. Therefore, Off-Line simulation is used in this master thesis.

1.3.2 Circuit Equation Formulation

Transient simulation tools must formulate circuit equations and solve them to provide the waveform of the power system state variables to the user. The most commonly used methods are *nodal* analysis and *state-space* method. These methods can be formulated in the frequency-domain and in the time-domain. Nodal analysis in power systems results in solving sparse matrices which enhance the capabilities to solve very large scale network. Solving nonlinearities is generally not a problem using nodal analysis formulation. State-space equations generation in large power systems is not an easy task. For large power systems, the computation time required for the formulation of the state-space equations can become very high. It is also not simple to include and to solve nonlinearities using the state-space method [18].

1.3.3 EMTP-type, SPICE-type and General Purpose Tools

Three (3) types of simulation tools are presented in [18] : EMTP-type, SPICE-type and General Purpose Tools.

EMTP-Type tools are based on nodal analysis. EMTP-RV, ATP and PSCAD are examples. All these tools use fixed time-step trapezoidal method to solve the circuit system of equations in the time-domain. EMTP-type tools are designed for power systems application because of the availability of complex models such as machine models, surge arrester, frequency-dependent transmission line models, transformer models with core saturation, and circuit breaker arc models. EMTP-type tools are not intended to study detailed switching behavior in power electronics application [18]. Semiconductors such as diodes, thyristors, and transistors can be modeled using ideal switch and/or their equivalent VI relationships which can provide a smooth switching response and reduce simulation discontinuities leading to unrealistic numerical current or voltage spikes. Some extra components may also be added to take into account losses or the presence of snubber circuits.

SPICE-type tools (e.g. PSPICE, LTSPICE) are also based on nodal analysis. Most SPICE-type tools also use trapezoidal integration method but unlike EMTP-type program they can use a variable integration time-step. It provides an important advantage in solving high level of nonlinearities but can become computer-time consuming. SPICE-type tool are mostly designed for electronic circuits simulation because there is a large amount of device libraries available from manufacturers which can help to avoid the development of user-defined models [18].

MATLAB/Simulink is the most popular general purpose tool. It was not intended to simulate power system transient at first but it have been developed for this application with the SimPowerSystems toolbox. It is flexible and it provides a high level of customization to build user-defined models. The increasing number of users is also an advantage in using MATLAB/Simulink with the SimPowerSystems toolbox because it provides an important community of available models and knowledge. However, it is based on the state-space formulation which is currently a limitation to solve large scale power systems especially with non-linear elements.

For power electronics simulation, both SPICE-type and EMTP-type can be used. Because of the availability of semiconductor device models, SPICE-type is generally selected for application where detailed representation of the device switching behavior is necessary. However, EMTP-type can be used to analyze power electronics converters from a power system standpoint when detailed switching models are not necessary [19].

1.3.4 The Final Choice: EMTP-RV

Despite the fact that EMTP-RV is mainly developed for AC power systems, it has been selected to model railway vehicle DC power systems for the following reasons:

- EMTP-RV provides high capabilities of simulating very large scale power system networks with detailed models [20]: It is suitable to model each vehicle with a sufficient level of details and perform simulation on a train level with the required precision and within an acceptable simulation time.
- Work has already been performed by the Bombardier Aerospace division with EMTP-RV in [14]. Its capabilities have been demonstrated on a first Global Express aircraft benchmark.
- Subcircuit, masking and scripting provide powerful ways to develop user-defined models, calculate parameters automatically and perform parametric studies.

1.4 Methodology

In order to meet the general and the specific objectives, the following steps are followed:

1. *Literature Review:* A survey of the design issues, available technologies and solutions in both industry and academic researches on DC power systems is first performed. Railway vehicle DC power systems are in fact not very different as other DC networks and researches related to other DC power systems application can be used as reference for railway application.
2. *DC Power System Analysis Review:* Based on the literature, standards, field experiments, and railway industry experiences in developing and testing DC systems, a set of power system phenomenon is established and studied from a theoretical standpoint. The investigation on power system behavior using simulation tools

should always be done with an appropriate understanding of the theoretical influence of network parameters.

3. *Development of the Simulation Model:* Models of the network components are first developed and validated. For each component, an individual literature review is performed to determine model assumptions and to develop accurate models for the application. The validation process is performed based on the expected theoretical model behavior, applicable standards, manufacturer's data, or field measurements depending on the available information and data in each case. The models are then used to develop different single vehicle models. The complete train model is built by connecting multiple vehicle model blocks.
4. *DC Power System Integration Analysis using the Simulation Model*: Using the complete train simulation model, multiple power system studies are presented to demonstrate the capabilities and the advantages of the developed train model to investigate different power system phenomena under different operating scenarios. The influence of the network parameters is also analyzed.

1.5 Thesis Structure

The thesis structure is mainly oriented to follow the methodology defined previously. A survey of the literature is first presented to introduce the trend in DC distribution architectures and technologies, and identify major technical integration and operational issues encountered with DC distribution (Chapter 2). Then, power system phenomena are established and studied from a theoretical standpoint to provide an understanding of the influence of network parameters for a proper analysis of the simulation results (Chapter 3). A description of each individual DC auxiliary systems network components is then presented along with the development and the validation of each component models. Three (3) vehicle models and a complete train DC auxiliary systems simulation model are also developed (Chapter 4). Then, the capabilities of the complete train model are demonstrated with multiple examples such as overcurrent protection, ground fault analysis, overvoltage protection, battery sizing, stability, and inrush current analysis (Chapter 5). Recommendations on important simulation integration analysis and guidelines for architecture improvements are finally provided. Further improvements to extend the application of the developed simulation model are also presented (Chapter 6).

CHAPTER 2 LITERATURE REVIEW

There is a clear trend in the industry and into academic researches toward the development of novel DC distribution systems. They are classified here into three (3) categories depending on the network nominal voltage level [21][22]:

- Low Voltage Direct Current (LVDC): Below 1.5 kV
- Medium Voltage Direct Current (MVDC): 1.5 kV to 35 kV
- High Voltage Direct Current (HVDC): Over 35 kV

It is important to mention here that this is not a standardized classification because there is in fact no standard yet on voltage levels for DC power systems [23].

DC distribution in aircrafts [24][25], unmanned aerial vehicles (UAV) [26], shipboards [27][28], commercial and industrial buildings [29][30][31] as well as in data centers [32][33] are being widely developed. Aircraft, UAV, commercial and industrial buildings, and data center industries are working toward LVDC networks while shipboard industry is mainly developing MVDC power systems. HVDC is used by electric utility for long distance power transmission.

There is currently worldwide effort in standardization of LVDC power systems for data centers and commercial buildings. The European Telecommunications Standards Institute (ETSI) and EMerge Alliance association are both working on the standardization of 380 V DC distribution [33]. According to [32], 380 V is in fact the optimum voltage level for equipment standardization, safety, efficiency, and cost balance for application in data centers.

These new developments are interesting for standardization of on-board DC auxiliary distribution in railway vehicles. Among the topics covered in the literature, a particular attention is paid to technical integration and operational considerations for higher voltage LVDC systems such as fault protection, stability, power quality, grounding/bonding, and safety. Although these considerations will be covered separately, systems integration requires the knowledge of the interrelationship between these considerations.

2.1 Fault Protection

Fault protection in DC systems has been over the past an issue for many power system designers due the lack of general protection and grounding standards compared to AC power systems [34]. Based on the litterature review performed, the problems associated with the detection and isolation of fault in DC systems are divided into three (3) categories: architectural, behavioral, and technological.

Architectural issues are related to the topologies of the DC distribution. MTDC (Multi-Terminal DC) systems (or meshed systems) are widely developed and their protection schemes need to be designed carefully to enhance the system operational performance [35][36][37]. Railway vehicle DC auxiliary distribution can be considered as a MTDC system. The various operating conditions (eg. Normal, Temporary, or Degraded) and the location of the sources and loads should be also considered in protection studies. As for AC systems, both system grounding and bonding considerations should also be included in complete protection analysis [38][39].

Behavioral issues mainly refer to DC system behavior under abnormal conditions. From field testing in railway vehicles and literature review, these power system events have been classified into three (3) categories: slow, medium and fast front transients. Slow front transients (0 – 10 Hz) are voltage and current variations caused by voltage dependent loads, load shedding, converter control, and battery charging and discharging cycles. These are important to be considered for appropriate sizing of the protective devices. Medium front transient (10 Hz – 5 kHz) may be referred mainly as short circuit current and charging (inrush) or discharging current of the filter capacitors [11][26]. Medium front transients should be considered when selecting the settings of protective devices. For example, when backup batteries are directly connected on the DC system, protection study should consider the high level of current provided by the batteries during a short circuit as well as the decay of the current over the time as the battery is discharging [40]. Converter current-limiting behavior is also important to be considered [11]. Fast front transients (5 – 20 kHz) are switching overvoltages [41] and transient recovery voltage at the opening of protective devices [42]. Arcing faults are difficult to classify but should also be considered. At any fault location the arc current from an arcing fault is expected to be smaller than the available bolted fault current for a fault at the same location [43].

Technological problems in protection mainly refer to the commercialy available protection technologies, their limitations and their characteristics in DC systems. Protective devices such as conventional fuses and circuit breakers have been used in railway vehicles auxiliary distribution for the last decades. DC standards for fuses and circuit breakers do exist and DC ratings can upon request be provided in many cases by the manufacturers [44][45]. The detection and arcing mechanisms of these protective devices depend on the circuit parameters (voltage, time-constant and available fault current). As an example, the impact of the circuit time-constant on fuse Time-Current Curve (TCC) is well shown in Fig. 3 of [46]. Current-limiting and non-current-limiting protective devices also exist. Non-current-limiting devices are likely to break the fault current during a steady-state condition while current-limiting devices are likely to break the fault current during a transient condition. Traditional assessment of protective devices performance using AC RMS time-current curves and AC peak let-through curves are limited practices with current-limiting devices in DC systems [44][47]. In fact, selectivity determination of current-limiting fuses and current-limiting circuit breakers should be performed by taking into account the energy limitation of the downstream device on the energy seen by the upstream device [47][48]. Since there is no natural zero-crossing, breaking DC current requires to also increase the arc voltage beyond the system operating voltage to quickly force the current towards zero [45]. By looking into the details of [49][50][51], it can be seen that the mechanisms behind DC protective devices are similar to AC current-limiting devices because the latter are built to break the current inside the first half-cycle of the AC waveform.

As of today, there is no standard related to protection analysis in on-board railway DC auxiliary distribution even though DC distribution has been used for many decades. Going with higher voltage auxiliary DC distribution will required the definition of standardized practices because of the inherent safety aspect. For fault analysis, Chapter 16 of the IEEE Std 399 (Brown Book) [52] can be used in reference even if it is not intended at first for railway application. In particular, they recommend the use of simulation tools to perform fault calculation because of the increasing complexity of the industrial and commercial DC power systems.

Finally, secondary effects such as transient overvoltage at fault clearing should be quantified and compared to IEC 60571 [53] standard which specifies voltage tolerance in DC auxiliary system of railway vehicles.

2.2 Stability

Power system stability must be guaranteed under a large number of contingencies [27]. Power system stability is defined as the system ability to reach a new stable operating state after being subjected to a disturbance. In AC power systems, stability is classified into three (3) categories: Rotor Angle Stability, Frequency Stability, and Voltage Stability [54].

In DC systems, rotor angle and frequency stability do not make any physical sense. However, voltage stability should be considered. Voltage stability in DC systems must be treated differently from AC systems because reactive power flow and phase voltage angle do not exist. The active power flow between two (2) nodes in DC systems can be controlled by the voltage magnitude difference between these two (2) nodes or by controlling the current circulating from one node to the other [55].

Power Electronic Converters (PEC) such as Voltage Source Converter (VSC) and Current Source Converter (CSC) can be used to control both the voltage and the current in DC systems. The two commonly used dc bus voltage control schemes are the master-slave method and the droop control. In master-slave control the master is responsible of controlling the voltage and giving the power set-point to the slave converters. Communication between the converters is required in this case. In droop control, all the converters share the power demand from the loads by controlling individually their output voltages. The output voltage of each converter is controlled such as it decreases linearly as the output current increases providing a sharing mechanisms between the converters [56]. Droop control emulates a series resistance at the output of the converters [57].

In DC Distributed Power System (DPS), large Constant Power Load (CPL) supplied by tightly regulated power electronics converter can yield to negative resistance behavior [58]. In railway vehicle, DC loads are classified according to the variation in current demand when their input voltage fluctuates. These are defined in IEEE Std 1476 as constant power, resistive and constant current loads [9]. A survey of different projects shows that as an average 50% of the loads in low voltage auxiliary systems are constant power while 33% are constant current and 17% are resistive loads (Figure 2.1).

The negative resistance behavior of CPL does not mean that the resistance seen is negative (i.e, $V/I < 0$) but means that the incremental resistance is negative ($dV/dI < 0$) [59]. Because of the presence of LC filters, the system can oscillate and may become unstable if the negative resistance seen at the input of the equipment cancels the positive resistive losses of the circuit [60]. The destabilizing effect of CPL can also bring the system into a breakdown condition because CPL act as a positive feedback following a disturbance [59].

Researches have been performed to determine stability criteria for both small and large disturbances as well as to develop converter stable control schemes [56][59][61]. For large multi-converter DC power systems, simulation provide a good way to assess stability under small and large disturbances and under multiple contingency scenarios.

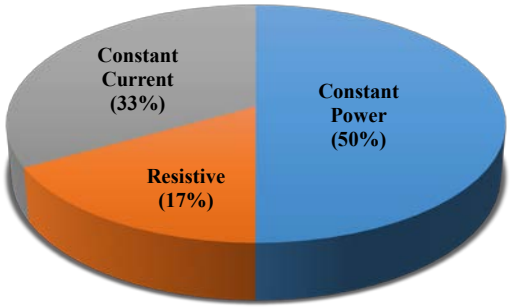

Figure 2.1: Typical Low Voltage Auxiliary Load Distribution in Rapid Transit Train

2.3 Power Quality

Power Quality is highly related to power system availability. Power quality is defined in [62] as the combination of voltage and current quality. This definition is not unanimously recognized in the industry but it is somehow what makes the most sense. In DC systems, it is defined here as the deviation of the voltage and the current magnitude from their nominal or ideal values.

Current quality phenomena such as overload, inrush and fault currents have been introduced in section 2.1 because they are all part of protection studies. Harmonic current distorsion should also be added to the list of current quality phenomena. Harmonics will not be considered in this project but the influence of the Electromagnetic Interference (EMI) filters on power system transients will be studied. Only voltage quality is covered in this section. Voltage quality phenomena can be divided into two (2) categories: variations and events [62].

- *Voltage Variations:* Voltage magnitude variation refers to slow voltage deviation while voltage fluctuation refers to fast voltage deviation from their ideal values. Harmonic distorsion, ripples and high frequency noise are also categorized as voltage variations.

- *Voltage Events:* A voltage event is generally sporadic. It is characterized by a deviation magnitude, a duration and a Vt-integral value which combines both the magnitude and the duration of the event in a single indicator. Voltage events examples are: interruption of the supply voltage, undervoltage, voltage magnitude steps, overvoltages, impulsive voltage transients (eg. Lightning), and oscillatory transients (eg. switching transients).

Voltage quality requirements can be represented by a voltage against time curve. In railway vehicles auxiliary distribution, the voltage tolerance envelope used is depicted in Figure 2.2. It is a personal representation of the most restrictive voltage tolerance described in the IEC 60571 standard [53]. The voltage tolerance envelope proposition of the Electric Power Research Institute (EPRI), Power Standards Lab (PSL) and NTT Facilities for new 380 V distribution system in data centers is also shown in Figure 2.3 [33]. No interruption is allowed and only fast voltage transient lasting less than 3 ms can exceed 385 V (1.01 pu). Therefore, the voltage must be tightly controlled around the nominal voltage of 380 V.

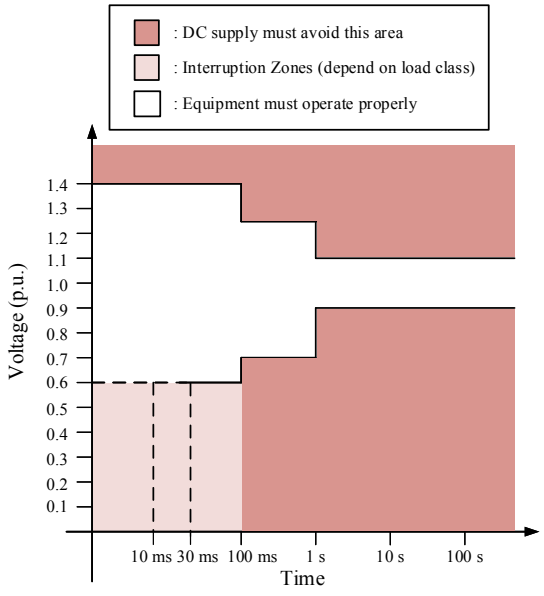

Figure 2.2: Voltage Quality Requirements in Railway Vehicles from IEC 60571

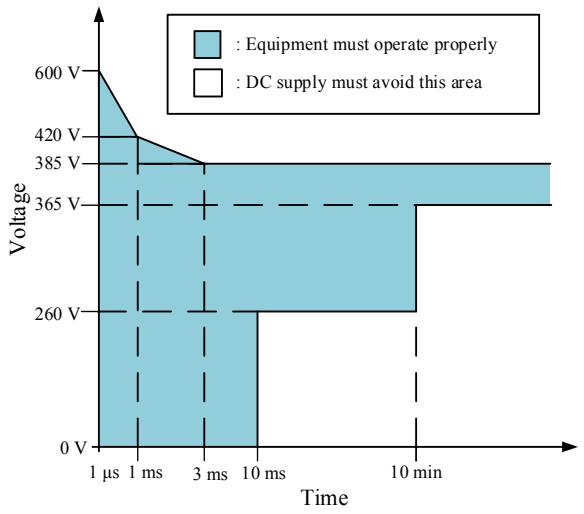

Figure 2.3: Voltage Quality Requirements in Data Centers from EPRI, PSL and NTT

2.4 Grounding and Bonding

The main reasons for grounding and bonding is to ensure human safety and reduce fire-hazards. Other reasons include improving system tolerance to electrostatic and lightning discharges, reducing radiated and conducted electromagnetic emissions and system susceptibility, improving system availability, and reducing equipment damage under fault [63]. Grounding and bonding definitions are however often confused. According to [38], grounding is in fact bonding to earth. Grounding gives a reference to ground. From a human safety standpoint, grounding reduces the touch-potential between equipment and the ground while bonding reduce the potential difference between different equipment especially under fault conditions. Both grounding and bonding also have an impact on the available type of fault and fault magnitude. This in turn influences the speed of operation of the overcurrent protective devices which is important to consider in both human and equipment protection analysis [38][39].

Grounding and bonding concept definition in railway vehicles must be done by considering the DC traction system grounding techniques which differ between transit authorities. In modern DC traction systems, the return is virtually never grounded but in old installations it can be grounded directly or through a diode. The trend is to keep the system ungrounded under normal conditions in order to minimize stray current between running rails (or vehicles) and the ground. However, when the rail-to-ground voltage is considered unsafe (typically around 60 V to 90 V), the negative lead is grounded automatically using protective relays and switching devices [6].

The definition of a new higher DC voltage standard in railway vehicle auxiliary distribution must consider grounding and bonding concepts carefully as it is done for the new 380 V distribution systems in data centers [63][64]. There is actually no standard for grounding and bonding in railway vehicles. However, even if standard IEC 60364-1 [65] is not intended to cover rolling stock electrical systems, the type of system and equipment grounding presented in this standard can be considered for grounding design within rail environment operational considerations. Depending on design considerations and particularities to transit authorities, the reference may also be provided by a grounding plane system and/or the vehicle chassis itself.

Before to present system and equipment grounding and bonding concepts, general characteristics of DC systems should be introduced. DC systems may be composed of multiple conductors having the following functions: line conductor(s) (L+ or L-), midpoint conductor (M), and protective conductor (PE). PEL and PEM conductors are the combination of protective/line and protective/mid-point conductors respectively. IEC 60364-1 defines two (2) conductors arrangement for DC systems: Two-Wire and Three-Wire (Figure 2.4) [65].

The choice of the conductor arrangement leads to the second step which is the selection of grounding and bonding methods. The grounding point may be at one pole or at the mid-point and in both cases can be directly connected to the ground or through a high resistance. The system can also be floating or isolated from the ground [63]. It leads to the definition of multiple types of grounding/bonding methods according to IEC 60364-1. The main three (3) types are [65]:

- TN: **System** direct connection of one point to ground (T) and **equipment** direct connection to the system grounding point (N).
- TT: **System** direct connection of one point to ground (T) and **equipment** direct connection to a dedicated grounding point (T).
- IT: **System** floating or high impedance connection of one point to ground (I) and **equipment** direct connection to a dedicated grounding point (T).

It has been found in the literature that authors do not agree on the safest choice of grounding/bonding methods for DC systems. For example, the authors in [63] state that the high resistance mid-point grounding (mid-point IT) should be used in new 380 V distribution system because it increases personal safety by reducing the touch potential and eliminating the arc-flash

hazard for a first fault to ground. At the opposite, the authors in [64] state that negative pole TT and TN systems should be used in new 380 V distribution system because IT grounding method requires the use of a ground fault detector to detect the first ground fault.

Another grounding method in DC system which is not directly covered in IEC 60364-1 is shown in Figure 2.5. This grounding scheme is widely used in DC auxiliary power systems for generating station [66]. System grounding is done through high resistances connected to the positive and negative leads and a Ground Fault Detector (GFD). This configuration is interesting because it uses only two wires and provides a connection point to detect ground fault. High resistance grounding can enhance the system availability because it allows the operation under a single fault to ground condition. A similar but not identical configuration is proposed by EPRI and Emerson Network Product for ±190 V (380 V) DC distribution in data centers [32].

In high resistance grounding networks, the detection of the first fault to ground is mandatory because a second fault to ground can lead to undesired high fault energy conditions. Two-pole circuit breakers interrupting capability is generally not guaranteed under such condition because the location of the two (2) faults may lead to a single pole interruption of the circuit breaker while it is rated to break the fault current using its two (2) poles [67].

It is finally important to mention that grounding and bonding architecture should ensure that the touch potential in fault condition is below the maximum human safety level of ventricular fibrillation as defined in IEC 60479-1 [68].

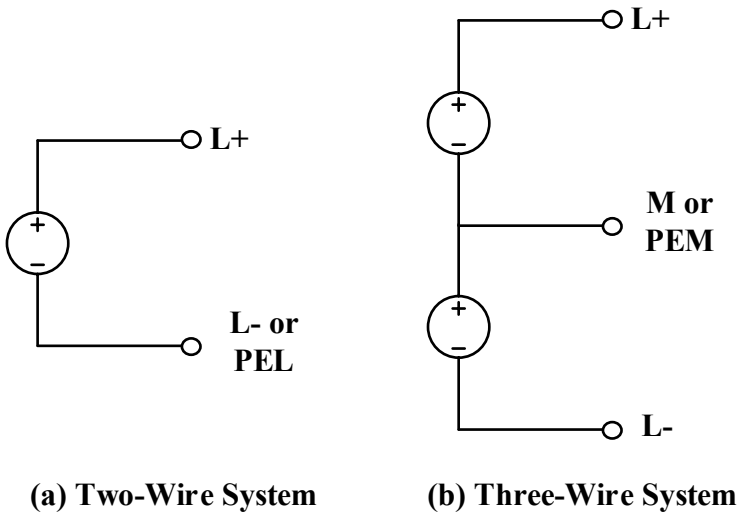

Figure 2.4: Conductor Arrangements in DC Systems from IEC 60364

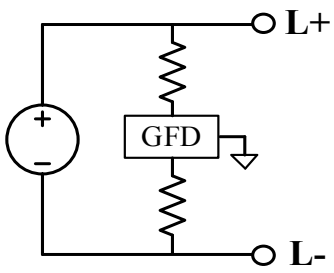

Figure 2.5: High Resistance Grounding DC Systems through a Ground Fault Detector

2.5 Safety

Safety is the number one priority of vehicle manufacturers. Two (2) important terms must be understood in safety: Hazard and Risks. Risks identification requires to translate hazards into risks. Hazard refers to "a condition or circumstance that could lead to an unplanned or undesired event". Risk is defined as the "expression of the impacts of an undesired event […] in terms of severity and likelihood" [69].

The United States Federal Transit Administration provides in their 2009 rail safety statistics report interesting data on safety in rail transit (heavy and light rails) for the period of 2003 to 2008 [70]. Figure 2.6 shows the US injury risk profile in rail transit for this period. The inner circle "Risk to" represents who is affected by the injury risk while the outer circle "Risk from" shows who is responsible for causing the risks.

This report is analyzed here by taking into account the risks that can be related to railway vehicle electrical system failures. First, the risks related to vehicles are most likely to affect passengers and workforce. On this, Figure 2.6 shows that 55% of all the injury risks are to passengers while 5% are to workforces. Of all the injury risks to passengers, 49% are related to workforce behavior which includes poor maintenance and 9% is related to equipment failure. Among the 55% of all passenger injury risks, 255 cases are the consequence of fires (Figure 2.7).

The safety in electrical system is highly related to appropriate grounding and protection practices [34]. Equipment and human protection should both be part of protection studies [71]. Equipment should be protected against abnormal operating conditions which could lead to equipment failures, potentially fires, and human safety hazards. For example, overcurrent, overvoltage, and arcing fault may lead to equipment failure and possibly fires which can in turn

cause service interruption or in worst cases human injuries or fatalities. Arc-flash and touch-potential (shock) hazards are also direct causes of human injuries or fatalities.

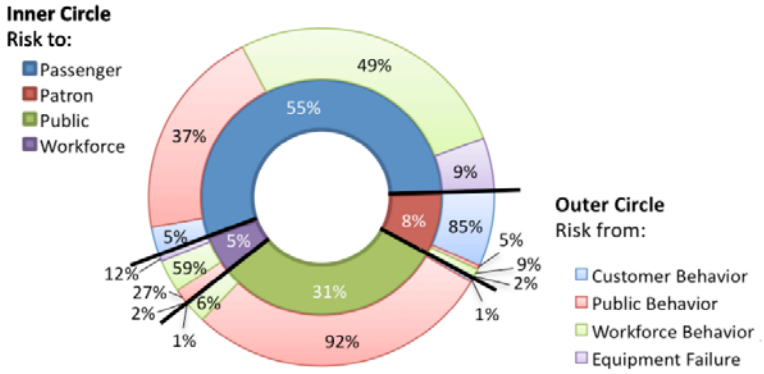

Figure 2.6: US Injury Risk Profile in Rail Transit: 2003-2008 [70]

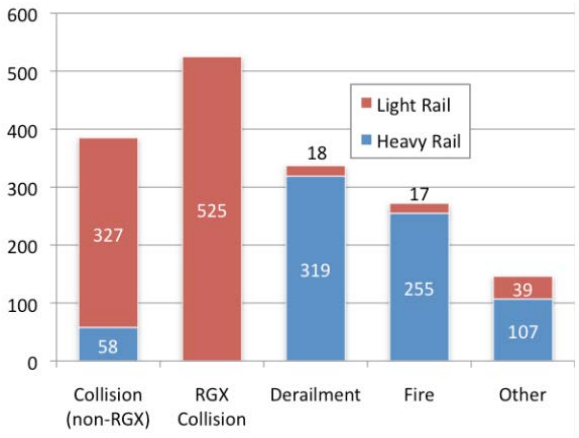

Figure 2.7 Passenger Injuries by Mode in Rail Transit: 2003-2008 [70]

Electrical safety hazards must be “analyzed, assessed, prioritized, and resolved, accepted or tracked” [69]. In order to identify and mitigate the risks, vehicle manufacturers perform Failure Mode and Effects Criticality Analysis (FMECA), Failure Modes and Effects Analysis (FMEA) and Fault Tree Analysis (FTA). FMECA is done to guarantee safe and reliable operation of the manufactured vehicles. It is based on the assumption that any piece of hardware or software will sooner or later fail which will affect the operation of one of the train system or in worst cases the complete train consist. FMEA is performed to ensure that the design will execute the required functions. It is based on the assumption that eventually design errors will impact the required functions. FTA is finally performed to identify the sequence of events that may lead to the loss of a pre-determined system function.

In accident analysis research, FTA is classified as a non-systemic accident analysis approach or more precisely as a sequential (or cause-effect) accident modeling method [72]. Sequential accident models represent the sequence of events leading to an accident where the links between the cause and the effect are simple and deterministic. Other models such as epidemiological accident models and systemic accident models have been developed with different objectives to overcome the limitations of the sequential approach [73].

Sequential accident models are widely used in engineering because they are easy to represent graphically. Nevertheless they should be analyzed within the knowledge of their limitation especially for complex dynamic systems. Detailed simulation models can be used as an efficient complementary tool to identify, analyze, assess, and resolve safety hazards at an early design stage such as it reduces the cost of the mitigation process. The main advantages of simulation is the ease to observe the evolution of the electrical state variables at any location in the power system.

CHAPTER 3 DC POWER SYSTEM ANALYSIS

In this chapter a set of DC power system phenomenon is established and studied from a theoretical standpoint. The investigation on power system behavior and problem mitigation using simulation tools should consider the theoretical influence of network parameters. The power system transient phenomena presented in this section are based on railway industry experience in manufacturing and testing DC systems, field experiment as well as a literature review related to other DC system applications.

3.1 Stability

The general concept of stability in DC systems has been introduced in section 2.2. The stability is now studied from a mathematical standpoint. Stability criteria are presented to understand the various parameters behind stability as well as to introduce simple criteria which can be used to reduce the potential of instability at the design phase but also to analyze the simulation results. The symbols used in this section are presented in Table 3.1.

Table 3.1: Symbols used for Stability Analysis

Description	Symbol
Equivalent Negative Resistance of the Load	R_{in}
Output Power of the Power Electronic Converter	P_L
Constant Power Load (CPL) Power Set-Point	P_{CPL}
Resistive Load Power	P_R
Constant Current Load (CCL) Power Set-Point	P_{CCL}
Source Current	i_{in}
Constant Current Load (CCL) Equivalent Current Set-Point	I_{CCL}
Power Electronic Converter Efficiency	η_c
Load Voltage	v_o
Source Voltage	v_s
Equivalent Circuit Resistance (Source, Cable and Inductor ESR)	R_{eq}
Equivalent Filter Inductance	L_{eq}
Equivalent Filter Capacitance	C_{eq}
Capacitor ESR	R_{ceq}
Load Resistance	R_L

3.1.1 Sokal Criterion

The Sokal Criterion [60] has been developed in 1973 and is the first DC voltage stability criterion found in the literature. It is based on the equivalent circuit of Figure 3.1. The negative resistance (R_{in}) is defined by (3.1) using Figure 3.2 and by taking the following assumptions:

- The load power (P_L) at the output of the power electronic converter (PEC) does not depend on the PEC input voltage (v_o).
- The input power of the PEC (P_{CPL}) is also independent of the PEC input voltage (v_o).
- The converter efficiency (η_c) is independent of v_o (generally a weak coupling).

$$R_{in} = \frac{\eta_c v_o^2}{P_L} = \frac{v_o^2}{P_{CPL}} \tag{3.1}$$

From [60] oscillations will not occur if:

$$P_{CPL} < \frac{v_o^2 \left(R_{eq} + R_{ceq} \right) C_{eq}}{L_{eq} + C_{eq} R_{eq} R_{ceq}} \tag{3.2}$$

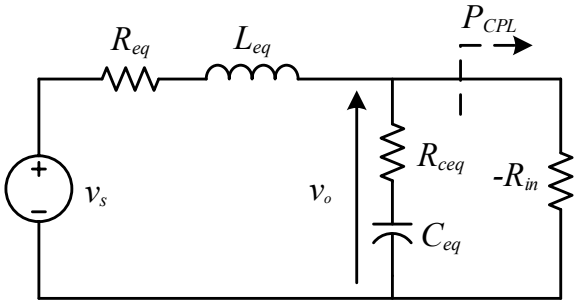

Figure 3.1 Sokal Criterion System Configuration

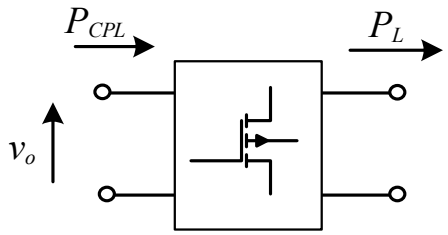

Figure 3.2 Sokal Equivalent Load Model for Negative Resistance (R_{in}) Definition

3.1.2 Emadi et al. Criterion

The approach presented by Emadi et al. [74] has been introduced in the context of the development of vehicular DC power systems. In their definition of voltage stability, the authors neglect the capacitor ESR (Equivalent Series Resistance) but they add the influence of what they call “constant voltage loads”. The use of the term “resistive load” is preferred here to the use of the term “constant voltage load” because the power of resistive load is voltage-dependent.

The circuit used to establish this criterion is shown in Figure 3.3. It can be demonstrated (ref. Appendix A) that necessary and sufficient condition for small-signal stability is given by [74]:

$$P_{CPL} < \frac{v_o^2}{R_L} + \frac{R_{eq}C_{eq}}{L_{eq}} v_o^2 \tag{3.3}$$

Or:

$$P_{CPL} < P_R + \frac{R_{eq}C_{eq}}{L_{eq}} v_o^2 \tag{3.4}$$

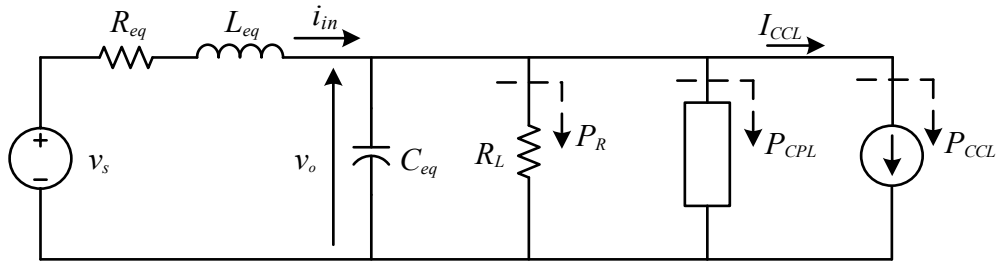

Figure 3.3 Emadi et al. Criterion System Configuration with Constant Current Load

3.1.3 Stability Analysis

By analyzing and comparing the Sokal [60] and Emadi et al. [74] criteria, design considerations for DC voltage stability margin improvements are established:

- For $C_{eq}R_{eq}R_{ceq}$ small compared to L_{eq}, increasing capacitor ESR (R_{ceq}) enhance stability margin according to (3.2). However, filter effectiveness will be reduced. For example, changing an old electrolytic capacitor with a high ESR by a new film capacitor with low ESR should be done by keeping in mind that stability margin will be reduced. This case has already been observed experimentally in the past.

- According to (3.4), increasing R_{eq} improves stability margin. Adding a series resistance is not desirable because it increases losses, generates heat and reduces system efficiency. However, increasing R_{eq} by increasing the converter internal droop as presented in section 2.2 can enhance stability without inserting extra losses. Nevertheless, the internal droop cannot be increased infinitely. The maximum droop value depends on the minimum load voltage and maximum power transfer requirements [61].
- According to (3.4), increasing C_{eq} or decreasing L_{eq} improves stability margin. This is often the easiest solution but it is important to keep in mind that C_{eq} and L_{eq} both determine the filter cutoff frequency. Increasing C_{eq} can also lead to high inrush current which may have to be managed by adding extra components.
- Increasing the system voltage (v_o) according to (3.4) can also improve system stability. However, it is a design choice only available at the beginning of a project. This is generally not an option.
- Adding resistive loads (P_R) improves system voltage stability. As can be seen in (3.4) the presence of P_R increases the amount of constant power loads (P_{CPL}) that can be connected on the system thus improving system voltage stability margin. However, this is also not really an option especially if resistive loads are not necessary for system functionalities.
- Controlling the internal power electronic converter of the load such as it does not behave as a pure constant power load seen from the DC power system is also a solution which is often preferred in late design phases. An example of control strategy to eliminate the negative impedance behavior over a specified bandwidth of a three-phase synchronous machine drive can be found in [75].

Finally, constant current loads (CCL) are not considered because they do not impact small-signal stability under linear assumptions. Appendix A shows how the CCL term vanishes into the mathematical formulation of the small-signal stability problem. However, during simulation in section 5.2.1, it will be observed that it is not the case in the presence of non-linear series resistive elements such as diode or converter variable output droop resistance.

3.2 Current Transient

Current transients are very important during components sizing. Moreover, overcurrent protection system design must consider current transients to avoid power system blackout, undesirable trip and poor coordination. Four (4) major types of current transient events are generally recognized: overload, inrush current, short-circuit, and arcing fault. This section covers each of these individually.

3.2.1 Overload

Overload condition refers to low and slow increase in the load demand. It can be controlled or not. For example, a controlled overload can occur when a major load or multiple loads are voluntarily increased to perform the required system functionalities. An uncontrolled overload can occur during degraded operating mode such as the loss of one or multiple sources or during long duration voltage drops due to the increase of the current of constant power loads.

Overload conditions need to be taken into account in battery and converter sizing. These overloads can also lead to undesired trip of the protection system if the load voltage dependency is not considered during protection system design.

From a theoretical standpoint, overloads from constant power loads are the most interesting to study. In fact, the current drawn by these loads increases/decreases when the voltage decreases/increases. Analytically, these loads react to voltage fluctuation following:

$$i = \frac{P}{v} \tag{3.5}$$

Resistive loads will act at the opposite of constant power loads following Ohm's law:

$$i = \frac{v}{R} \tag{3.6}$$

Constant current loads simply draw a constant current value independently of the voltage magnitude.

3.2.2 Inrush

Inrush current is typically a very fast transient with time-constant less than few milliseconds. Inrush current is likely to happen when filter capacitors are energized.

Important inrush current due to the load front-end LC filters has been observed in railway vehicle DC auxiliary systems when simultaneously switching ON multiple DC loads. Undesired circuit breaker trips have also been observed during field testing. Analytical equations based on simple circuit equations can be derived to provide a better understanding of the inrush current in DC systems. All the equations presented in this section have been validated with EMTP-RV.

The simple series RLC-circuit of Figure 3.4 is used to study analytically capacitor inrush current when the switch (S) is closed. The initial inductor current ($i_L(0)$) is neglected. The initial capacitor voltage ($v_C(0)$) is not neglected in order to consider capacitor trapped charge.

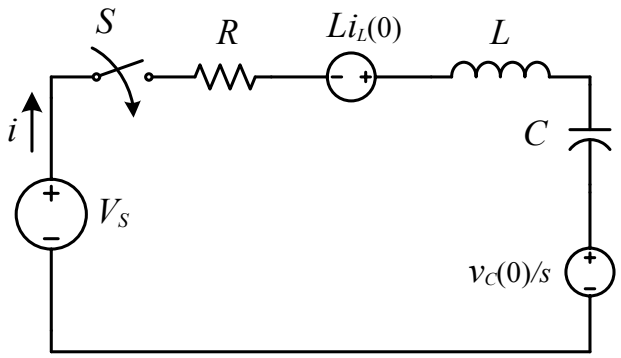

Figure 3.4 Series RLC-Circuit for Capacitor Inrush Current Calculation

The inrush current can be defined in the Laplace domain by:

$$I(s) = \frac{\left(V_S - v_C(0)\right)/L}{s^2 + \frac{R}{L}s + \frac{1}{LC}} \tag{3.7}$$

The roots ($\lambda_{1,2}$) of this system are the zeros of the characteristic equation:

$$\lambda_{1,2} = -\frac{R}{2L} \pm \sqrt{\Delta} \tag{3.8}$$

With Δ being calculated by (3.9) and defines the inrush current dynamic response which can be critically damped (3.10), damped (3.11), or oscillatory (3.12).

$$\Delta = \left(\frac{R}{2L}\right)^2 - \frac{1}{LC} \tag{3.9}$$

$$\frac{R}{2L} = \frac{1}{\sqrt{LC}} \tag{3.10}$$

$$\frac{R}{2L} > \frac{1}{\sqrt{LC}} \tag{3.11}$$

$$\frac{R}{2L} < \frac{1}{\sqrt{LC}} \tag{3.12}$$

Only the damped and oscillatory conditions will be studied because the critically damped case is a unique case which is unlikely to happen. From the characteristic equation, we can also define the well-known equations giving the natural frequency (ω_o), the damping coefficient (ζ), and the coefficient (α):

$$\omega_o = \frac{1}{\sqrt{LC}} \tag{3.13}$$

$$\zeta = \frac{R}{2}\sqrt{\frac{C}{L}} \tag{3.14}$$

$$\alpha = \frac{R}{2L} \tag{3.15}$$

These equations allow to see that increasing L and C leads to a lower natural frequency while increasing R and C, or decreasing L provides extra damping.

For the damped case, the real roots are given by:

$$\lambda_{1,2} = -\alpha \pm \sqrt{\alpha^2 - \omega_o^2} \tag{3.16}$$

It can be shown that the transient current response is given for the damped case by:

$$i(t) = K\left(\frac{1}{\lambda_1 - \lambda_2}e^{\lambda_1 t} + \frac{1}{\lambda_2 - \lambda_1}e^{\lambda_2 t}\right) \tag{3.17}$$

With K defined as follow:

$$K = \frac{V_S - v_C(0)}{L} \tag{3.18}$$

For the oscillatory case, the complex roots are calculated by:

$$\lambda_{1,2} = -\alpha \pm j\sqrt{\omega_o^2 - \alpha^2} = -\alpha \pm j\beta \tag{3.19}$$

In this case, it can be shown that the transient current response follows:

$$i(t) = \frac{K}{\beta} e^{-\alpha t} \sin(\beta t) \tag{3.20}$$

Using (3.17) and (3.20), typical waveforms for damped and oscillatory inrush current conditions are plotted in Figure 3.5. In both cases the current tends toward zero as the time tends to the infinity which is typical of a transient inrush current because the capacitor act as an open-circuit once it is completely charged.

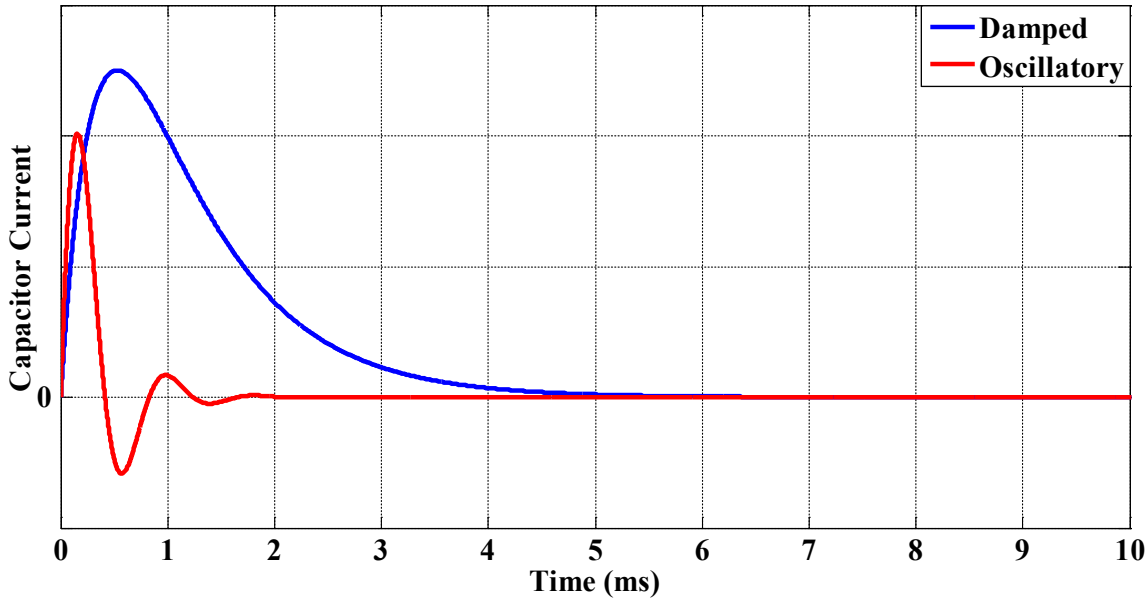

Figure 3.5 Inrush Current Typical Waveforms

3.2.3 Short-Circuit

The calculation of short-circuit currents in DC auxiliary installations of power plants and substations is presented in IEC 61660-1 [76]. This approach is based on evaluating the contribution of each of the sources to the total short-circuit current. Standardized waveforms and typical adjustment factors are used. IEC 61660-1 is not intended for other auxiliary installation systems such as aircraft, ship, and railway DC systems [77]. This standardized approach can also become a very demanding task when studying complex meshed systems. Nevertheless, the

decomposition into individual source contribution can be used to at least understand the contribution of each component to the total short-circuit current.

Filter capacitors, batteries and auxiliary converters are the main sources of short-circuit current in railway DC auxiliary distribution systems. The contribution of each of these sources to the total short-circuit current is different depending on many factors (e.g. Distance, Dynamic Control, Filter). The total short-circuit current at any fault location is the superposition of the individual sources contribution. Evaluating the short-circuit current in DC distribution systems also implies the calculation of both the minimum (battery low SOC, arcing, high resistance) and the maximum (battery maximum SOC, bolted) short-circuit current values.

3.2.3.1 Filter Capacitor

Filter capacitor contributes to short circuit current for a very short period of time. However, during this period the peak contribution can be very high. It can be studied by neglecting the initial current of the inductor using the simple series RLC-circuit of Figure 3.6. When the switch (*S*) is closed, a short circuit between the initially-charged capacitor is created through the RL path. The RL path is mainly constituted of the capacitor ESR and ESL, and the DC bus resistance and inductance from the capacitor up to the faulty point.

Similarly to capacitor inrush current, capacitor discharge during short circuit can be written using (3.17) and (3.20) with *K* now being:

$$K = \frac{v_C(0)}{L} \tag{3.21}$$

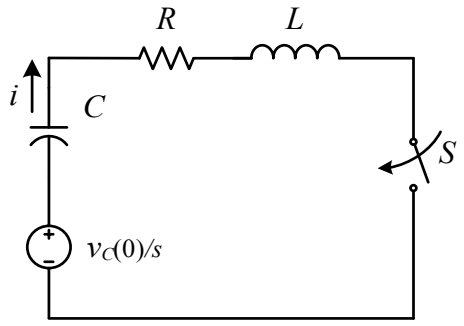

Figure 3.6 Series RLC-Circuit for Capacitor Discharge Current Calculation

3.2.3.2 Battery

Unlike capacitor, battery contributes to the short-circuit current over a long period of time. Battery is often modeled as a simple fixed internal voltage source behind its internal resistance and inductance. However, field tests have shown that the discharge of a battery over time during a fault has a significant impact on the fault current magnitude which in turn has an impact on the speed of operation of thermal overcurrent protective devices. A more sophisticated battery model should be implemented to consider the discharge of the battery during a fault.

A simple battery model (Figure 3.7) is compared to a more detailed model (presented in section 4.2.2) in order to provide a rationale to the importance of using a detailed battery model and to understand the behavior of a real battery under short-circuit condition.

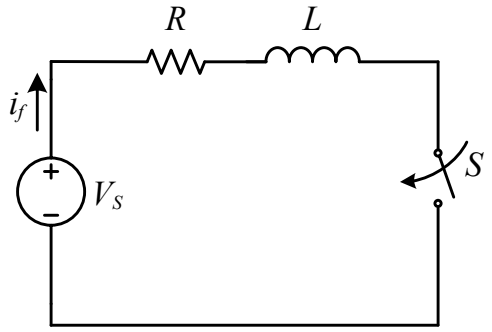

Figure 3.7 Simple RL Battery Model for Short-Circuit Current Calculation

The transient short-circuit current when switch (*S*) is closed in Figure 3.7 is described using the well-known first order current transient response of a RL-circuit:

$$i_f(t) = I_{SS}\left(1 - e^{-t/\tau}\right) \tag{3.22}$$

Where I_{SS} is the prospective current and τ is the time-constant calculated by:

$$I_{SS} = \frac{V_S}{R} \tag{3.23}$$

$$\tau = \frac{L}{R} \tag{3.24}$$

The initial rate-of-rise is also an important parameter in protection studies. It is given by:

$$\left.\frac{di_f}{dt}\right|_{t=0} = \frac{I_{SS}}{\tau} = \frac{V_S}{L} \tag{3.25}$$

The comparison between the short circuit current for simple and detailed battery models is presented in Figure 3.8. The detailed battery model initial voltage is the same as the simple battery model constant internal voltage. The fault RL path including the battery internal resistance is the same in both cases. In Figure 3.8, it is seen that the fault current is constant in steady-state using the simple model of Figure 3.7 while the current decreases significantly with the time using the detailed model which considers the discharge of the battery. Field testing have shown that the fault current decreases of approximately 5% to 15% for fault duration between 5 to 10 seconds.

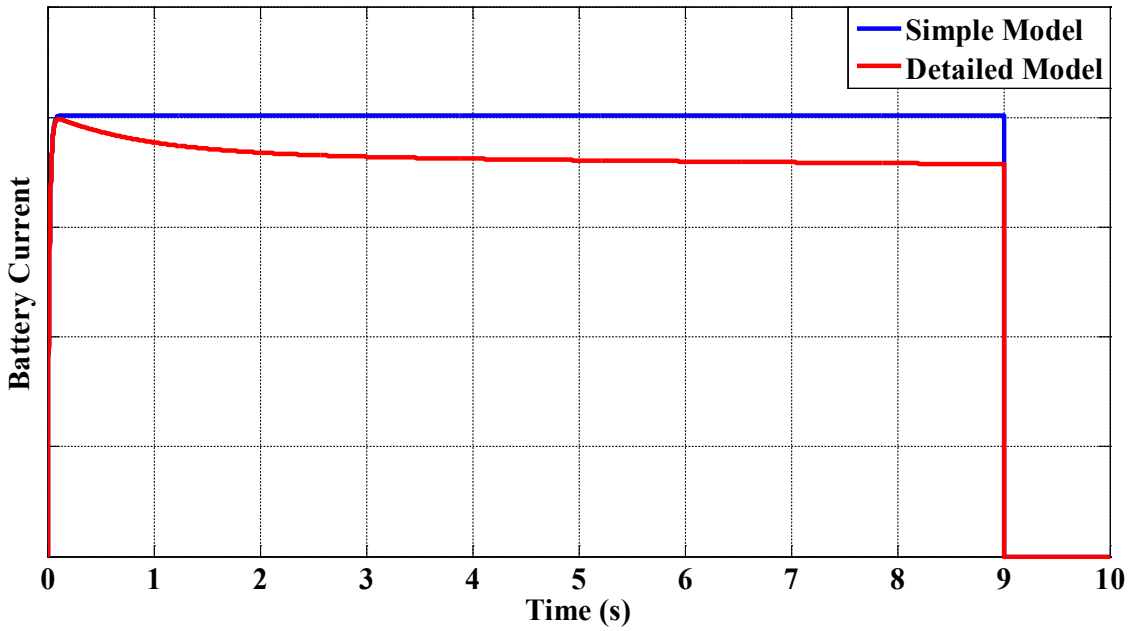

Figure 3.8 Simple and Detailed Battery Models Short-Circuit Current Comparison

3.2.3.3 Auxiliary Converter

Assessment of auxiliary converter contribution to short-circuit must consider its control structure and its dynamic under fault condition. In railway application, similarly to what is presented in [57] for DC microgrid, three (3) levels of converter control can be defined:

- **Internal Control:** These controls are typically inner voltage and current control loops of the converter. They do not influence the converter from a power system standpoint (e.g. Built-in protection of the semiconductors, pulse-to-pulse current limit feature). They are generally faster than the switching period.

- **Primary Control:** These controls are outer voltage and current loops defined by a VI-characteristic. These controls are based on averaged (or filtered) value at the output of the converter. Voltage control, battery charging temperature compensation, and soft-start are examples. They are slower than the switching period.
- **Secondary Control:** In railway auxiliary converter, the secondary control (if present) is used to slowly restore current deviation between multiple parallel converters. It is based on a communication scheme between the converters.

DC auxiliary converters used on-board of DC supplied railway vehicles are generally isolated DC-DC buck converter. Primary control is the main level to be considered in short-circuit analysis on the DC auxiliary system side. A general VI characteristic is shown in Figure 3.9. Converters are controlled following a VI characteristic that allows current sharing between the converters, and power and current limiting actions. The characteristic can be shifted up or down in battery charging mode for battery temperature compensation. The following control zones can be defined:

- Zone (1): Current Sharing (or Droop Control)
- Zone (2): Constant Power (or Overload Protection)
- Zone (3): Short-Circuit Protection

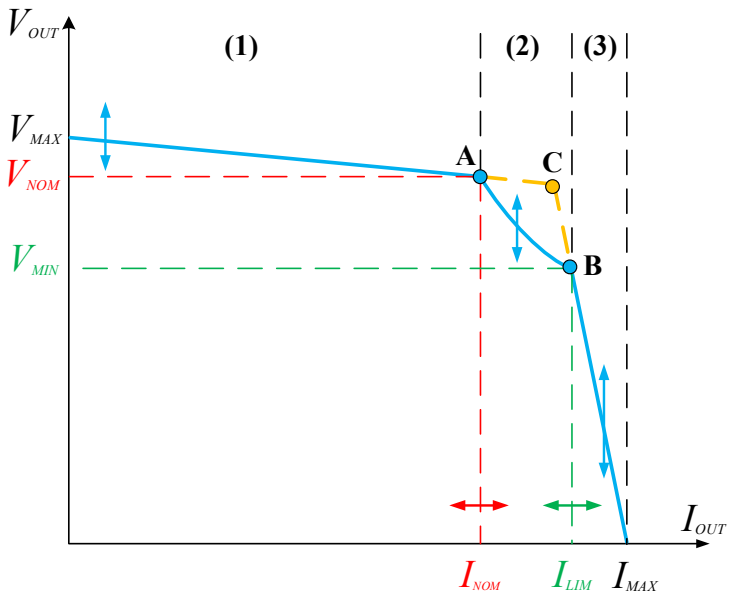

Figure 3.9 General VI Characteristic of Auxiliary Converter

As seen before, zone (1) is important for current sharing and the stability of the power system. Zone (2) is used to reduce the stress applied to the semiconductors under high power conditions. Instead of operating on the dashed orange lines (A-C-B), the converter is controlled to keep a constant power on the blue curve (A-B). Zone (2) is not always necessary. Under short-circuit conditions in zone (3), the converter is controlled to limit its output current rapidly. As the average output current rise, the converter limits its output voltage to provide a current-limiting effect. It mainly acts as a constant current source during fault condition. Figure 3.10 shows that the converter output filter capacitor will also have a high contribution to the fault current during the first milliseconds of the fault but the current will rapidly settle to a constant value following the converter VI-characteristic in zone (3).

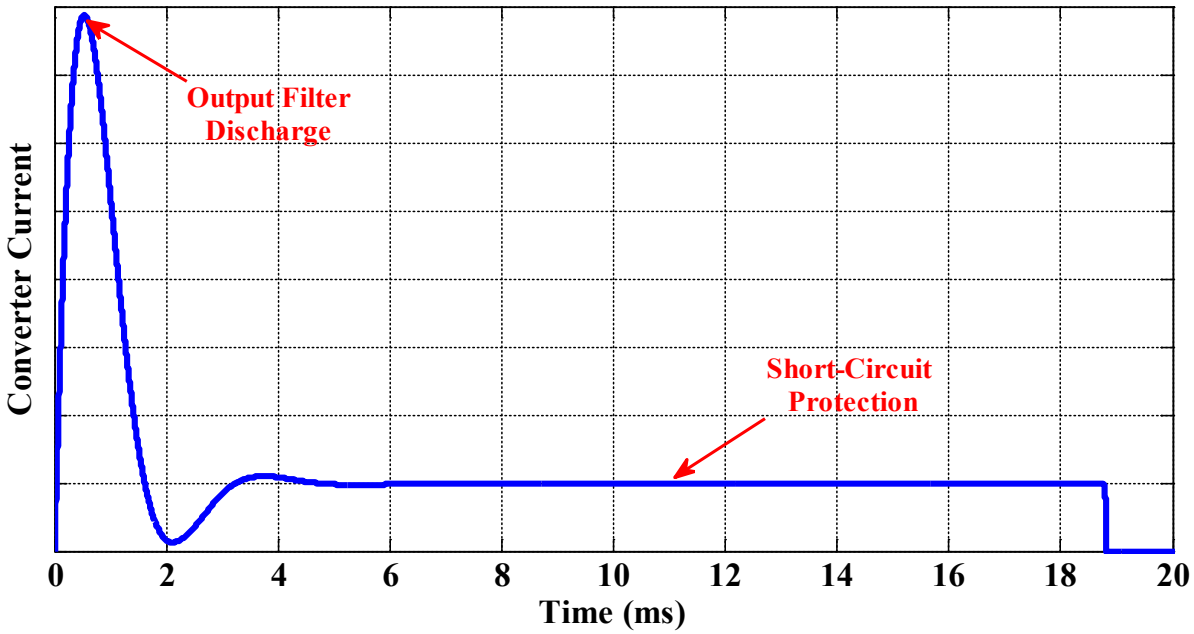

Figure 3.10 Auxiliary Converter Output Current Typical Waveform

3.2.4 Arcing Fault

Arcing fault are now frequently integrated into protection studies. Fire and arc-flash hazards originating from arcing fault are the main reasons to this increasing interest in arcing fault. Arcing fault current must be well understood in order to reduce the potential of fire and arc-flash hazards caused by arcing fault in power systems.

3.2.4.1 Low Fault Current

Many fires in residential home have been generated by arcing fault on 120 VAC circuits [78]. Fires also occurred in DC rapid transit and mine trolley systems due to arcing fault [79]. One of the main problem of arcing fault in both AC and DC systems is the fact that it remains undetected by the overcurrent protective devices [78][79].

An arcing fault occurs when an electric arc is created between two (2) electrodes. Loose connections and damage to wire insulation are two (2) examples of situations which may lead to an arcing fault. If the conditions for arc sustainability are met, the arc is established permanently and an arcing fault condition is created. This condition can lead to a fire if combustible materials are exposed. Arcing fault are difficult to detect by overcurrent protective devices because arc sustainability conditions can be established with less than one (1) ampere of arc current and the arc impedance reduces considerably the available fault current [78].

Arcing fault escalating rapidly into a low impedance fault can result in overcurrent protective devices trip. However, it is not always the case and low arcing current may lead to a fire before it is even detected by the overcurrent protective devices.

There is two (2) types of arcing fault: series and parallel (Figure 3.11). Series arcing fault occurs when there is a breach within a single conductor while parallel arcing fault results of an indirect connection through the air by an electric arc between two (2) conductors or a conductor and the ground. In AC circuit, series arcing fault results into very low fault current in the range of the protective device circuit rating but shows high Radio Frequency (RF) content. Parallel arcing fault results in a higher fault current but low RF content. High current rate-of-rise (di/dt) are expected in comparison to the normal load current. In AC systems, the arc extinguishes and reignites periodically at each zero-crossing of the normal current waveform which is a very helpful indicator of arcing fault. Since 2008, Arc Fault Circuit Interrupters (AFCI) detecting both series and parallel arcing faults are also required by the National Electrical Code (NEC) in bedroom circuits [78].

In DC systems, there is no zero-crossing. In solar applications, arc detection scheme are implemented in compliance to the UL 1699B standard. Arcing fault in DC systems changes the power frequency spectrum between 40 kHz to 100 kHz [80]. Experimentation seems to be the preferred way to identify arcing fault spectrum and to validate different protection algorithms.

This is mainly explained by the complexity of the physics behind and the high level of parameters that need to be taken into account. Similarly to AC systems, arcing fault detection mechanisms in DC systems are based on signal processing and analysis of the current frequency spectrum [81]. In this master thesis, no attempt will be made to model the frequency behavior of arcing fault.

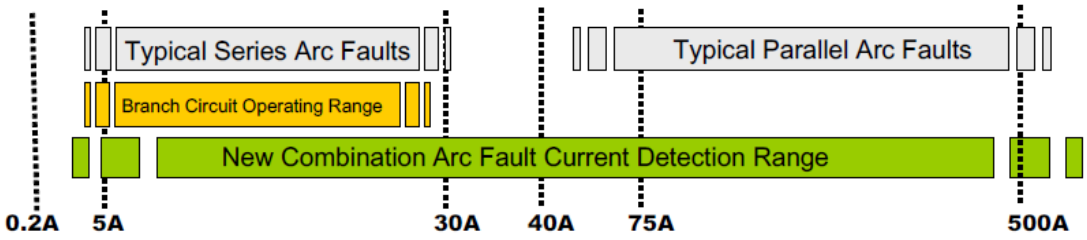

Figure 3.11 Current Level of Series and Parallel Arcing Faults in Home Circuit [78]

3.2.4.2 Arc-Flash Hazard

Arc-flash hazard exposure for workers is also an important concern due to the large number of listed incidents. Arc-flash hazard is a high release of energy generated by an electric arc. Many workers have been seriously burned or even died from arc-flash exposure in commercial and industrial sites, electric utility installations and mine sites. A large number of incident occurred in system with nominal voltage as low as 480 VAC [82]. The main purpose of arc-flash hazard analysis is to evaluate the potential maximum incident energy exposure of workers and determine the appropriate personal protective equipment (PPE) for given working distance and working conditions [46][71].

In AC systems, IEEE Std 1584 [82] is widely used for arc-flash hazard analysis. During arc-flash event, the current flowing into the circuit is the arc current, not the bolted fault current. Therefore, to evaluate the potential maximum arc-flash energy exposure the arc current must be evaluated. Obviously, the time of exposure must be evaluated as well. The time of exposure depends on the worker escape time from the hazard location but also the speed of operation of the protective devices. Since arcing fault results into lower fault current in comparison to a bolted fault at the same location the operating time of the protective devices increases. Since there is a non-linear relationship between the current and the time on conventional time-current curve, the maximum incident energy can occur at the maximum arcing current or at the maximum

protective devices operating time. For this reason, arc current must be well defined during this process and this is why there is an increasing number of researches on arc current in DC systems. Empirical models are being developed and an example is summarized here.

It is well-known that the bolted fault current (I_{bf}) in a given power system depends on the location of the fault. It is then obvious that the arc current (I_{arc}) for a fault at the same location depends on the available bolted fault current (I_{bf}). The arc current also depends on the gap distance (G) between the arc electrodes (points of contact). Based on field experimentation on a 600 VDC transit system, an empirical equation relating the open-air arc current (I_{arc}), the bolted fault current (I_{bf}) and the gap distance (G) has been defined in [43]:

$$I_{arc} = 0.9063 I_{bf}^{0.8927} - 0.1051 e^{0.1093 I_{bf}} \left(G - 1\right) \tag{3.26}$$

In (3.26), the arc current (I_{arc}) and the bolted fault current (I_{bf}) units are both in (kA) while the gap distance (G) units are in inches (in). This equation is valid for bolted fault current ranging from 1 kA to 25 kA and for gap distance ranging from 0.2 in to 6 in [43].

The incident energy (IE) which depends on the arc current (I_{arc}), the exposure time (t_{exp}), the gap distance (G), and the working distance (D) has also been defined in [43]:

$$IE = \left(0.9694 I_{arc} - 0.0589\right)\left(0.4793 ln\left(G\right) + 1.0027\right) \times \left(\frac{t}{0.1}\right)\left(\frac{6^2}{D^2}\right) \tag{3.27}$$

The gap distance (G) is also given in inches (in). This equation is valid for exposure time ranging from 10 ms to 2 s and working distance from 6 in to 34 in [43].

Equations (3.26) and (3.27) can be also used to conservatively assess incident energy for 125 VDC and 250 VDC systems assuming slow protection [43]. The ratio of I_{arc} against I_{bf} is plotted in Figure 3.12 using equations (3.26) to show the non-linear behavior of the arcing current against the bolted fault current and the gap distance.

As of today, NFPA 70E [83] appears to be the only standard that covers DC arc-flash calculation. The NFPA 70E method is based on the formulation of the maximum power transferred into the arc proposed by [46]. According to the NFPA 70E standard this method is considered to be conservative. The maximum power transfer theorem in DC systems states that the maximum power is transferred by a source to a load when the source resistance (R_s) and the

load resistance (R_L) are matched ($R_s = R_L$). Applying this theorem to the arcing current problem leads to a maximum arc power transferred when the arc resistance (R_{arc}) is equal to the system resistance (R_s), leading to:

$$I_{arc} = 0.5 I_{bf} \tag{3.28}$$

Equation (3.28) can be used as a rule of thumb for arc current estimation. However, by comparing (3.26) to (3.28), it is seen that it is not really accurate over a wide range of fault location and gap distance.

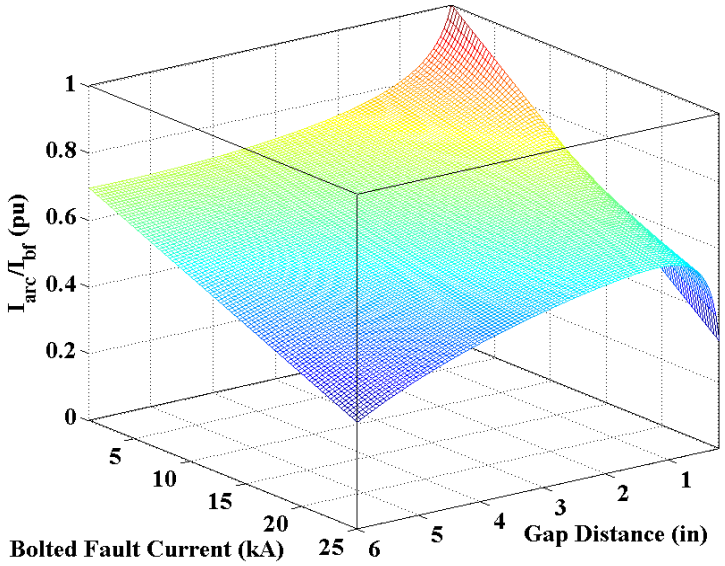

Figure 3.12 Arcing Current against Bolted Fault Current and Gap Distance

3.3 Voltage Switching Transient

During the design phase, it is important to validate that the designed system will meet the voltage tolerance envelope requirements (ref. Section 2.3). This section covers voltage switching transients in DC systems because it is a concern for railway vehicle manufacturers. One of the main concern is the transient overvoltage at fault clearing.

In a first step, a theoretical review of switching overvoltage at the opening of an ideal switch in a simple RLC-circuit is presented to observe the impact of the circuit parameters. However, it should be kept in mind that protective devices such as circuit breaker and fuse are not ideal switches. Breaking DC current requires in fact sophisticated arcing mechanisms similar to AC current-limiting devices to increase the arc voltage and force the current towards zero.

Considering an ideal switch to study voltage transient will overestimate the expected transient overvoltage since the energy absorbed by the arc is not taken into account.

Also, when the current reaches zero, an oscillatory response called the transient recovery voltage (TRV) may also leads to dangerous overvoltage conditions. Arc voltage and transient recovery voltage will be covered separately.

3.3.1 Theoretical Review of Voltage Switching Transient

Dangerous overvoltage condition can occur when a switching device breaks the current flowing into the circuit. It can also be studied with a basic circuit. This section is intended to present the impact of circuit parameters on overvoltage and understand the worst case conditions and the available mitigation techniques. All the equations presented have been validated by simulation on an equivalent circuit in EMTP-RV.

For the purpose of understanding, let's consider first the theoretical circuit on the left of Figure 3.13. The switch (S_F) is initially closed through the fault resistance (R_F) to simulate a fault condition on the load side of a LC filter. The initial current into the inductor ($i_L(0)$) and the initial capacitor voltage ($v_C(0)$) are then known from steady-state circuit equation during the fault condition:

$$i_L(0) = \frac{V_S}{R + R_F} \tag{3.29}$$

$$v_C(0) = R_F i_L(0) \tag{3.30}$$

When the switch (S_F) is opened, the circuit response is mathematically equivalent as if we close the switch (S) in the circuit on the right of Figure 3.13 with the initial conditions $i_L(0)$ and $v_C(0)$ given respectively by (3.29) and (3.30).

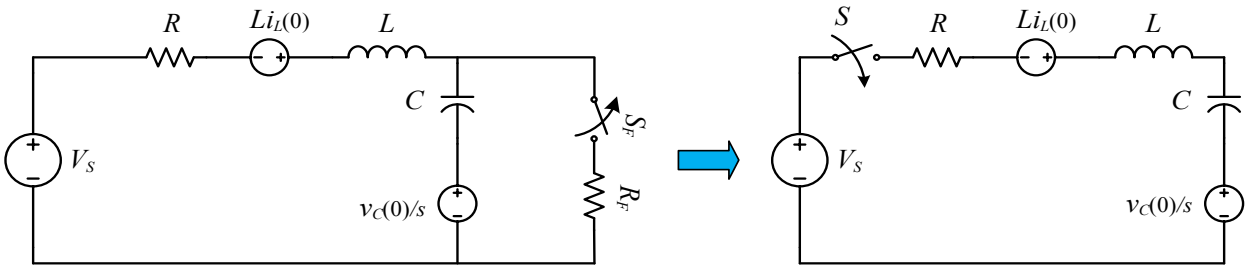

Figure 3.13 RLC-Circuit for Transient Overvoltage Study

It can be shown in the Laplace domain that the capacitor voltage is given by:

$$V_C(s) = \frac{K_1}{s\left(s^2 + \frac{R}{L}s + \frac{1}{LC}\right)} + \frac{K_2}{s^2 + \frac{R}{L}s + \frac{1}{LC}} + \frac{v_C(0)}{s} \tag{3.31}$$

The coefficients K_1 and K_2 are given by:

$$K_1 = \frac{V_S - v_C(0)}{LC} \tag{3.32}$$

$$K_2 = \frac{i_L(0)}{C} \tag{3.33}$$

Overvoltage occurs when the system is oscillatory. In this case, equation (3.12) is met. Again, using the residue method for partial fraction decomposition with complex roots, equation (3.31) becomes in the time-domain:

$$v_C(t) = 2|C_1|e^{-\alpha t}\cos\left(\beta t + \theta_{C_1}\right) + \frac{K_2}{\beta}e^{-\alpha t}\sin(\beta t) + v_C(0) \tag{3.34}$$

Where C_1 is a complex number defined by solving:

$$C_1 = \left.\frac{K_1}{s(s+\alpha+j\beta)}\right|_{s=-\alpha+j\beta} = |C_1|\angle\theta_{C_1} \tag{3.35}$$

Recall also that the coefficient α and β are obtained from (3.15) and (3.19) respectively.

The influence of each circuit parameters can be studied by keeping all the other parameters constant (Figure 3.14). From this, it is possible to say that:

- Fault conditions (large value of $i_L(0)$) and large inductor (L) lead to a large amount of energy stored into the inductor, thus increasing the maximum overvoltage.
- Adding capacitance (C) helps to reduce the potential of overvoltage in DC system. However, it also increases the inrush current and short-circuit current contribution such that capacitors should be added carefully.
- Initial capacitor voltage ($v_C(0)$) increases the maximum overvoltage available.
- Resistance (R) provides extra damping. Therefore, increasing the resistance reduces the maximum overvoltage.

Another phenomenon that needs to be considered is the trapped charge on capacitor. Let's use the circuit on the right of Figure 3.13. If the switch (*S*) is closed, according to section 3.2.2 an inrush current is expected. If the switch (*S*) is a circuit breaker and the inrush current reaches its instantaneous trip region for a time long enough, the circuit breaker will eventually trip. The worst trapped charge condition occurs if the circuit breaker trips at the first peak of the voltage waveform (Figure 3.15). It leaves a maximum trapped charge on the capacitor and any connected equipment on the bus will have to support the voltage condition unless the capacitor is discharged rapidly. Adding a parallel discharge resistance is mandatory for large capacitor to avoid dangerous long duration overvoltage conditions.

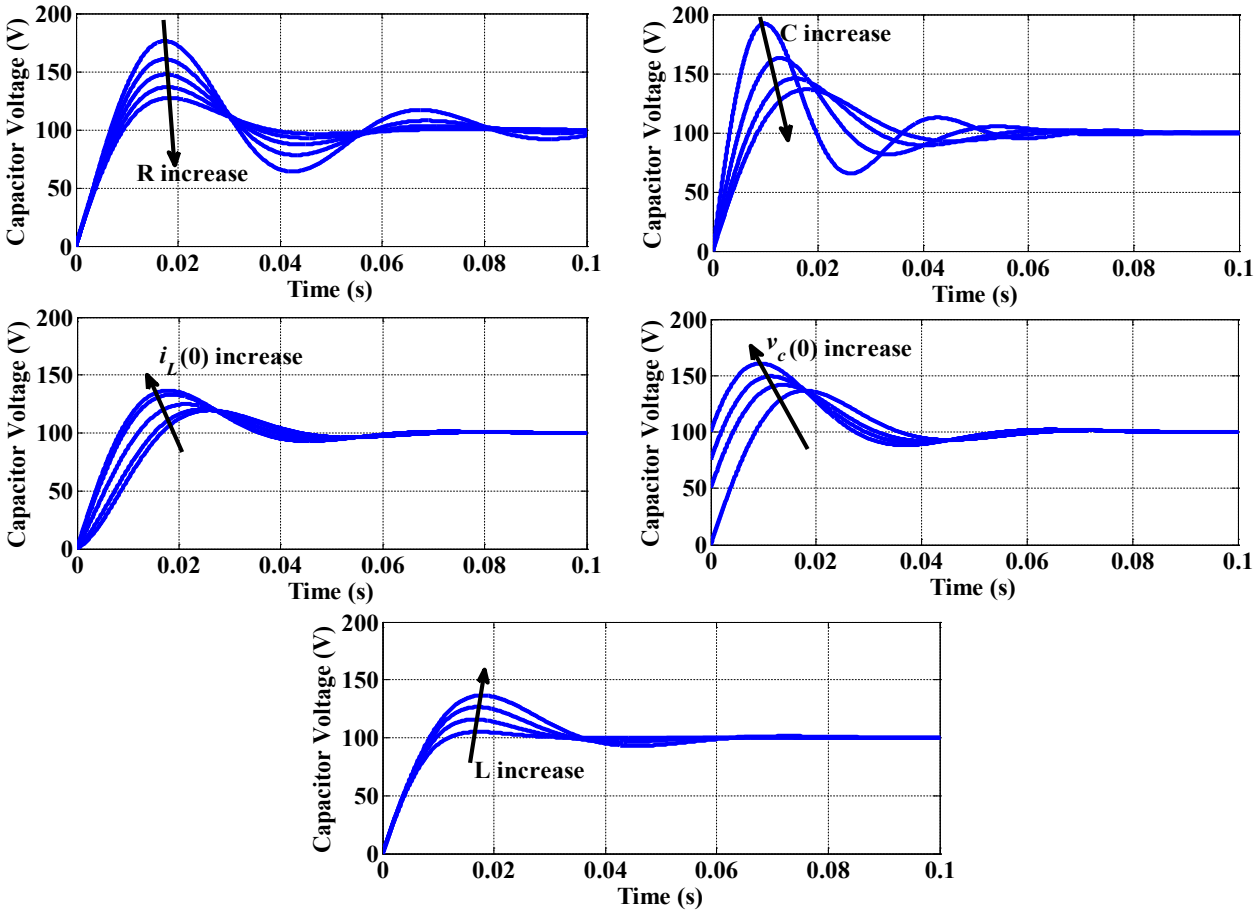

Figure 3.14 Circuit Parameters Impact on Transient Overvoltage

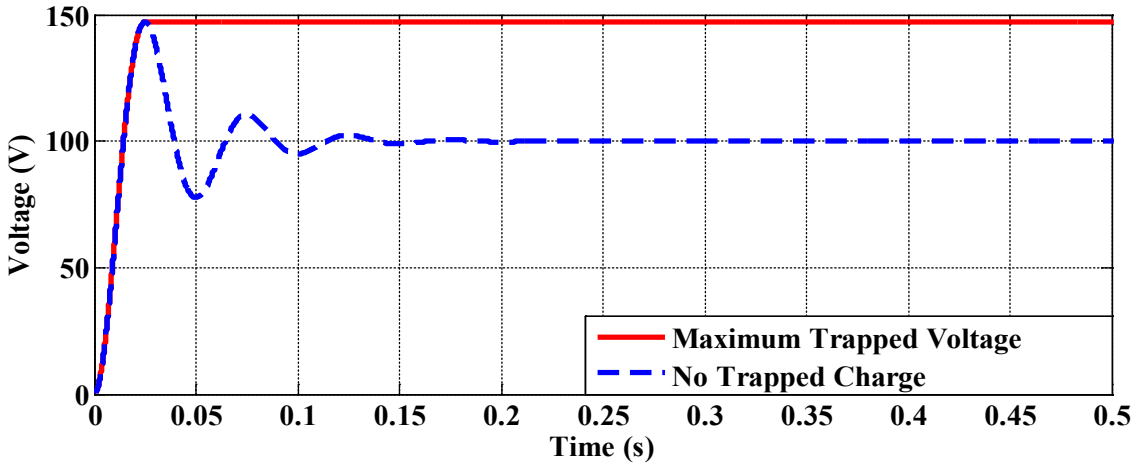

Figure 3.15 Trapped Charge when Opening at Peak Capacitor Overvoltage

3.3.2 Arc Voltage

The mathematical development in the previous section considers that the switching devices are ideal. However, DC protective devices are using sophisticated arc elongation mechanisms to break the fault current. The arcing phenomenon can be explained using a simple RL circuit. A DC voltage source (V_S) is applied to a RL load through a circuit breaker (Figure 3.16). It is well-known that the prospective fault current is given by (3.22).

In (3.22), the current can only be decreased to zero if V_S=0 or if R is infinite. However, V_S and R are both fixed by the system. Arc voltage is introduced to break the fault current. Once the protective device starts to open, an arc voltage (v_a) is created across the circuit breaker and the arcing current (i_a) starts to decrease and becomes smaller than the prospective fault current (i_f).

Current interruption in current-limiting devices can be explained using an arc voltage (v_a) following a ramp function starting at time t=0 [49][84]:

$$v_a(t) = Mt \tag{3.36}$$

with M being the slope (in V/s) of the arc voltage ramp.

By neglecting the initial voltage drop, the current that will flow into the circuit during the current breaking process can be approximated by [84]:

$$i_a(t) = \left(V_S / R + ML / R^2\right)\left(1 - e^{-Rt/L}\right) - Mt / R \tag{3.37}$$

Using (3.37), it can be shown in Figure 3.17 that the arcing current (i_a) is always smaller than the fault current (i_f) if the arc voltage (v_a) is applied at t=0. The maximum current (I_p) on the arcing current (i_a) is also smaller than the prospective current value (I_{SS}) on the fault current (i_f) and the current starts to decrease when v_a is greater than V_S-Ri_a. The rate-of-decrease of the arcing current (i_a) is highly dependent on the circuit inductance (L) and on the arc voltage value (v_a). According to Schneider Electric [42] the maximum arc voltage for a circuit breaker is optimum around 1.5 pu to 2.5 pu of the nominal network voltage.

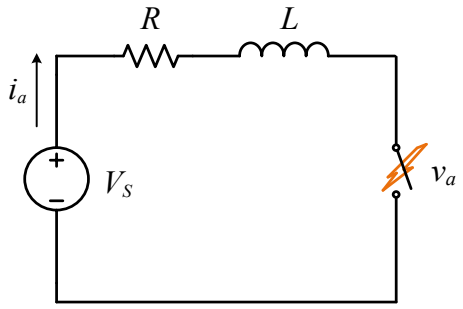

Figure 3.16 RL-Circuit for Arcing Voltage Study

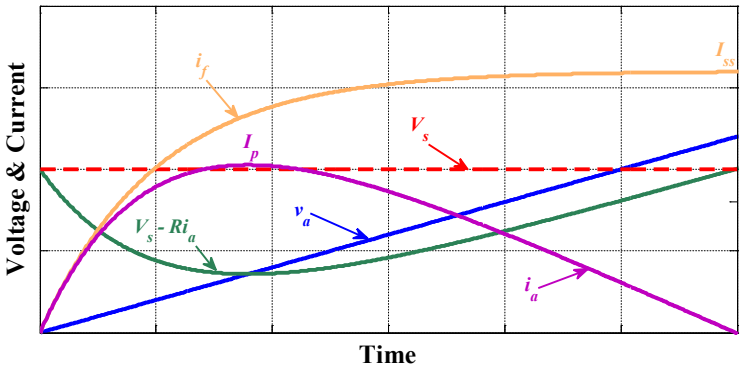

Figure 3.17 Current Breaking Process by Electric Arc

3.3.3 Transient Recovery Voltage (TRV)

In the previous section, it has been shown how the fault current can be interrupted by increasing the arc voltage. When the current is finally interrupted the presence of system capacitance combined with system inductance leads to transient recovery voltage (TRV) which can also create undesired overvoltage conditions. The transient recovery voltage occurs when the voltage between the circuit breaker poles is going back from the arc voltage (U_a) to the network voltage (U_r) (Figure 3.18).

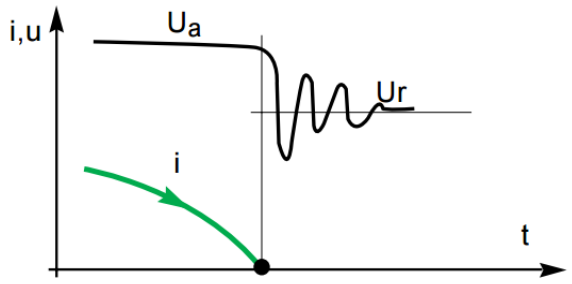

Figure 3.18 Final Current Interruption Transient Recovery Voltage (TRV) [42]

CHAPTER 4 MODEL DEVELOPMENT

4.1 Introduction

This chapter covers the development of the DC auxiliary system component models. Due to proprietary information related to Bombardier Transportation projects it is not possible to present the model development within the context of a particular project. Instead, three (3) generic rail vehicles (A-, B- and C-car) and a typical 5-car rapid transit train DC auxiliary system model are built in EMTP-RV based on past and recent projects data (Figure 4.1). Also, since each transit authority has their particular requirements it would become easily heavy to consider every configuration and every solution implemented. The generic train power system is presented in Appendix B.

In sections 4.2 to 4.6, individual models of the power system components are first developed and validated. In section 4.7, the models are used to develop three (3) vehicle models (A-, B- and C-car) and a complete train model is implemented by connecting the vehicles as in Figure 4.1.

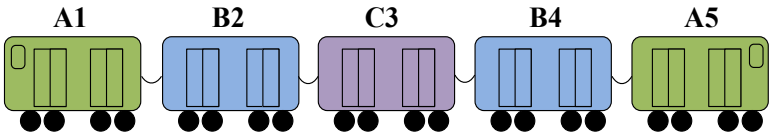

Figure 4.1 Train Configuration for Simulation Case Study

4.2 Sources of Power

4.2.1 Auxiliary Power Supply (APS)

4.2.1.1 Context

The Auxiliary Power Supply (APS) in railway vehicles is the main source of power on the auxiliary distribution under normal operating condition. It can be composed of five (5) types of converter: an Intermediate Voltage Power Supply (IVPS), a Low Voltage Power Supply (LVPS), a Battery Charger (BC) a Reverse Voltage Power Supply (RVPS), and one or multiple inverters (INV). The APS is directly supplied by the third rail or the catenary system and the converters are generally galvanically isolated. If present, the IVPS is used to supply an Intermediate Voltage Bus (IVB). If no inverter (INV) is implemented in the APS, distributed Variable Frequency

Drives (VFD) are connected on the IVB to supply the AC loads. The LVPS is used to power a Low Voltage Bus (LVB). The RVPS can be used to power the IVB from the backup batteries connected on the LVB under degraded conditions. A dedicated battery charger (BC) can also be used to charge the battery but in some cases the batteries are simply floating on the LVB and charged by the LVPS.

In the train power system of Appendix B, only the LVPS and the IVPS are present to simplify the architecture. The battery charger (BC) is excluded because it is never supplying the LVB simultaneously to the LVPS because of the isolation provided by the Battery Charger Switch (BCS). Since only DC systems are targeted and the system includes an IVB, there is no inverter in the APS. The RVPS is also excluded because decoupled simulation on the IVB and the LVB are performed. However, the RVPS should be integrated into the model in the future to study complete emergency scenarios in a system including a RVPS.

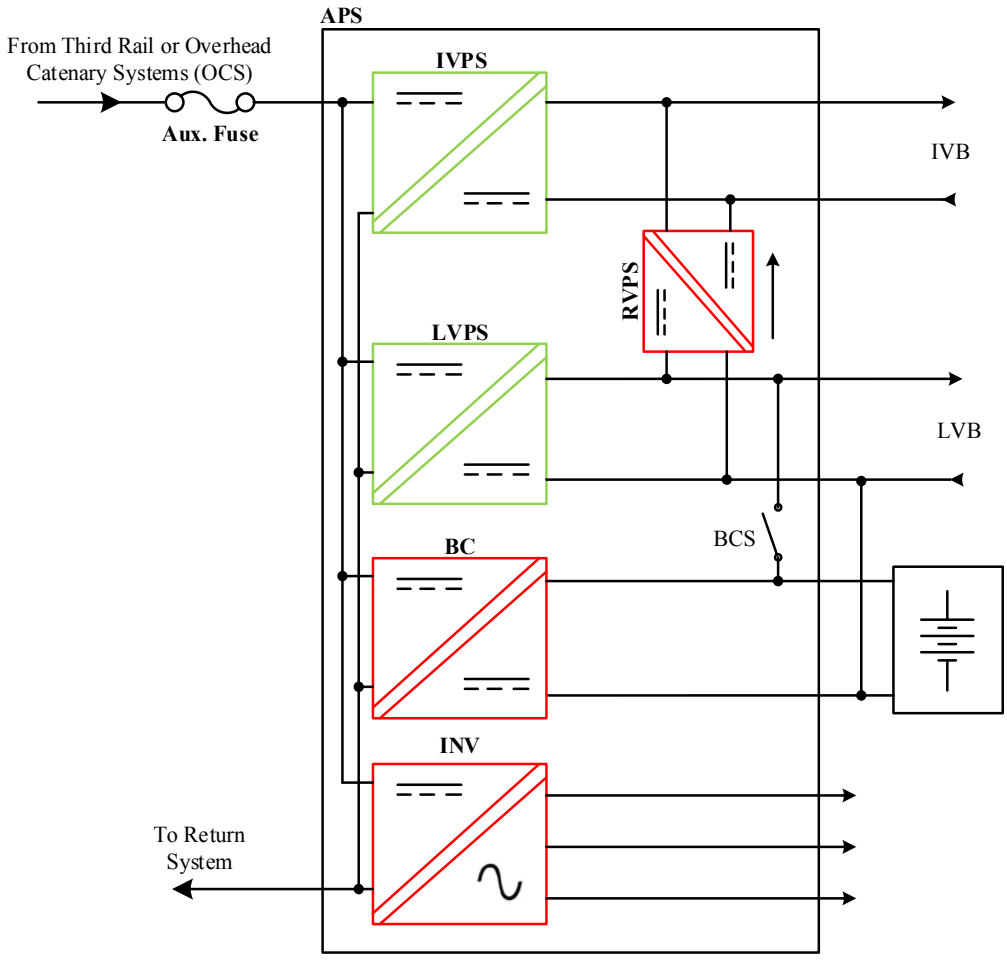

Figure 4.2 General Auxiliary Power Supply (APS) System

Selecting an appropriate converter model is important because there is a trade-off between computation time and accuracy [85]. Depending on the simulation objectives, there is two (2) major level of modeling for power electronics converter: *Switching Model* and *Average Model*. Switching model of converters are used when the objective is to study the device switching behavior. In this case, the surrounding network is generally reduced since the analysis of converter semiconductors is targeted. With average model, all the switching information is removed and the main objective is to study the dynamic response of the converter which results into computation speed orders of magnitude faster than with the switching model [86].

For the specific objectives of this project, it is sufficient to use an average model. It is also sufficient to model only the output stage since the converters are galvanically isolated from the primary power and the impacts of the converter on the primary power and vice and versa are not studied. However, it does not mean that it should not be integrated into the model in the future.

4.2.1.2 Model Description

Because of the complex and various topologies used and the lack of information on the control structure and on the dynamic behavior of the converters, a simple converter model is implemented based on the generally known information provided by the converter suppliers. The converter is modeled using a voltage source and a non-linear resistance to replicate its VI characteristic behind its output LC filter (L_F, C_F). The VI characteristic is flexible but fixed during the complete simulation duration.

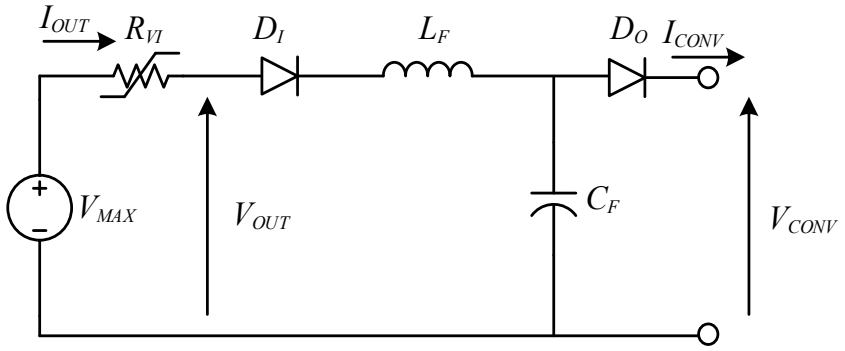

Figure 4.3 Converter Model Schematic Representation

From basic circuit equations, it can be defined that:

$$V_{OUT} = V_{MAX} - R_{VI} I_{OUT} \tag{4.1}$$

Thus,

$$R_{VI} = \frac{V_{MAX} - V_{OUT}}{I_{OUT}} \tag{4.2}$$

To reproduce the general VI characteristic (V_{OUT}, I_{OUT}) of Figure 3.9, it is necessary to define the equivalent resistance in each of the three zones:

$$R_{VI}^{1} = \frac{V_{MAX} - V_{NOM}}{I_{NOM}} = \frac{\Delta V_1}{I_1} \tag{4.3}$$

$$R_{VI}^{2} = \frac{V_{MAX} - V_{MIN}}{I_{LIM}} = \frac{\Delta V_2}{I_2} \tag{4.4}$$

$$R_{VI}^{3} = \frac{V_{MAX}}{I_{MAX}} = \frac{\Delta V_3}{I_3} \tag{4.5}$$

Using the non-linear resistance model in EMTP-RV, it requires simply to enter the couples (ΔV_x, I_x) to replicate the given converter VI characteristic. The internal diode (D_I) is used to block the reverse current from the filter capacitor (C_F) to the voltage source (V_{MAX}) and the output diode (D_O) is used to avoid reverse feed current into the converter. These diodes are generally present in real converter output stage. They are also modeled by non-linear resistance using their equivalent forward voltage and current characteristic from manufacturer's data.

4.2.1.3 Conclusion

This model can be used to reproduce the VI characteristic of typical converters used in railway vehicles. This model well represents the converter behavior under load variation from the network. Since the primary control is generally much slower than the filter time response, it is expected that the dynamic behavior of the converter model seen from its output terminals should not be very far from the real converter dynamic. The output filter and the output diodes are important to be modeled in order to take into account the filter effect during transients. Obviously, this model is not intended for converter internal analysis.

The two (2) main limitations of this model are the following. First, as already mentioned the model does not take into account the control structure of the converter and its dynamic is determined by its output filter characteristics combined with its VI characteristic. Secondly, the diodes D_I and D_O introduce a voltage drop which will not be compensated by the internal voltage

source and the VI output characteristic of the whole converter (V_{CONV}, I_{CONV},) is slightly shifted down from the internal converter VI output characteristic (V_{OUT}, I_{OUT}).

4.2.2 NiCd Battery

4.2.2.1 Context

There is four (4) major types of battery commonly used in transportation: Lead-Acid, Nickel-Cadmium (NiCd), Nickel-Metal-Hydride (NiMH), and Lithium-Ion (Li-Ion). Most auxiliary distribution in the railway industry use NiCd batteries. NiCd batteries are used as a good compromise between the cost ($/kWh) and the energy density (kWh/kg). NiCd batteries also provide a good cycle life range and safe operation but have a high self-discharge [87].

The model presented in this section is mainly developed for NiCd battery sizing and short-circuit analysis. In these cases, the battery voltage must be known over complete charge and discharge cycles.

For battery sizing, the battery voltage as a function of the battery state-of-charge (SOC) is important because the current of constant power and resistive loads depends on the load voltage which in turn has an impact on the battery discharge rate.

For short-circuit analysis, it has been observed experimentally that the battery can be discharged at many times its rated capacity which leads to a rapid discharge of the battery and therefore a decay of the voltage at the battery terminal over time. Short-circuit can last many seconds which can be enough for the battery internal cell voltage to have a non-negligible impact on the available fault current.

4.2.2.2 Model Description

The NiCd battery model developed in EMTP-RV is based on the NiCd battery model implemented in the SimPowerSystems toolbox of Matlab/Simulink, and presented in [88] and [89]. This model has been validated from SOC_0=100% to SOC=20% [88]. It has been modified in this master thesis to consider the loss of available capacity with the current magnitude (Peukert Effect) which is generally considered by railway battery manufacturers during the sizing process.

The NiCd battery model schematic representation is shown in Figure 4.4. The model symbols and the units used are provided in Table 4.1.

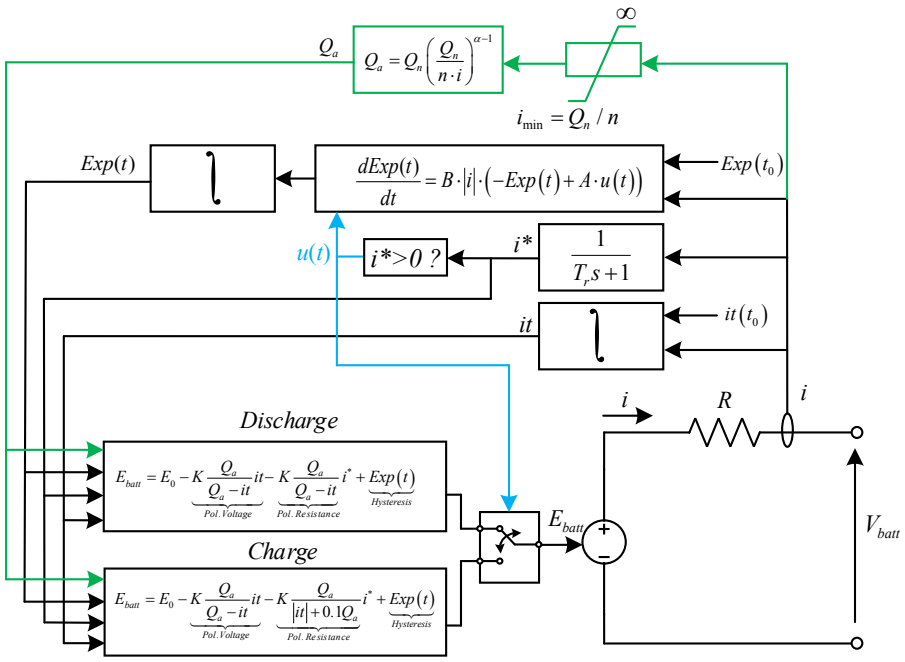

Figure 4.4 Battery Model Schematic Representation

Table 4.1: Battery Model Symbols and Units

Description	Symbol	Unit
Battery Terminal Voltage	V_{batt}	V
Battery Open-Circuit Voltage	E_{batt}	V
Battery Internal Resistance	R	Ω
Battery Current	i	A
Battery Constant Voltage	E_0	V
Polarization Constant	K	V/Ah
Available Battery Capacity	Q_a	Ah
Battery Nominal Capacity	Q_n	Ah
Actual Battery Charge	$it = \int idt$	Ah
Exponential Zone Amplitude	A	V
Inverse Exponential Zone Time-Constant	B	Ah^{-1}
Filtered Current	i^*	A
Exponential Zone Voltage	$Exp(t)$	V
Initial State-of-Charge	SOC_0	%
Filter Time-Constant	T_r	s
Discharge Time of the Battery to obtain Q_n	n	h
Peukert Coefficient	α	n/a
Battery Nominal Current	i_n	A

The NiCd battery model terminal voltage is given by:

$$V_{batt} = E_{batt} - R \cdot i \tag{4.6}$$

The internal voltage (E_{batt}) is given by (4.7) when the battery is discharging and it is given by (4.8) when the battery is charging:

$$E_{batt} = E_0 - \underbrace{K\frac{Q_a}{Q_a - it}it}_{Pol.Voltage} - \underbrace{K\frac{Q_a}{Q_a - it}i^*}_{Pol.Resistance} + \underbrace{Exp(t)}_{Hysteresis} \tag{4.7}$$

$$E_{batt} = E_0 - \underbrace{K\frac{Q_a}{Q_a - it}it}_{Pol.Voltage} - \underbrace{K\frac{Q_a}{|it| + 0.1Q_a}i^*}_{Pol.Resistance} + \underbrace{Exp(t)}_{Hysteresis} \tag{4.8}$$

The physical signification of the terms in (4.7) and (4.8) needs to be explained for a good understanding of the model.

The polarization voltage is implemented to model the non-linear variation of the battery open-circuit voltage as a function of the battery SOC.

The polarization resistance is used to model the non-linear variation of the battery internal voltage as a function of the battery current and the battery SOC. During the charge, NiCd battery also shows a particular behavior. When the battery is completely charged (it=0), the voltage starts to drop as a function of the current if the battery is continued to be charged. This phenomenon is represented by using the absolute value of the charge ($|it|$) in the polarization resistance term. Experimental results have also shown in [88] that the contribution of the polarization resistance is shifted by 10% of the capacity in typical NiCd battery, which is modeled by the $0.1Q_a$ term.

The hysteresis phenomenon between the charge and the discharge also leads to a potential on charge that is higher than the potential on discharge [90]. The hysteresis term ($Exp(t)$) is calculated by solving the following differential equation:

$$\frac{dExp(t)}{dt} = B \cdot |i| \cdot \left(-Exp(t) + A \cdot u(t)\right) \tag{4.9}$$

where:

u(t) is equal to 1 in charge mode (i^*< 0) and 0 in discharge mode (i^*> 0)

Initial conditions must be implemented in the model to initialize the model depending on the selected initial state-of-charge (SOC_0):

- The initial value of $Exp(t)$ is defined similarly to the SimPowerSystems model:

$$Exp(t_0) = Ae^{-B \cdot it(t_0)} \tag{4.10}$$

- The initial value of the charge integral (it) is calculated by:

$$it(t_0) = (1 - SOC_0 / 100) \cdot Q_a \tag{4.11}$$

Furthermore, the current filter transfer function is given by:

$$\frac{i^*(s)}{i(s)} = \frac{1}{T_r s + 1} \tag{4.12}$$

Moreover, Peukert's theory states that the available capacity of a battery decreases as the current discharge rate increases. In fact, manufacturers specify the nominal battery capacity (Q_n) at a given nominal discharge rate (i_n). The available capacity (Q_a) for a battery discharge current (i) can be approximated by [91]:

$$Q_a = Q_n \left(\frac{Q_n}{n \cdot i} \right)^{\alpha - 1} \tag{4.13}$$

Equation (4.13) is added into the model and is used to dynamically update the value of the available capacity (Q_a) at the discharge current rate (i).

In the model, when the current is under (4.14) or when the battery is charging, the prospective available charge capacity (Q_a) is equal to the nominal battery capacity (Q_n).

$$i_n = Q_n / n \tag{4.14}$$

The Peukert effect can be shown by plotting the impact of the discharge current (i) on the available battery capacity (Q_a) (Figure 4.5).

Finally, the battery state-of-charge (SOC) (in %) is calculated based on the nominal battery capacity (Q_n):

$$\text{SOC} = 100 \left(1 - \frac{it}{Q_n} \right) \tag{4.15}$$

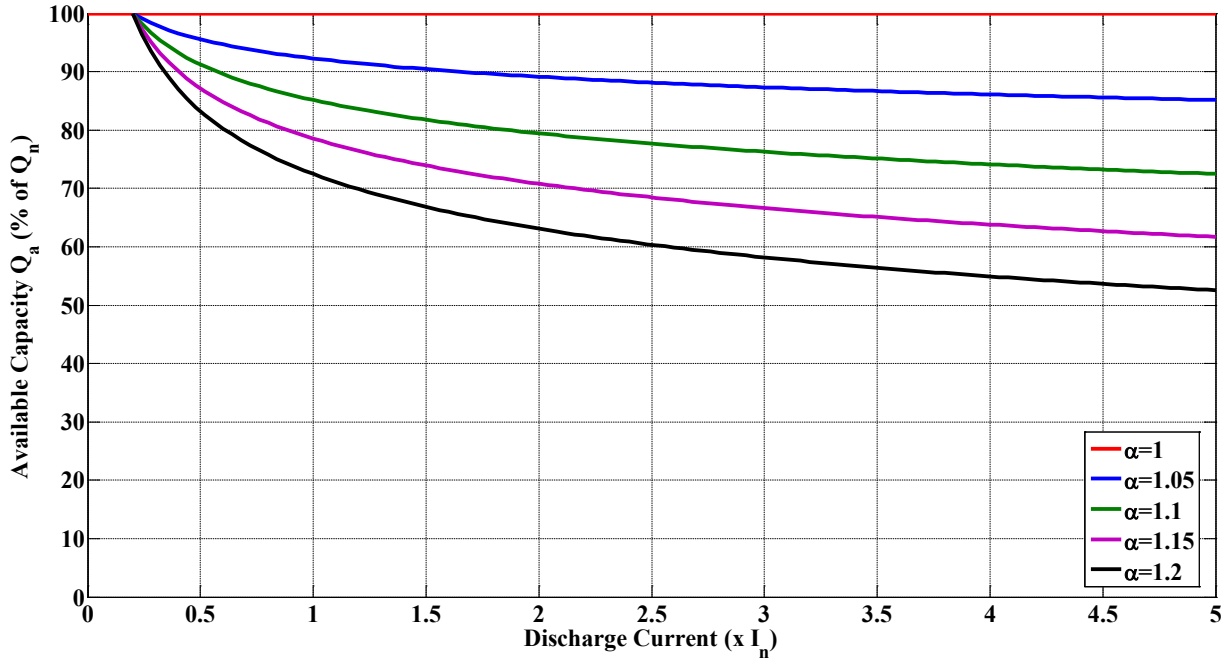

Figure 4.5 Theoretical Peukert Effect for Different Peukert Coefficient

4.2.2.3 Model Validation

The model developed in EMTP-RV needs the following input parameters: A, B, K, E_0, Q_n, α, n, R, SOC_0, and T_r.

A commonly used NiCd battery has been modeled as an example. The nominal voltage of each cell is 1.2 V. The parameters have been adjusted to best fit the manufacturer discharge curve and the experimental results. However, the battery parameter values are not provided here because of proprietary and confidential information related to the tested battery.

The manufacturer cell voltage for a discharge of 1 C at 20 Celsius is first compared to the cell voltage using the EMTP-RV battery simulation model (Figure 4.6). Figure 4.6 shows that over a depth of discharge of 80% the battery model leads to a large error in comparison to the manufacturer curve. However, recall here that the initial model has been only validated from SOC_0=100% to SOC=20% [88]. This error is acceptable in battery sizing because it is never assumed that the battery will have its complete available capacity during its entire service life. In fact, the battery capacity can be reduced by memory effect, operating temperature, and aging. This error is also acceptable in short-circuit protection analysis because battery should not be discharged completely before the protective devices clear the fault.

The cell voltage for a train emergency discharge field test is also compared to an averaged similar discharge test in EMTP-RV (Figure 4.7 and Figure 4.8). The minimum SOC of the battery is 26% at the end of the emergency condition. The battery model is finally validated during a short-circuit test (Figure 4.9, Figure 4.10, and Figure 4.11).

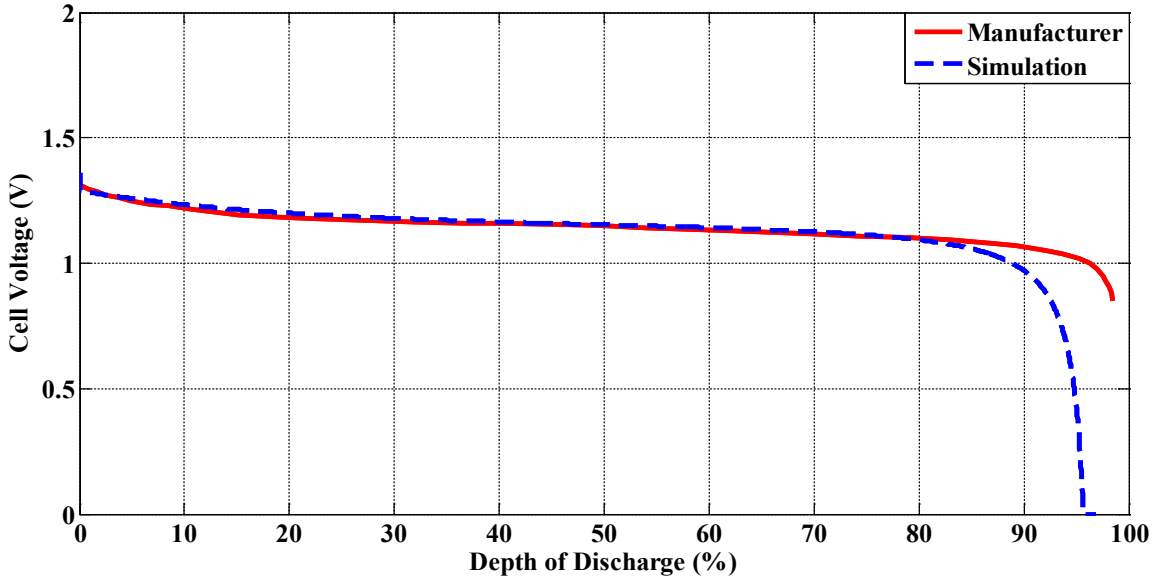

Figure 4.6 NiCd Battery Discharge Curve Validation

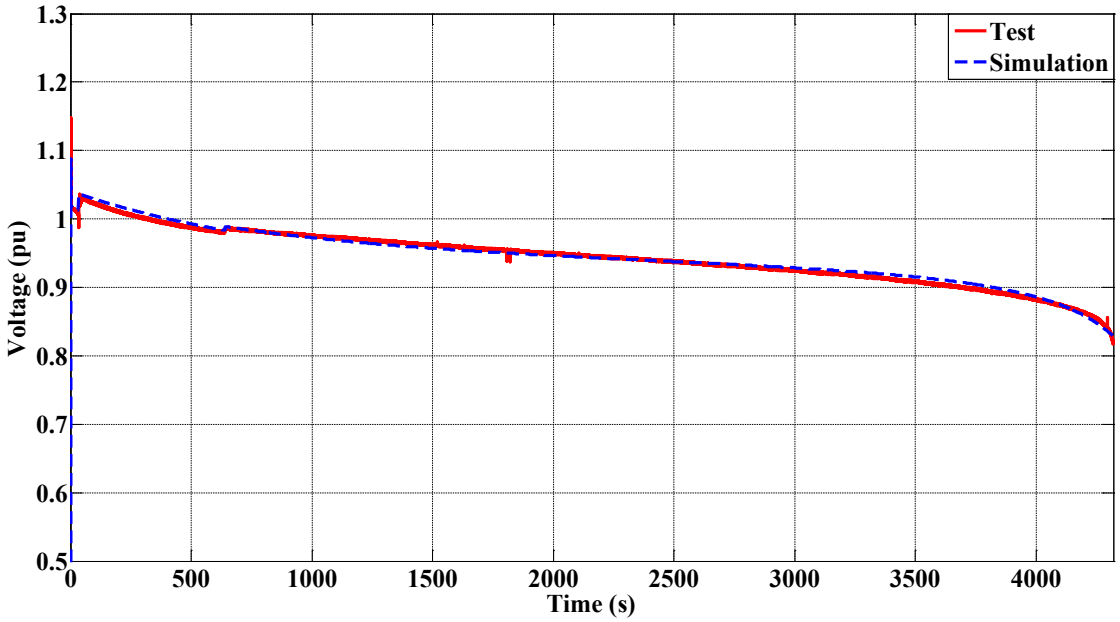

Figure 4.7 NiCd Battery Voltage Validation in Train Emergency Condition

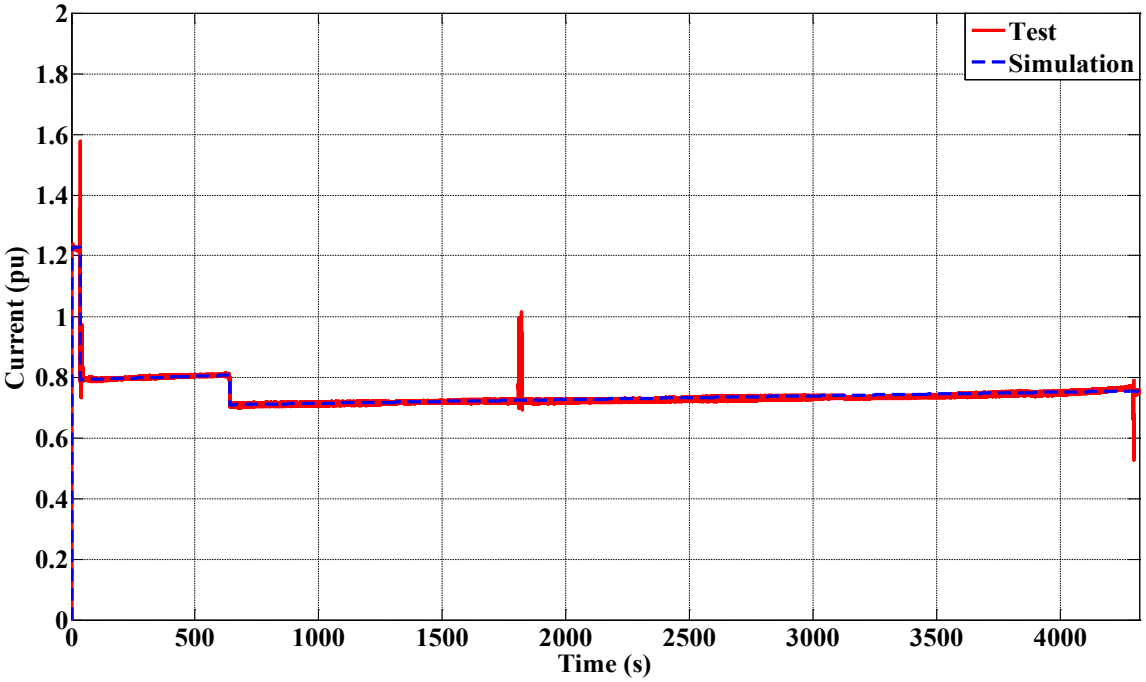

Figure 4.8 Train (Test) and Averaged (Simulation) Current in Emergency Condition

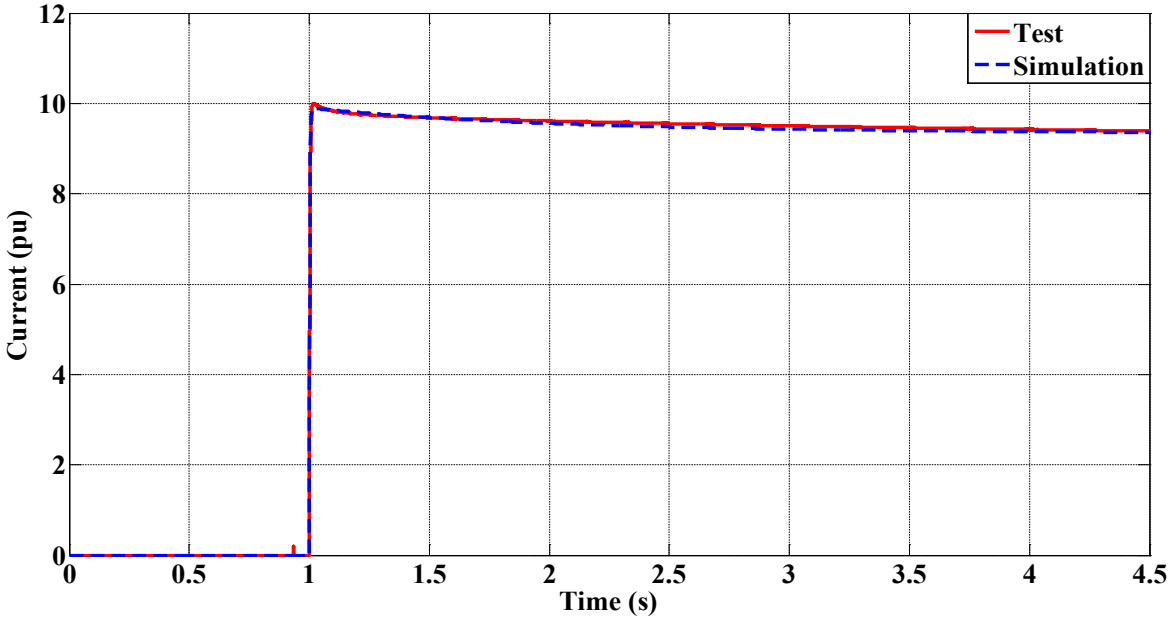

Figure 4.9 Battery Current in Short-Circuit Condition

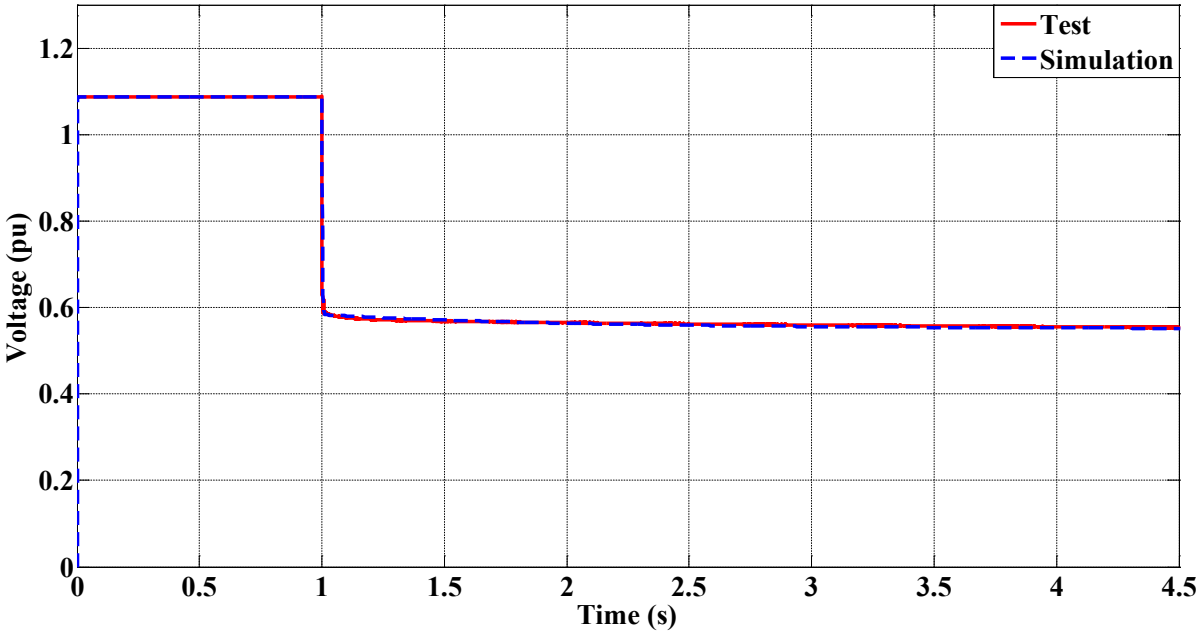

Figure 4.10 Battery Voltage in Short-Circuit Condition

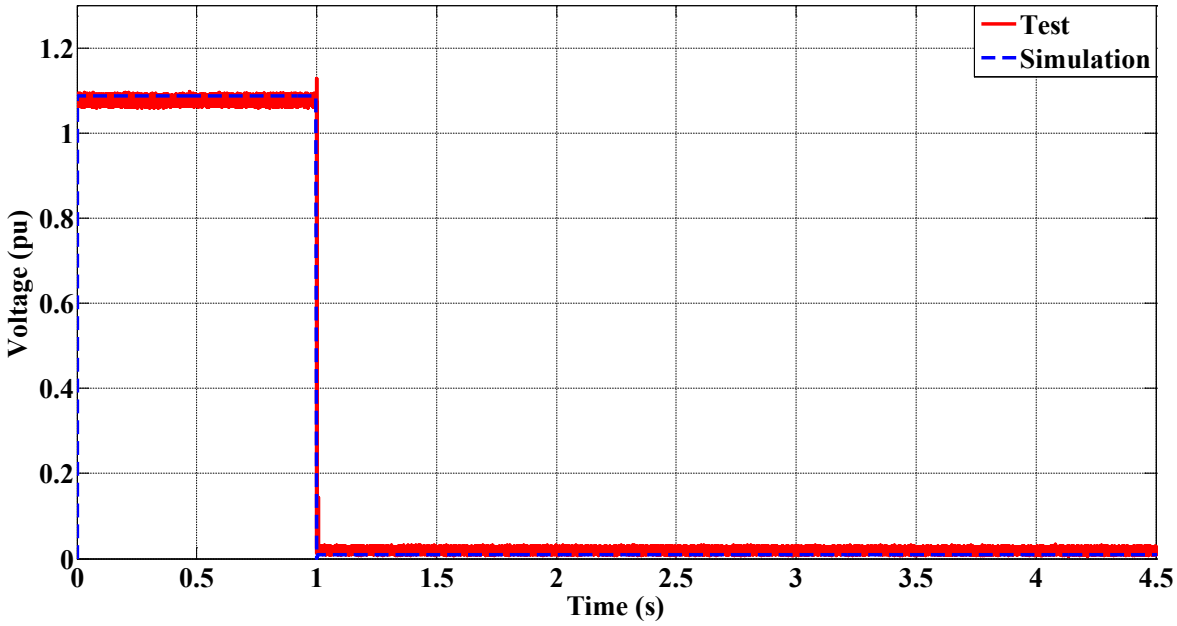

Figure 4.11 Fault Voltage in Short-Circuit Condition

4.2.2.4 Conclusion

It is finally possible to conclude that this model can be used to reproduce NiCd battery discharge characteristic from manufacturer for SOC_0=100% to SOC=20%. It is also expected good results with successive charge and discharge cycles as obtained in [88]. Experimental

validation in emergency condition (sizing) and under short-circuit condition have also shown that the battery model can be used to reproduce accurately these conditions. For all the validation, the parameters were identical. The Peukert coefficient (α=1.02) is also necessary to reproduce with more accuracy the experimental results (Figure 4.7 to Figure 4.11) even if it increases the difference between the simulation model and the manufacturer curve (Figure 4.6).

It should be kept in mind that the battery internal resistance is considered constant and the battery model does not consider the memory effect. Historically, the memory effect in NiCd battery referred to the loss of battery capacity as a function of previous discharge cycles. Modern NiCd battery technology suffers less from this phenomenon. However, battery may show another memory effect which is due to crystalline formation. Frequent exercise and reconditioning help to reduce the memory effect [92]. The memory effect can be simply modeled as a reduced initial state-of-charge (SOC_0) because of the very long time-constant involved (months).

Even if the temperature effect and the self-discharge of the battery are not modeled, when data are provided the battery parameters in the model can be adjusted to fit the manufacturer curves at different temperature. Self-discharge can be simply modeled as an equivalent parallel leakage resistance.

4.3 Wiring

4.3.1 Conductor

During short-circuit, battery sizing and inrush current field testing, it has been observed that conductor characteristics have an important impact on the simulation results validity because of the long cable length in typical trains. Typical length of railway vehicles is around 15 m to 25 m. Overall train length depends on the number of vehicles connected together. Train length between 120 m to 150 m are commonly seen during revenue service.

Modeling conductors can be done by defining the four (4) generally used transmission-line parameters: resistance, inductance, capacitance, and conductance. Lumped- or distributed-parameter models can also be used depending on the simulation objectives.

Because of the typical conductor arrangements, environmental conditions, voltage levels, conductor length involved and frequency range to be studied, a lumped-parameter model

neglecting the conductance and capacitance is used. Only the series resistance (R) and the series inductance (L) are considered (Figure 4.12). Each conductor is modeled separately because it allows to study different grounding scheme as well as the voltage level on both conductors.

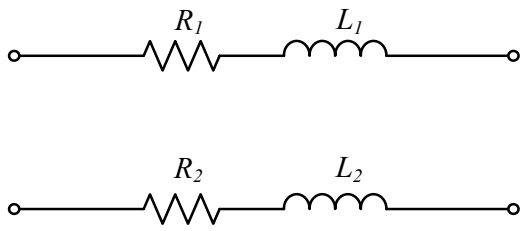

Figure 4.12 Two (2) Conductors Equivalent Model

4.3.1.1 Series Resistance

The conductor series resistance per unit length depends on the conductor material, operating temperature, cross-sectional area, stranding, and the frequency (skin effect).

Since the conductor resistance does not depend on the conductor arrangement, the DC resistance value from the manufacturer data at a given temperature is used. The skin-effect is neglected because no information are generally provided.

4.3.1.2 Series Inductance

The calculation of conductor series inductance per unit length requires to consider the conductor arrangement. To model each conductor following Figure 4.12, the internal inductance (L_{int}) and the equivalent external inductance (L_{ext}) of each conductor need to be determined.

The internal inductance per unit lenght due to the internal magnetic field can be approximated by [93]:

$$L'_{int} = \frac{\mu_o}{8\pi} (\text{H/m}) \tag{4.16}$$

where $\mu_o = 4\pi \cdot 10^{-7}$ (H/m). If available, the manufacturer internal inductance value should be used for more accuracy.

The external inductance is a function of the conductor physical arrangement. For two (2) parallel cylindrical conductors with one of the conductor used as the return, the total external inductance per unit length can be approximated by [93]:

$$L'_{ext} = 4 \cdot 10^{-7} \ln\left(\frac{D}{r_x}\right) (\text{H/m}) \tag{4.17}$$

Where D is the distance between the two (2) conductors and r_x is the geometric mean radius (GMR) of the conductor-x.

The inductance (L_x) of a single conductor-x of length (l_x) can be approximated by:

$$L_x = \left(L'_{int} + L'_{ext}/2\right) \cdot l_x = L'_x \cdot l_x \tag{4.18}$$

The conductor parameters used in the train model are presented in Table 4.2. The series resistance and the internal inductance are from manufacturer's data for 4/0 AWG cables. The external inductance is calculated for two (2) 4/0 AWG cables (r_x=7.4 mm) at a distance (D) of 55 mm.

Table 4.2: Conductor Parameters used in the Train Model

R'_x	L'_{int}	L'_{ext}
0.177 mΩ/m	0.239 μH/m	0.820 μH/m

4.3.2 Electrical Connection

The connection between two (2) conductors are typically made using a bolted-joint configuration (Figure 4.13). These connections are never electrically perfect. The crimping and the contact resistance between the two (2) lugs increase the resistance of the bolted-joint. According to [94] the resistance of a good electrical connection should be smaller than 50 μΩ.

Tests have been performed using a 400 A current injection at 60 Hz under the conditions of Table 4.3 to determine the total resistance of a bolted-joint connection between two (2) 4/0 AWG cables. By measuring the voltage drop between different points, the resistance of the different sections can be evaluated as well as the total resistance. The results are presented in Table 4.4. Comparing the connection resistances to the cable resistance per unit length, it should be realized that the connection resistance is negligible in railway vehicle power system studies if the number of connection is small and the cable length is large enough. However, if the studied zone is very small with multiple connections, the connection resistances should not be neglected. At this point, engineering judgment is important.

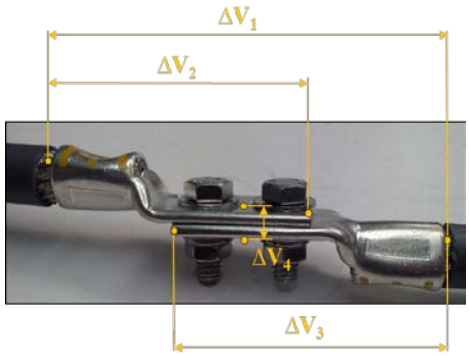

Figure 4.13 Bolted-joint Connection Example

Table 4.3: Bolted-joint Connection Test Conditions

Cables	Lugs	Bolt	Torque
4/0 AWG	4/0 AWG 2 holes 3/8 in. dia. 1in. between holes	3/8-16 in. F593C Stainless Steel	240 lbs/ft

Table 4.4: Bolted-joint Connection Test Results

$R_1=R_{tot}$	R_2	R_3	R_4
45 μΩ	15 μΩ	20 μΩ	10 μΩ

4.4 Overcurrent Protective Devices

4.4.1 Circuit Breaker

4.4.1.1 Context

Circuit breaker generally used in low voltage DC distribution of railway vehicles are Molded-Case Circuit Breaker (MCCB) - type equipped with thermomagnetic or magnetic trip units. The MCCB used are generally non-current-limiting (or zero-crossing type). The MCCB used are typically qualified for both AC and DC application. Manufacturer's specification must be well understood to ensure their correct use in DC conditions which may be different from the AC specifications.

The thermomagnetic trip unit consist of two (2) tripping regions. In the thermal region the release delay varies inversely with the current flowing through the circuit breaker. This trip unit

is intended for protection against continuous overload while allowing momentary current surges. In the magnetic region the release delay of the circuit breaker is almost constant when the current flowing through the circuit breaker is beyond the instantaneous trip value. This trip unit is intended for protection against short circuit. The thermal unit reacts to the current thermal effect (RMS) while the magnetic trip is current sensitive [95][96]. Both trip units act independently and are mechanically coupled to the trip mechanism to open the circuit breaker contacts. It is also well-known that the level of thermal energy varies as a square of the RMS current while the magnetic forces vary as a square of the instantaneous current.

Once the trip mechanism energy is high enough, the breaker contacts start to separate to interrupt the fault current. Once the contacts are slightly separated an arc is formed in the air between the contacts. The arc is moved into the arc chute where it is segmented into small arcs. There is two (2) types of circuit breaker depending on how they manage the arc: zero-crossing circuit breaker (or non-current-limiting) and current-limiting circuit breaker. Current-limiting circuit breakers are faster to extinguish the arc than the zero-crossing circuit breakers. They break the fault current within the first half of the AC cycle. The speed of extinction of the electric arc in current-limiting circuit breakers leads to a significant lower peak let-through current (I_p) and let-through energy (I^2t) [47][96]. It should be mentioned that for operation in times less than one (1) AC cycle, the thermal effect is greatly affected by the transient waveform of the current [97].

Three (3) important curves are generally provided by the protective devices manufacturers [95]: Time-Current Curve (TCC), Peak let-through current (I_p), and Let-through energy (I^2t). These curves can be used to assess the coordination and the performance of the circuit breaker but also to develop models based on these information that are easy to use in the future. The peak let-through current (I_p) and the let-through energy (I^2t) are given only for current-limiting devices.

Since the MCCB commonly used in railway vehicle auxiliary systems are non-current-limiting, the model presented in this section is based on this important assumption. However, the propulsion High Speed Circuit Breaker (HSCB) is a current-limiting device. Modeling a HSCB is different from what it will be presented in this section. The development of a HSCB model for transient overcurrent protection analysis has been covered in [7].

4.4.1.2 Model Description

A non-current-limiting circuit breaker with thermomagnetic trip model is developed. The model is divided into two (2) sections: the *detection* block and the *opening* block. The circuit breaker model symbols and units are tabulated in Table 4.5.

Table 4.5: Circuit Breaker Model Symbols and Units

Model	Description	Symbol	Unit
Detection	Measured Current	i_{mes}	A
	Trip Time (*T*=Thermal, *I*=Magnetic)	t_{trip}	s
	Pick-up Current	I_{pickup}	A
	Travel Time (*T*=Thermal, *I*=Magnetic)	t_{travel}	pu
	Simulation Time	t	s
	Thermal Time-Constant	T_{ther}	s
Opening	Arc Voltage	v_a	V
	Schwarz Equivalent Voltage Gradient	e_{eq}	V/cm
	Contact Resistance	R_c	mΩ
	Anode-Cathode Voltage Drop	U_0	V
	Arc Length	l_{eq}	cm
	Schwarz Arc Conductance	G_s	Ω^{-1}
	Arc Length Equation Parameters	c	n/a
		d	n/a
	Schwarz Arc Model Parameters	P_0	n/a
		a	n/a
		b	n/a
		τ_s	n/a

Detection

The detection circuit model is implemented to reproduce the thermomagnetic trip feature of the circuit breaker as in Figure 4.14. The detection circuit model is shown in Figure 4.15. Since the thermal trip and the magnetic trip act independently, they are also modeled separately. The TCC provided by manufacturers is typically giving the total clearing time. Since the detection

time is typically much higher than the arcing time, the total clearing time TCC is used to determine the detection time (or trip time). Non-current-limiting circuit breakers are also likely to break the fault current in steady-state especially if the fault path inductance is low. Therefore, it is not necessary to calculate the RMS value of the measured DC transient current as in [7].

In the model, the measured current (i_{mes}) flowing through the circuit breaker is compared directly to the circuit breaker TCC to define the trip time (t_{trip}). The trip time is infinite if the measured current is under the pick-up current (I_{pickup}). In the thermal region, the trip time is a function of the simulation time (t) and the measured current (i_{mes}). In the magnetic (or instantaneous) region, the trip time is constant and equal to T_{inst}. Once the trip time is known, the travel (t_{travel}) which represents the amount of thermal or magnetic energy transferred to the trip units is calculated dynamically using the general equation:

$$t_{travel} = \int \left(1 / t_{trip}(t)\right) dt \tag{4.19}$$

In the thermal region, if the current falls under the pickup current (I_{pickup}) the travel should not be reset to zero since the thermal time-constant of the fusing element needs to be taken in account. Assuming that the maximum time for the fusing element to cool down is given by T_{ther}, the thermal travel decreases following:

$$t^{T}_{travel} = \int \left(-1 / T_{ther}\right) dt \tag{4.20}$$

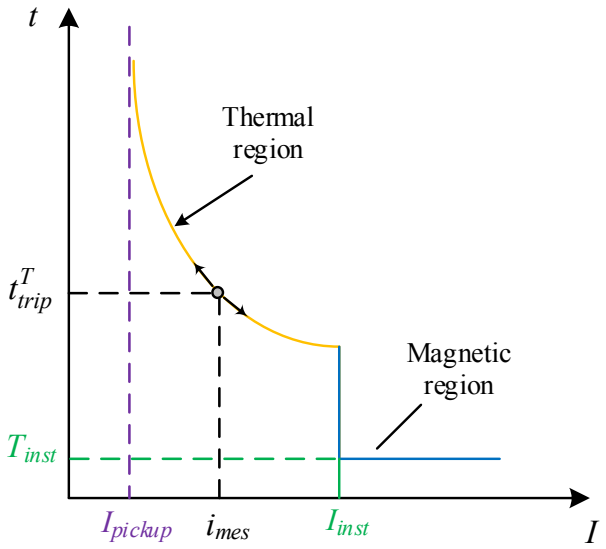

Figure 4.14 Thermomagnetic Circuit Breaker Time-Current Curve Model

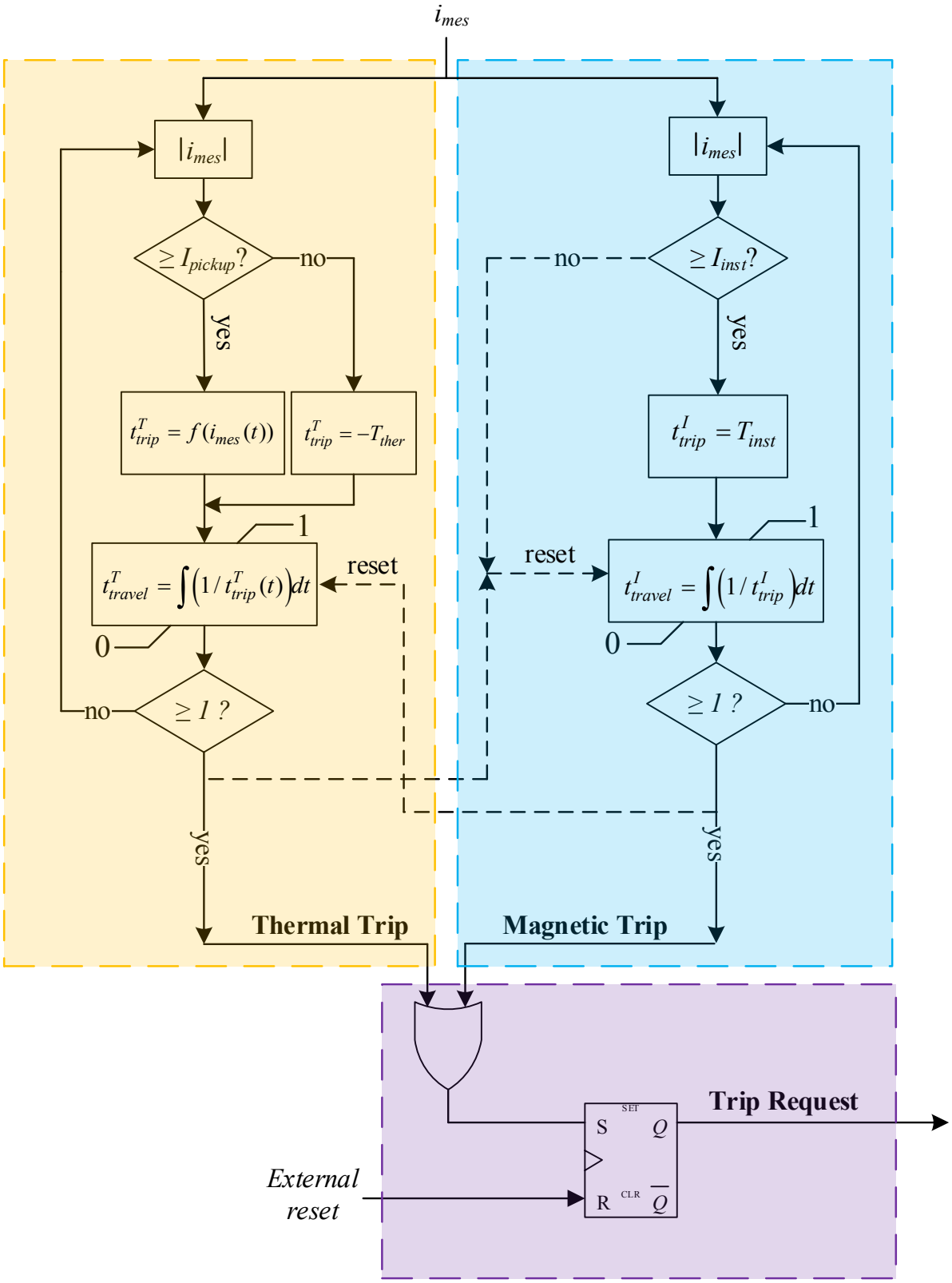

Figure 4.15 Thermomagnetic Circuit Breaker Detection Model Diagram

In the magnetic region, if the current falls under the instantaneous current, the magnetic travel is automatically reset to zero since magnetic time-constant does not really exist.

To provide additional simulation flexibility, the two (2) detection modules are mutually reset when one of the trip modules reaches the release time; if a thermal trip occurs, the magnetic trip module is reset and if a magnetic trip occurs, the thermal trip module is reset. A RS flip-flop is added to provide a latching effect on the trip signal. An external reset is also implemented to add simulation flexibility because some circuit breakers are equipped with a built-in shunt trip coil.

Opening

When the travel time (t_{travel}) reaches one (1) in (4.19), it means that the total thermal or magnetic energy is achieved and a trip signal request is sent to the circuit breaker opening model.

Circuit breaker opening (or arcing) phase is modeled as an equivalent arc voltage (v_a) depending on the arc characteristics as presented in [98]. This model has been used to reproduce the arc voltages of a three (3) pole current-limiting circuit breaker in a three-phase AC network [98]. Since DC circuit breakers do not wait current zero-crossing to interrupt the fault, it is expected that they break the fault current in a similar way to AC current-limiting devices even if they are not marked as current-limiting for DC application. The simplified model presented in [98] has been slightly modified and implemented in EMTP-RV to model MCCB used in DC systems during their opening phase. This model is obviously bi-directional because it has been developed at first for AC. Therefore, the current flow can be interrupted in both direction. The arc voltage (v_a) is calculated by solving (4.21) to (4.24) [98]:

$$v_a = R_c i + sign(i) U_0 + e_{eq} l_{eq} \tag{4.21}$$

The value of the equivalent voltage gradient (e_{eq}) is calculated using the Schwarz arc conductance (G_s) model [98]:

$$\frac{1}{G_s}\frac{dG_s}{dt} = \frac{1}{\tau_s G_s^a}\left(\frac{e_{eq} i}{P_0 G_s^b} - 1\right) \tag{4.22}$$

$$e_{eq} = \frac{i}{G_s} \tag{4.23}$$

The arc length (l_{eq}) is calculated by solving the following differential equation [98]:

$$\frac{dl_{eq}}{dt} = ci^2 + d|i| \tag{4.24}$$

Even if the simplified version presented in [98] considers a constant arc length ($l_{eq} = l_s$), it is proposed here to calculate the arc length using the complete version defined by (4.24) with c and d parameters being here constant. The arc voltage (v_a) is calculated in EMTP-RV using the control functions and the result is used to command a controlled voltage source model.

4.4.1.3 Model Validation

The model is validated for two (2) different scenarios. A fault with a current value inside the thermal region is first done to validate the detection model in the thermal region (case A). Then, a fault in the magnetic region is performed to verify the model in the magnetic region (case B).

The circuit breaker TCC implemented is a ABB Tmax T5 400A with minimum trip settings. The "hot" curve is used to reduce the simulation time but the "cold" curve is also implemented. The circuit breaker TCC implemented in EMTP-RV is shown in Figure 4.16 [99]. The nominal instantaneous trip setting (I_{inst}) is considered to be 2200 A because of the pole connection in DC application (ref. [100], Table 14, 1st Connection Modality). A tolerance of ±20% can also be considered on the instantaneous trip [100]. The main simulation parameters are also provided in Table 4.6. In both cases the fault is applied at t=0 and the simulation time step Δt is equal to 2 µs.

For the first case (Case A), the steady-state fault current (I_{SS}) is 1100 A and the fault circuit time-constant is 0.25 ms. According to the TCC of Figure 4.16, the detection time should be equal to 1.8 s and according to section 3.3.2 the peak arc overvoltage should be between 1.5 pu to 2.5 pu. The thermal travel should also slowly decreases after the fault is cleared following the thermal time-constant. The simulation results in Figure 4.17 show that the circuit breaker simulation model does meet the expected results.

Table 4.6: Circuit Breaker Model Validation Parameters

Model	Description	Symbol	Value
Detection	Pickup Current Setting	I_{pickup}	280 (A)
	Instantaneous Current Setting	I_{inst}	2200 (A)
	Thermal Time-Constant	T_{ther}	100 (s)
	Instantaneous Delay	T_{inst}	16 (ms)
Opening	Contact Resistance	R_c	0.12 (mΩ)
	Anode-Cathode Voltage Drop	U_0	20 (V)
	Arc Length Equation Parameters	c	Case A: 0.01 Case B : 0.003
		d	0.05
	Schwarz Arc Model Parameters	P_0	1000
		a	0.06
		b	1.3
		τ_s	0.00001

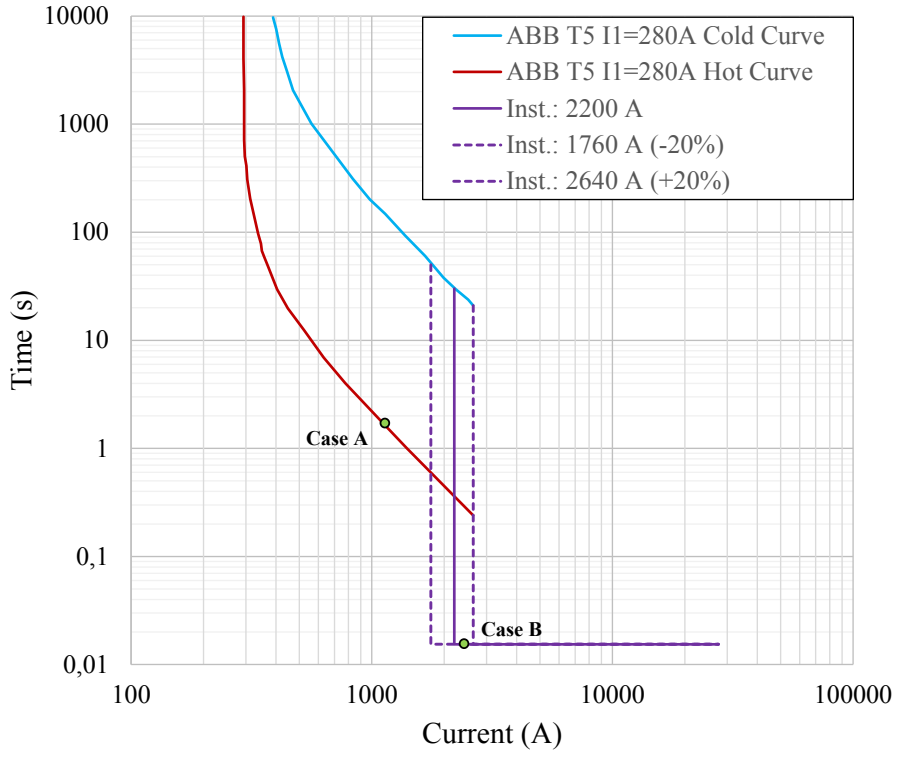

Figure 4.16 ABB Tmax T5 400A Thermomagnetic Circuit Breaker Time-Current Curve

For the second simulation (Case B), the steady-state fault current (I_{SS}) is now 2300 A and the fault circuit time-constant is 0.5 ms. According to the TCC of Figure 4.16 and Table 4.6 the detection time should be equal to 16 ms in the instantaneous region. The simulation results in Figure 4.18 show that the simulation model does also meet the expected results in the magnetic region. The detection time is slightly higher than 16 ms because the travel is calculated starting from the instant at which the current goes beyond the instantaneous current setting. The simulation results also show that there is no magnetic travel time-constant, which means that the travel is reset to zero once the current falls under the instantaneous current setting. The parameter *c* in the circuit breaker opening block has been adjusted to obtain a maximum arc voltage between 1.5 pu to 2.5 pu. The main reason is that the fault conditions are very different from case A.

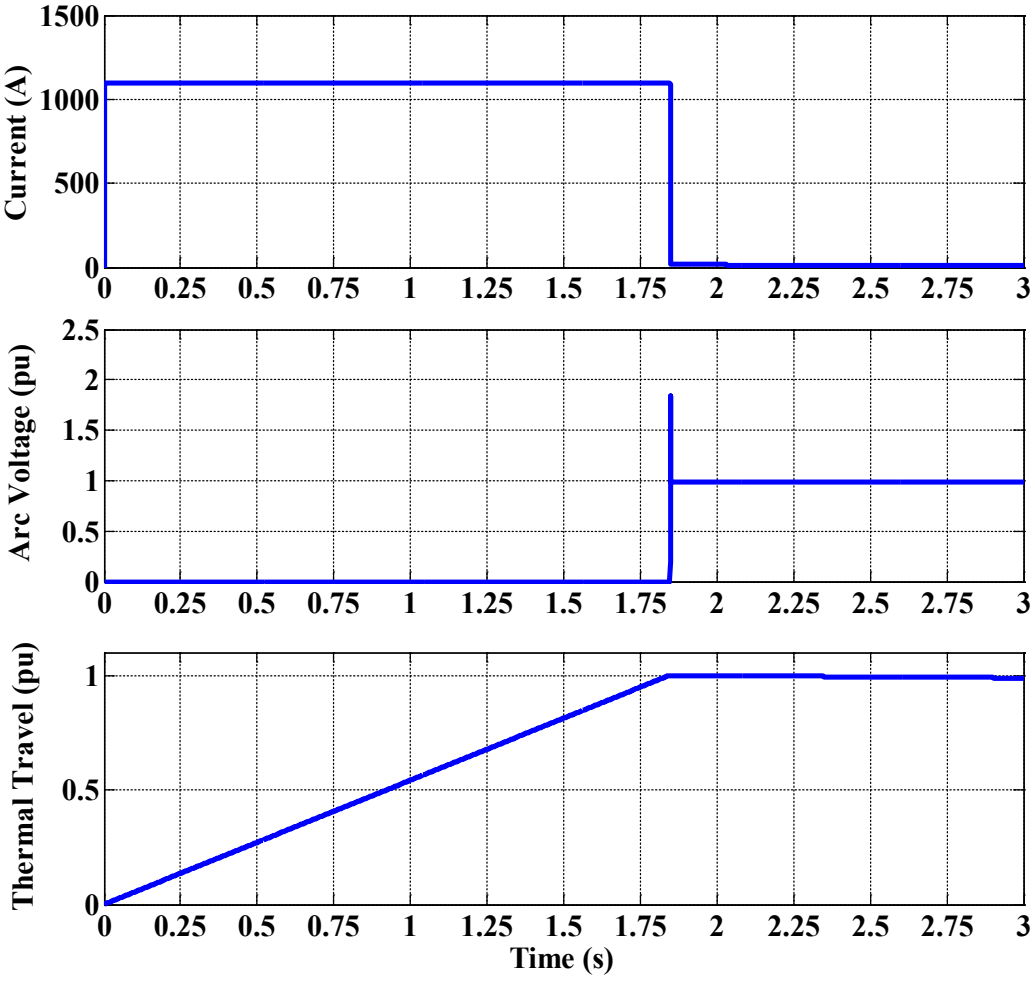

Figure 4.17 Case A: Validation of the Circuit Breaker Model in the Thermal Region

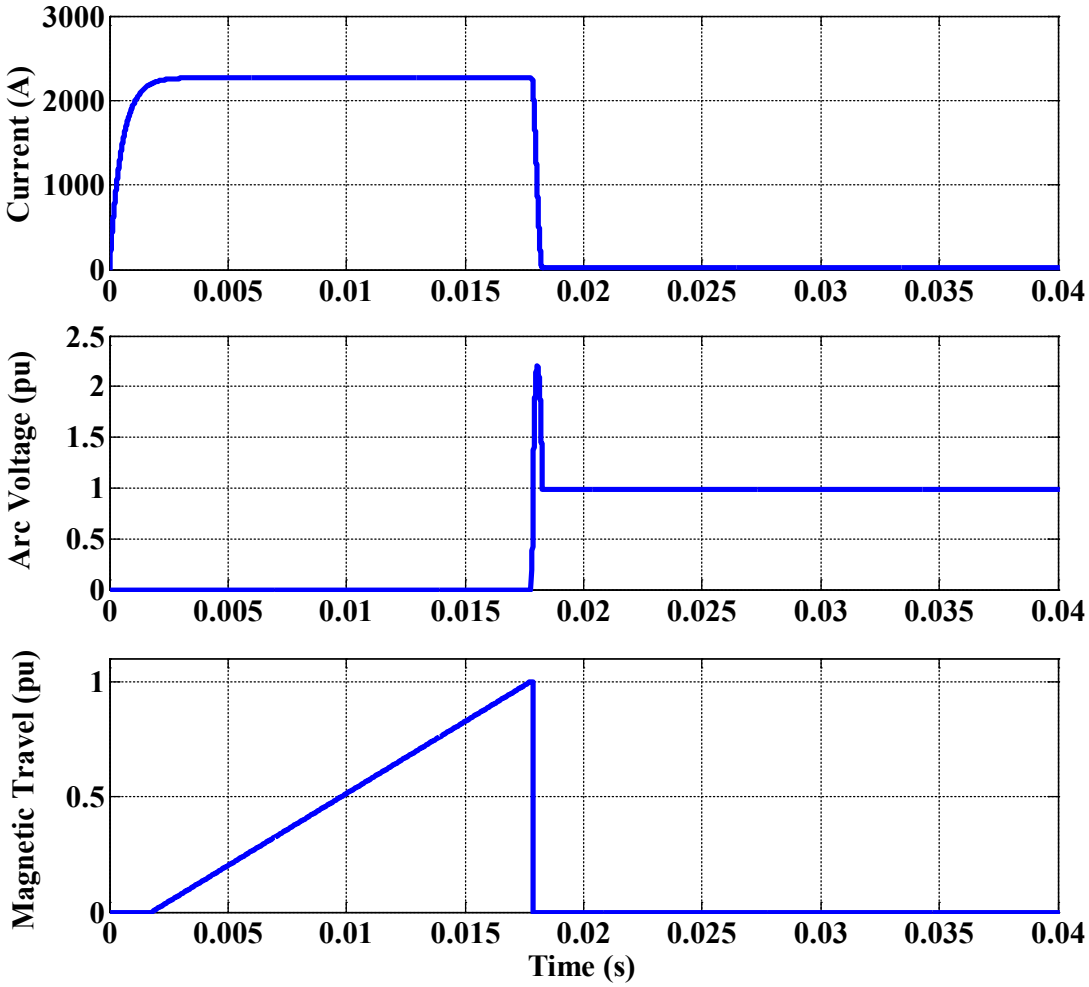

Figure 4.18 Case B: Validation of the Circuit Breaker Model in the Magnetic Region

4.4.1.4 Conclusion

The circuit breaker simulation model developed in this section is complete because it considers both the detection and opening mechanisms.

Modeling the detection mechanism is important because it allows to validate if the circuit breaker will detect the fault current or not based on the manufacturer's data and the fault current obtained by simulation under different scenarios. The available settings, the pole connections of the circuit breaker as well as the tolerance on the thermal and magnetic regions should be taken into account when entering the TCC data into the model [95][100] as seen in Figure 4.16. The detection accuracy highly depends on the number of points taken on the manufacturer TCC. The detection model is valid for slow transient and steady-state fault current.

Modeling the opening mechanism is also important because it reduces the numerical discontinuities associated with the opening of an ideal switch in a DC system, thus reducing the transient overvoltage to realistic values. The arc model is well-suited for fault current analysis and to reproduce approximately the arc voltage. It is not intended to study transient overvoltage at the opening of a circuit breaker. It is also important to mention that the circuit breaker leaves a small but negligible leakage current once it is opened.

4.4.2 Fuse

4.4.2.1 Context

Fuses are also used to protect the auxiliary distribution and the equipment in railway vehicles. Fuses used in railway vehicles auxiliary distribution are typically non-current-limiting such that they are likely to break the current during the final steady-state. The model developed in [7] for the collector shoe fuses on the primary power can be used with slight modification. By assuming that the fuses are non-current-limiting and low circuit inductance, the RMS calculation of the transient current is not necessary similarly to the circuit breaker model. The main problem with the calculation of RMS value of transient DC current is the selection of the integration window. The RMS calculation module must be initiated at the beginning of the fault to be studied and reset based on a predetermined condition. This is not user-friendly and wrong results may be obtained if the RMS calculation module is not used within its limits.

4.4.2.2 Model Description

The non-current-limiting fuse breaking process is shown in Figure 4.19 (a). Fuses are typically defined by two (2) TCC [44]. The melting TCC represents the minimum thermal energy required to melt the fuse element. The melting time (T_m) is the time at which the arc is initiated (also called pre-arcing time). The clearing TCC represents the total energy passed through the fuse as it clears the fault during its arcing time (T_a). The clearing time (T_c) is the time at which the fault is completely interrupted. The TCCs are generally given for AC RMS current values. For non-current-limiting fuse it is acceptable to consider that the fuse will break the current during the final steady-state such that the AC RMS curves can be used in DC.

The fuse melting time can be defined similarly to the circuit breaker detection time in section 4.4.1. The dynamic evaluation of the fuse melting time (t_{mf}) is done by comparing the fault current with the fuse AC RMS melting TCC implemented in EMTP-RV (Figure 4.19 (b)). The total melting time (T_m) is the time required for Tr_m to reach one (1) using:

$$Tr_m = \int \left(1 / t_{mf}(t)\right) dt \tag{4.25}$$

with Tr_m being an indicator of the fuse pre-arcing energy. In the simulation model, the fuse starts to melt once Tr_m reaches one (1).

Fuse melting process is modeled in [50] as a non-linear increasing resistance. The fuse melting process is then modeled as a non-linear increasing resistance following Figure 4.19 (c) using the controlled resistance model in EMTP-RV.

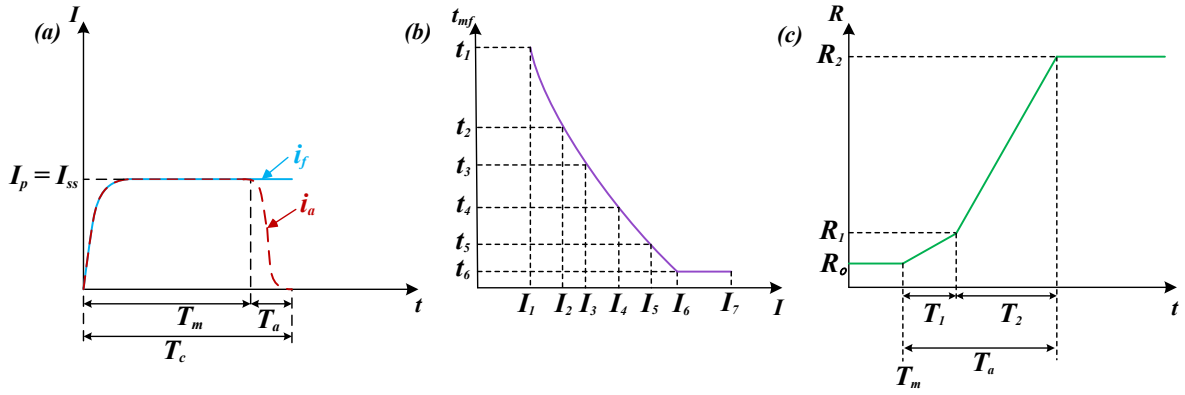

Figure 4.19 Non-Current-Limiting Fuse Model

4.4.2.3 Model Validation

The model has been validated using three (3) TCCs from typical fuse data used in the rapid transit industry [101]. The fuses are all rated 440 VDC. The current rating of the fuses are 100 A, 125 A, and 160 A. The fuse melting TCCs used for model validation are shown in Figure 4.20. The fuse non-linear resistance parameters are provided in Table 4.7.

For each case, a 600 A fault with a time-constant of 1 ms is applied at t=1 s. The simulation time step Δt is equal to 50 µs. According to Figure 4.20, the 100 A, 125 A, and 160 A fuses are expected to approximatively melt in 0.5 s, 1.1 s, and 7 s respectively. The results show that the fuse model does meet the expectation in both the detecting and arcing regions (Figure 4.21 and Figure 4.22).

4.4.2.4 Conclusion

Similarly to the circuit breaker model, it can be concluded the fuse simulation model developed in this section is also complete because it considers both the detection and arcing mechanisms. Analogous conclusion can be made regarding the importance of modeling both the detection and the arcing mechanisms. Again, this model is not intended to study transient overvoltage during fuse opening.

The overall precision of the model still rely on the number of points taken on the melting TCC and on the number of segments used to model the fuse arcing characteristic. At this point, field testing should be performed to evaluate the arcing behavior of different fuse types under different conditions. These information are generally not given by the fuse manufacturers because they depend on many factors.

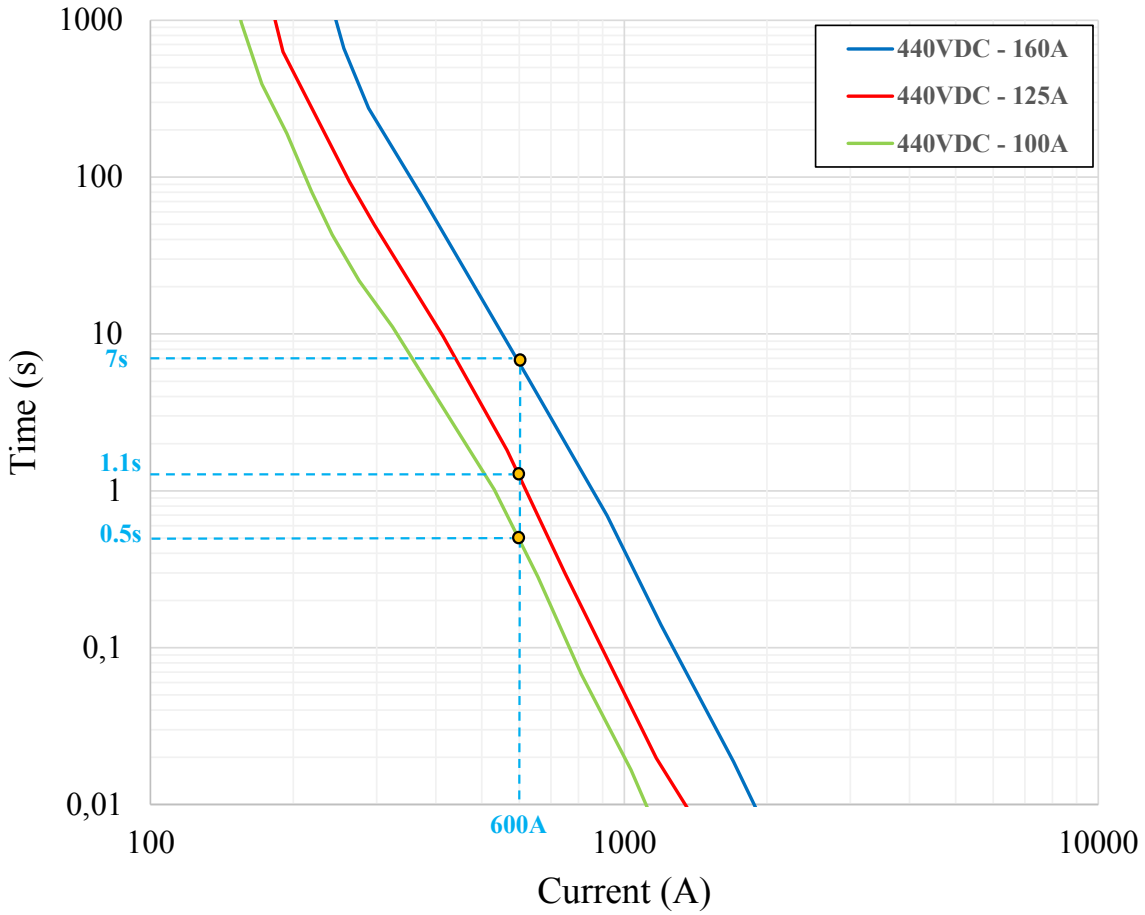

Figure 4.20 Fuse Melting Time-Current Curves

Table 4.7: Fuse Non-Linear Resistance Model Parameters

R_0	R_1	R_2	T_1	T_2
1 mΩ	5 Ω	100 Ω	10 ms	20 ms

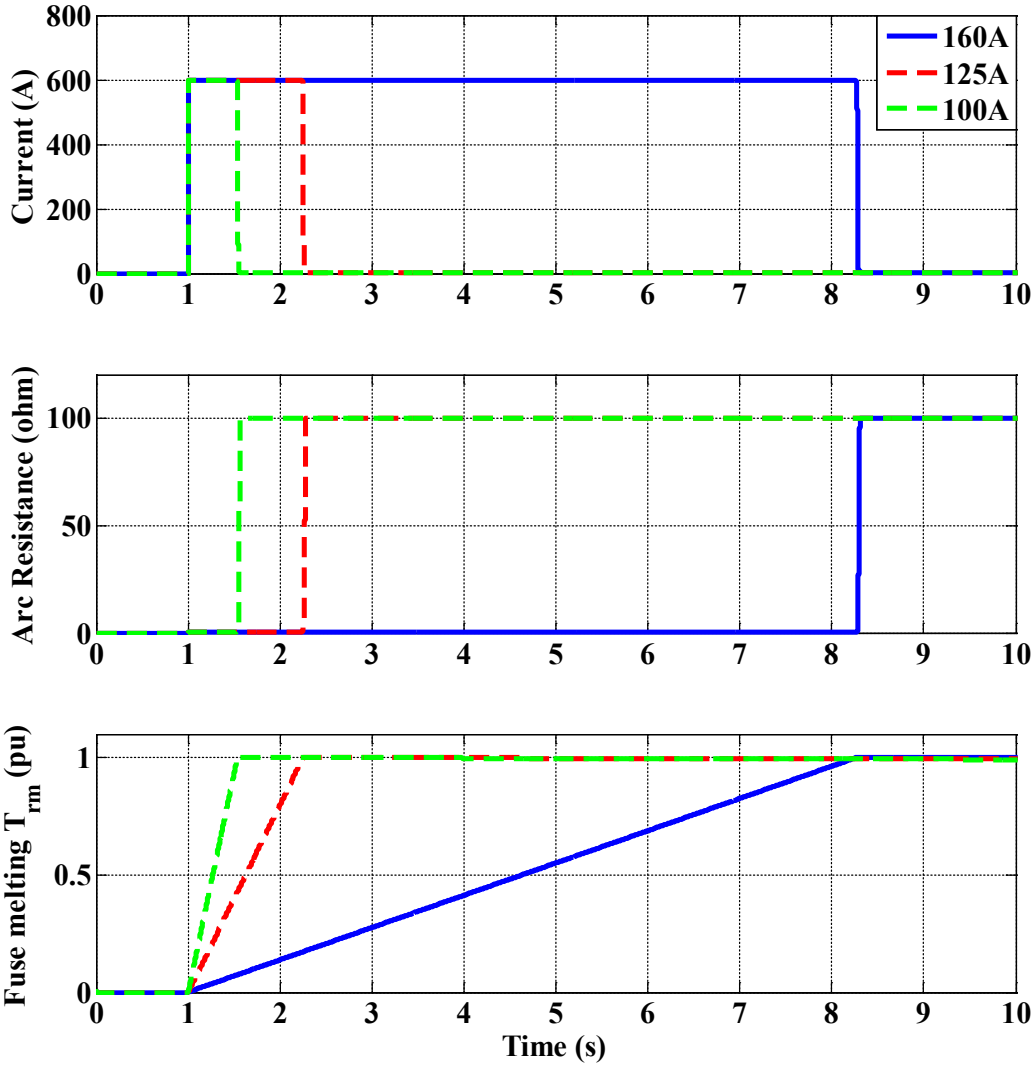

Figure 4.21 Fuse Model Validation for Three (3) Different Fuse Current Ratings

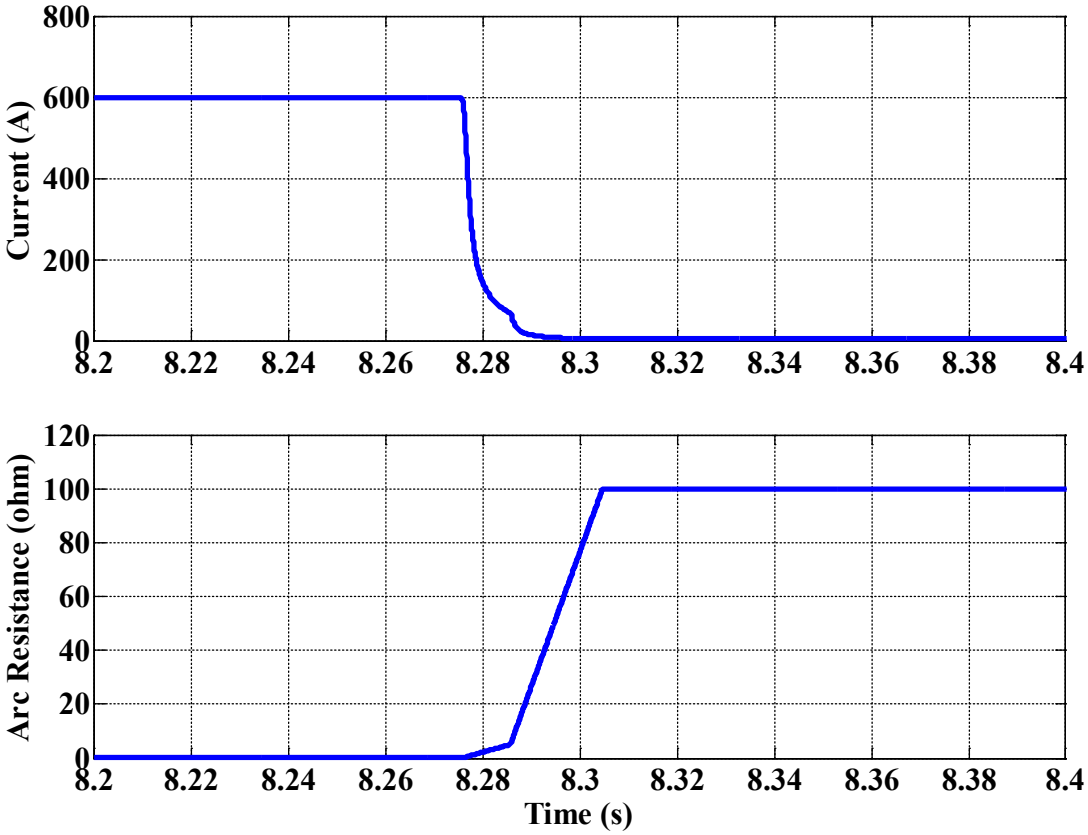

Figure 4.22 Fuse Model Validation – Arcing of the 160 A Fuse

4.5 Load Front-End

In railway vehicles, the electronic equipment generally need to meet the electrical requirements of the IEC 60571 standard (or EN50155). Many components are added on the front-end of the loads to ensure their compliancy with this standard. Understanding the voltage requirements in this standard is essential to at least model the expected behavior of the loads in railway vehicle under voltage fluctuations.

The various elements generally added on the load front-end are presented in Figure 4.23. Even if these elements may not all be present or may be disposed differently, the configuration presented in Figure 4.23 can be used as a general representation for the purpose of model development. In this section, each element is covered separately in order to understand their individual functions, their influence on the power system and to introduce the different modeling techniques.

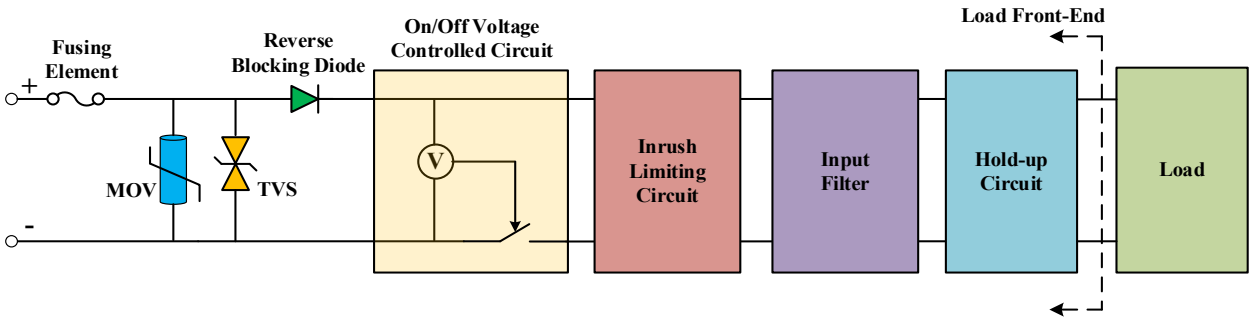

Figure 4.23 Typical Auxiliary Load Front-End in Railway Vehicle

4.5.1 Overvoltage Protective Devices

During transient overvoltage event, overvoltage protective devices are used to limit the surge of energy transferred to the load to be protected. In normal operating mode, these elements are inert and only a small leakage current is flowing through them. If well selected, during overvoltage condition, these devices become good conductors such that they absorb extra energy and keep the voltage under an acceptable level (clipping effect). The amount of current flowing through the protective devices depends on the voltage level and its VI characteristic. However, these devices have an energy limit which shall not be exceeded in order to guarantee multiple protective actions.

The generally used overvoltage protective devices are Transient Voltage Suppressor (TVS) and Metal Oxide Varistor (MOV).

TVS are generally faster and more reliable but their maximum clipping voltage is generally lower. Their leakage current is also lower. They are generally placed near each load to protect them individually [102].

MOV are self-sacrificial which means that their performance are degraded at each operation. They may also suffer from thermal runaway. For a similar low voltage application, MOV are generally bigger than TVS and have a much higher energy capability. Even if they may sometimes be used inside equipment, MOV are generally installed on the main bus for overall protection of the auxiliary distribution [102].

4.5.1.1 Transient Voltage Suppressor (TVS)

The model of Transient Voltage Suppressor (TVS) is based on manufacturer's nomenclature and typical available data. These information are generally sufficient to study the impact of TVS from a power system standpoint and to evaluate the energy absorbed during overvoltage events.

Bidirectional TVS VI characteristic is similar to the series connection of two (2) back-to-back Zener diodes. The VI characteristic of the TVS model implemented in EMTP-RV is shown in Figure 4.24. The VI characteristic is symmetrical. The symbols used to describe the model are given in Table 4.8. The TVS is modeled using a nine (9) points non-linear resistance approximation following Figure 4.24.

Table 4.8: TVS Model Parameters

Description	Symbol
Reverse Stand-off Voltage	V_R
Reverse Leakage Current	I_R
Breakdown Voltage	V_{BR}
Test Current	I_T
Clamping Voltage	V_C
Maximum Peak Pulse Current	I_{PP}

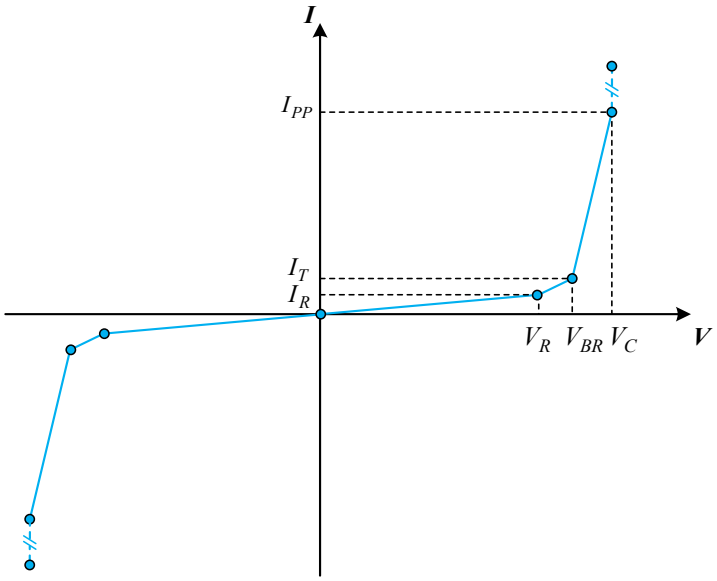

Figure 4.24 VI Characteristic of the TVS Model

One important thing with TVS is the fact that they can't be paralleled unless they are matched. As a matter of fact, manufacturer's data [103] provides tolerance on the value of the breakdown voltage (V_{BR}) for a given TVS (Figure 4.25). For a transient overvoltage event between V_R and V_C, even if the TVS are of the same part number, the TVS with the lowest breakdown voltage (red) will be the first to conduct and will need to sustain much more energy than the others (blue and green).

Since TVS are used in each load individually, they are distributed throughout the entire DC auxiliary system such that it is hard to evaluate their individual effects on power system transients. Modelling multiple TVS of the same part number or even from different part number in one or multiple aggregate is also not recommended because of the difference in their non-linear VI characteristics. Simulations and past experiences have shown that the cable resistance and inductance between the various TVS have also a high influence on the clipping capability of the TVS.

The developed TVS model can be used for power system transient studies in a reduced zone of work. Any attempt to include all the TVS effect in overall power system studies without taking into account all the TVS and their different location may lead to erroneous results. It is recommended not to consider the TVS for overall power system studies.

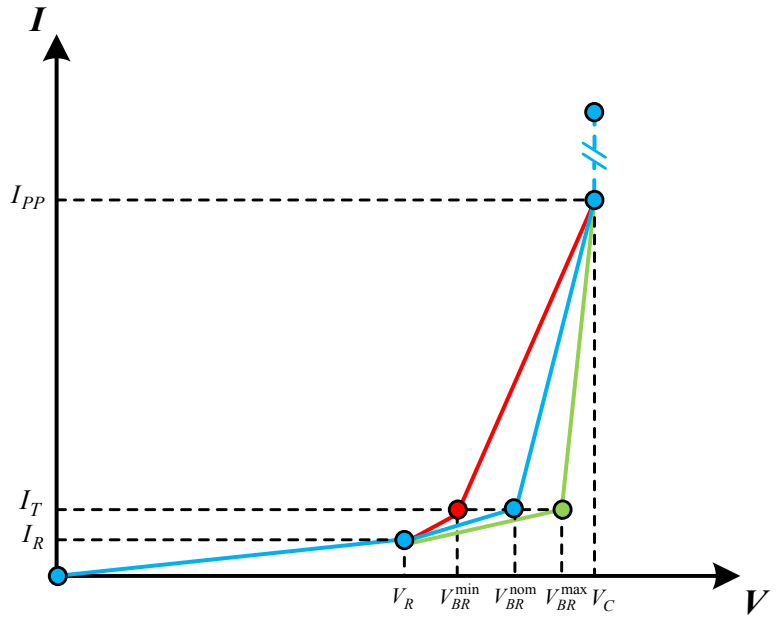

Figure 4.25 Breakdown Voltage Tolerance on TVS VI Characteristic

4.5.1.2 Metal Oxide Varistor (MOV)

The model of Metal Oxide Varistor (MOV) is also based on manufacturer's nomenclature and typical available data. The MOV are also generally defined by a VI characteristic but generally on a Log-Log scale. The VI characteristic of a MOV can be approximated by the following equation [104]:

$$i = Kv^{\alpha} \tag{4.26}$$

Where i is the current flowing through the varistor, v is the voltage across the varistor, α is the non-linearity exponent ($\alpha > 1$) and K is the ceramic constant depending on the type of varistor.

Low voltage MOV can be modeled using the ZnO arrester model in EMTP-RV by entering data points from the manufacturer VI-characteristic. An example of MOV overvoltage protection study is presented in Chapter 5.

4.5.2 Reverse Blocking Diode

The reverse blocking diode is used before the input filter to protect the load internal circuit against reverse polarity and to isolate the filter capacitor from the power system. These diodes can be modeled by a non-linear resistance using their equivalent forward VI characteristic from the manufacturer's data. It is important to consider the presence of the reverse blocking diodes in power system simulation analysis. For example, filter capacitors will not contribute to the short-circuit current for a fault on the DC bus when a reverse blocking diode is used. Diodes non-linear behavior is also important for stability investigation.

4.5.3 On/Off Voltage-Controlled Circuit

The On/Off Voltage-Controlled circuit is used to physically disconnect the loads during unacceptable undervoltage and/or overvoltage conditions. Since the loads are not guaranteed to operate outside the voltage envelope, the loads can be automatically disconnected in the simulation model. From a modelling standpoint, loads can be disconnected outside their voltage operating limits by developing the necessary logic to reproduce the voltage envelope. For the sake of simplicity, a simplified version of the voltage envelope of Figure 2.2 has been implemented (Figure 4.26). In the hold-up region, the load current is generally not provided by

the power system but by an internal hold-up circuit. Therefore the load can be considered disconnected from a power system standpoint in the model. The load is reconnected automatically (with a small delay : < 0.1 ms) in the model once the voltage is back within the operating range. The On/Off Voltage-Controlled module must be carefully used because it can create oscillations due to the rapid change in the load demand when the load is disconnected. Section 4.6 will show how to use this module in conjunction with the load models to reduce the risk of simulation instability.

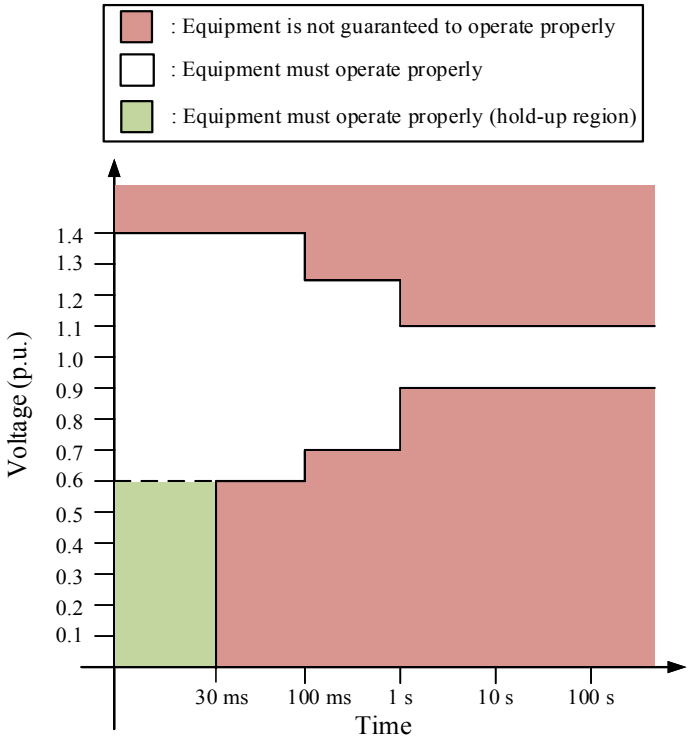

Figure 4.26 Voltage Envelope Implemented in EMTP-RV for Load Model Disconnection

4.5.4 Input Filter

Electromagnetic Interference (EMI) filter is used on the load front-end for differential-mode and common-mode noise attenuation as well as to improve stability. A general representation of EMI input filter configuration is shown in Figure 4.27. Because of the polarity and the magnetic coupling between the two (2) windings forming the common-mode choke (L_{cm}), common-mode currents are trapped into the core of the common-mode choke resulting in high impedance while differential-mode currents are cancelled resulting in low impedance.

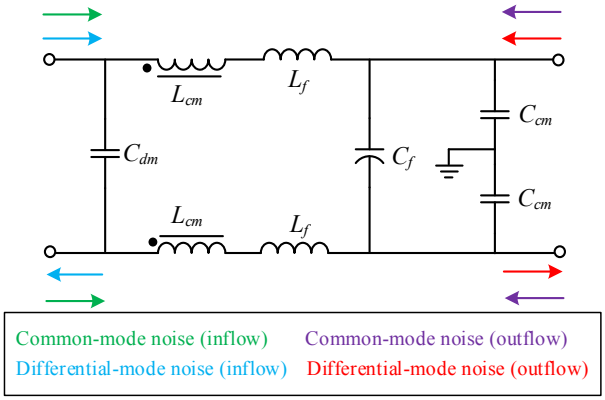

Figure 4.27 EMI Filter General Configuration

Since the power systems transient studied in this work are of differential-mode type, common-mode choke inductance can be neglected. However, the differential-mode filter inductors (L_f) forming the LC input filter with the capacitor (C_f) should be considered. The filter capacitor (C_f) is also used for bus stability such that its value is generally large. The common-mode capacitors (C_{cm}) connected to ground are generally very small and may also be neglected. The differential-mode capacitor (C_{dm}) placed at the very front-end of the filter is also generally much smaller than the filter capacitor (C_f) and therefore can be neglected in most cases.

4.5.5 Hold-up Circuit

The hold-up circuit is used to maintain the voltage applied to the load during power system voltage drops or when the load front-end is disconnected from the main power system. An example of simple hold-up circuit is shown in Figure 4.28. The hold-up capacitor (C_{hu}) is charged initially through a high resistance (R_{hu}) and is discharged through the diode (D_{hu}) when the front-end is disconnected from the power system by the On/Off Voltage-Controlled module. Hold-up circuit does not have a major impact on power system studies unless the load behavior is studied on a small network region. It is not considered in the final complete load model.

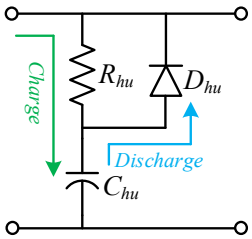

Figure 4.28 Simple Hold-up Circuit

4.5.6 Inrush Limitation

The inrush limitation circuit is used to reduce the speed at which the filter capacitor (C_f) is charged and therefore reducing the inrush current.

Transistor-based scheme are sometimes used in conjunction with the On/Off voltage-controlled circuit to smoothly introduce the capacitor into the circuit. This type of circuit is based on controlling analogically a transistor based on the load terminal voltage. However, this type of inrush limiting circuit is not the most used.

On large load, a charging contactor (CC) is generally used to pre-charge the filter capacitor (C_f) through a resistance (R_{pc}). An example is provided in Figure 4.29. Once the capacitor is charged, the resistance is bypassed using a bypass contactor (BC). On small load, pre-charge circuit using Negative Temperature Coefficient (NTC) resistor (R_{NTC}) are generally used even if they are of a limited use for multiple successive inrush events (Figure 4.30). Even if the value of R_{NTC} is small under loaded condition (hot), it can be optionally bypassed using a bypass contactor (BC) to increase system efficiency.

The NTC-based circuit is modeled following Figure 4.31. NTC resistor can be modeled by a simple resistor with its resistance value equal to its nominal value at ambient temperature (R_{cold}) for peak inrush current evaluation. Once the inrush event is finished, the cold resistance is removed by opening the switch (S_{cold}) and replaced by its hot value (R_{hot}) by closing the switch (S_{hot}).

Experimental validation on a complete train power system has demonstrated that considering a fixed resistance value equal to R_{cold} is accurate enough for evaluating the peak inrush current (Figure 4.32). This is explained by the fact that the inrush current peak duration is only of few milliseconds and the NTC resistor shows thermal inertia. The difference between the simulation and the experimental waveforms after the peak current occurred is mainly attributed to the converter model. As a matter of fact, the source behavior is important in load inrush studies. Nevertheless, from these results it is worth mentioning that the NTC-based model developed (Figure 4.31) can be used for inrush current studies on a complete train basis.

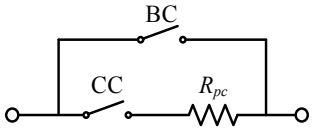

Figure 4.29 Pre-Charge Resistor Inrush Limiting Circuit

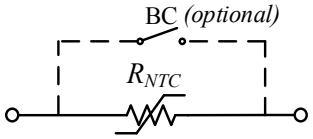

Figure 4.30 Inrush Limiting Circuit using NTC Resistor

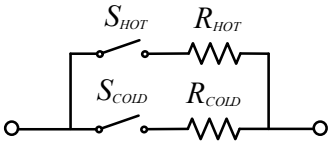

Figure 4.31 Inrush Limiting Circuit using NTC Resistor Model in EMTP-RV

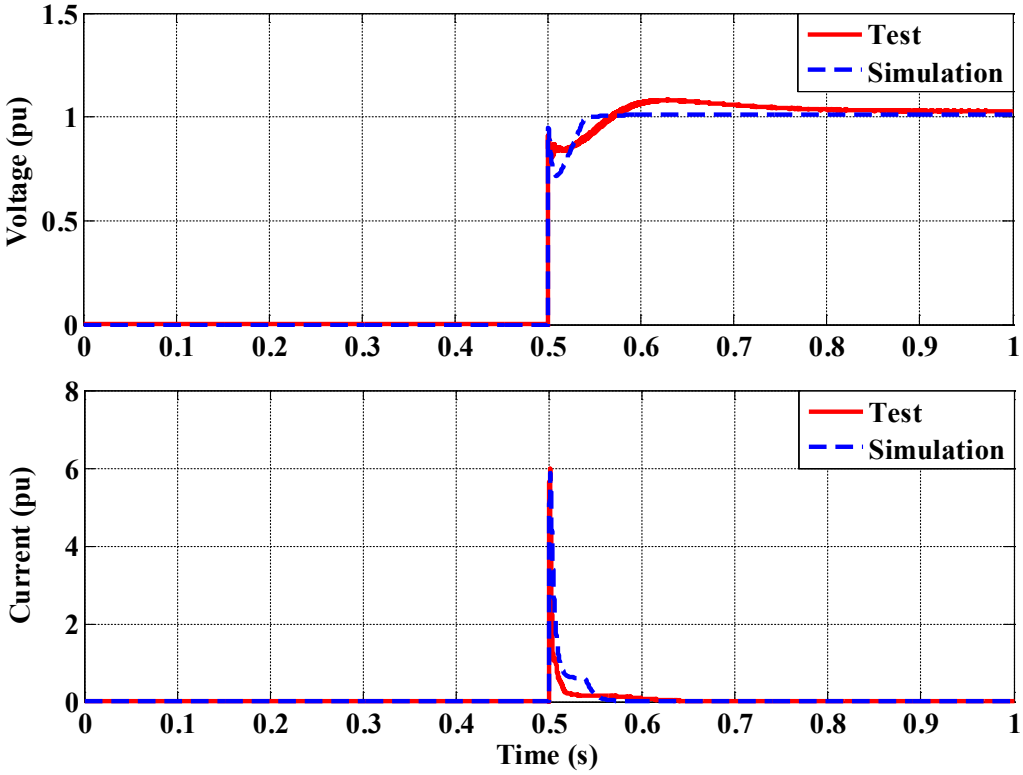

Figure 4.32 Inrush Experimental Validation using the NTC Resistor Model (cold)

4.6 Complete Load Model

The load in Figure 4.23 is modeled following its equivalent response to voltage variation. Constant power, constant current and resistive load models are developed. The complete models for constant current and constant power loads include both the load front-end and the equivalent load model blocks (Figure 4.33). Resistive loads are simply modeled by a resistance.

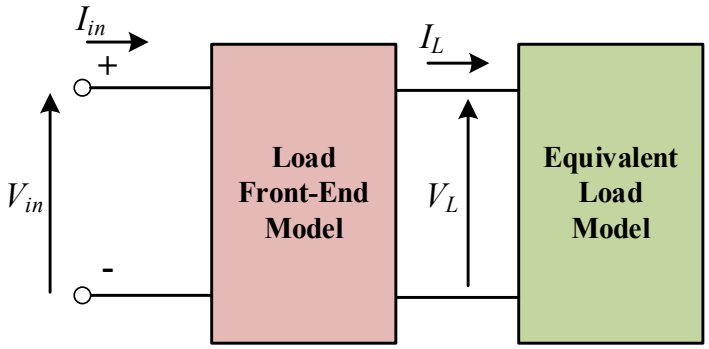

Figure 4.33 Complete Load Model Schematic Representation

4.6.1 Constant Power Load

As previously presented, constant power load reacts to voltage fluctuation following equation (3.5). Constant power load generally includes an internal power supply controlled such as it provides a constant power at its output, thus a constant power seen from its input terminals. Implementing DC constant power load model in DC circuit is not as simple as controlling a current source following equation (3.5).

The first problem is the fact that as the voltage tends toward zero in (3.5), the current goes to infinity. This can be managed by using the on/off voltage-controlled block presented previously (section 4.5.3) to ensure that the equivalent load model only reacts to voltage events inside its normal operating envelope.

The second problem is a consequence of the solution to the first problem. When the load is disconnected under abnormal voltage conditions, the sudden change in current may lead undesired behavior or simulation instability. This issue is managed by adding a filter on the current.

A schematic representation of the equivalent load model is shown in Figure 4.34. Depending on the output of the on/off voltage-controlled block, the load current is calculated using equation (3.5) or is equal to zero. The transition is always filtered. A first order approximation for the filter is used:

$$G(s) = \frac{\Delta I_L(s)}{\Delta I_i(s)} = \frac{1}{1 + s\tau_f} \tag{4.27}$$

To understand the complete load model, the theoretical behavior of the system can be written mathematically. Following a voltage variation given by (4.28), the current variation at the output of the dividing block is given by (4.29).

$$\Delta V_L(t) = \begin{cases} 0, & t < 0 \\ V_{L2} - V_{L1}, & t \geq 0 \end{cases} \tag{4.28}$$

$$\Delta I_L(t) = \begin{cases} 0, & t < 0 \\ P_{CPL}\left(\frac{1}{V_{L2}} - \frac{1}{V_{L1}}\right), & t \geq 0 \end{cases} \tag{4.29}$$

The load current (I_L) is then given by:

$$I_L(t) = P_{CPL}\left(\frac{1}{V_{L2}} - \frac{1}{V_{L1}}\right)\left(1 - e^{-t/\tau_f}\right) + \bar{I}_L \tag{4.30}$$

Thus the final steady-state current is given by:

$$I_L(t) = P_{CPL}\left(\frac{1}{V_{L2}} - \frac{1}{V_{L1}}\right) + \bar{I}_L \tag{4.31}$$

The complete load model is validated using successive voltage steps (Figure 4.35). The on/off voltage-controlled module is also implemented and validated in multiple zones. Load changes are always filtered using a first order approximation. The load is automatically reintroduced smoothly once the voltage is back within the operating range as implemented.

Equation (4.31) is validated using the voltage variation between t=240 ms to t=300 ms in Figure 4.36. For a voltage variation from V_{L1}=1.1 pu to V_{L2}=1.3 pu, a constant power load (P_{CPL}) of 1 pu, a filter time-constant (τ_f) of 2 ms and an initial current ($\bar{I}_L$) of 0.91 pu, the final steady-state value of the current should be equal to 0.77 pu according to (4.31). The final steady-state

should also be reached after approximatively five (5) time-constant which is equal to 10 ms. Figure 4.36 confirms that the developed constant power load model behave as expected.

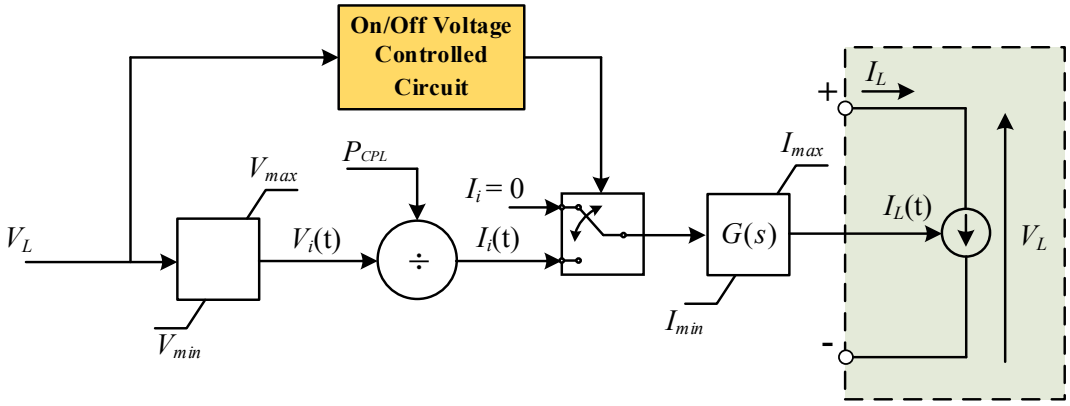

Figure 4.34 Constant Power Load Model Schematic Representation

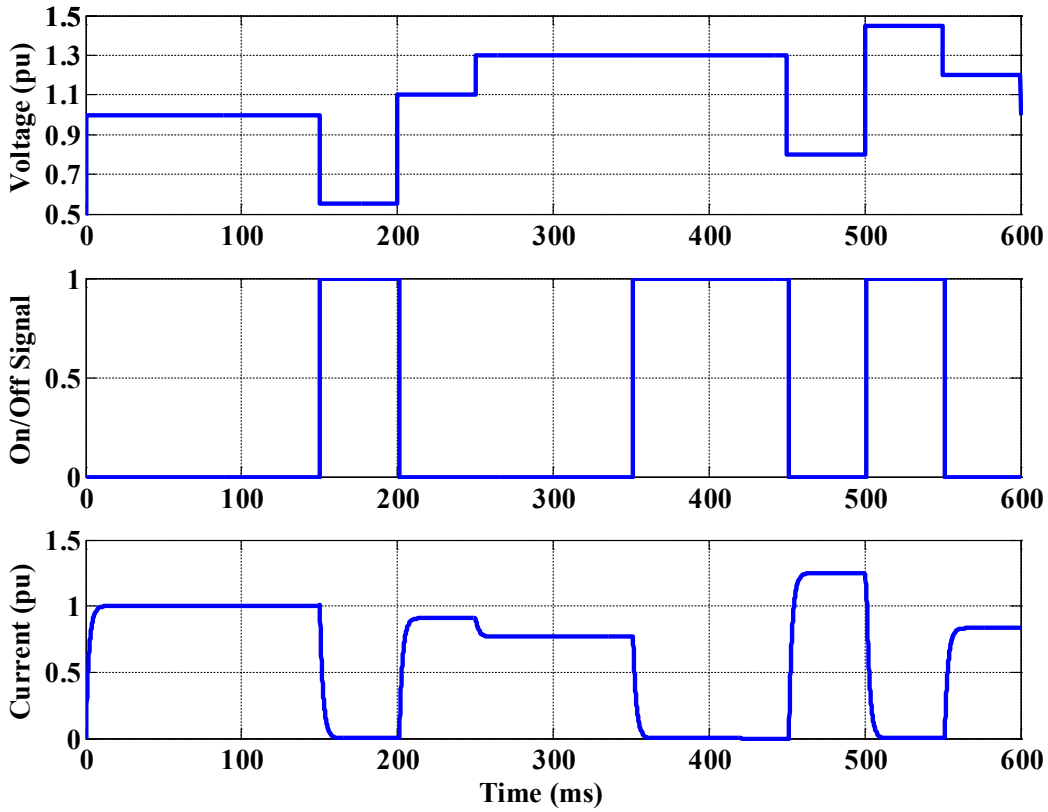

Figure 4.35 Complete Constant Power Load Model Simulation Validation

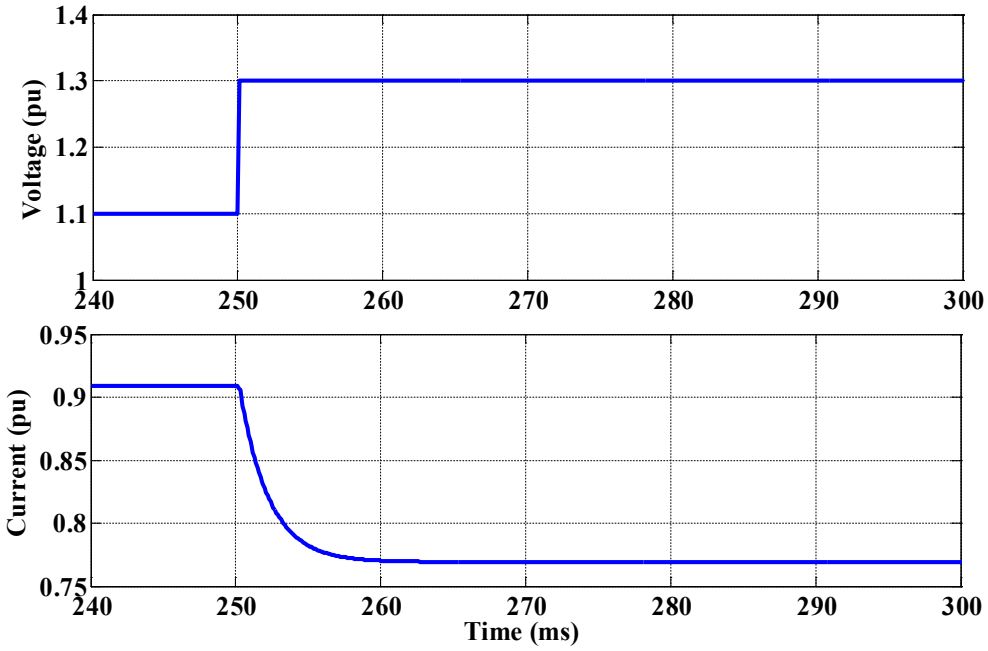

Figure 4.36 Validation of the Complete Constant Power Load Model Current Equation

4.6.2 Constant Current Load

Constant current load in railway vehicles also includes an internal power supply which keeps the input current approximatively constant. Some lighting fluorescent systems with electronic ballast behave approximatively as constant current loads seen from their input terminals.

Constant current load does not react to voltage variation. The current is constant even if the input voltage varies. Knowing the nominal power (P_{CCL}) and the nominal voltage (V_n), the load current (I_L) is given by:

$$I_L = \frac{P_{CCL}}{V_n} \tag{4.32}$$

Implementing a constant current load model in DC circuit is similar to implementing a constant power load model. These loads can also be disconnected when the voltage is outside the normal operating envelope.

When disconnecting the load under abnormal voltage conditions, the sudden change in current must also be managed properly. Similarly to the constant power load model this issue is managed by adding a filter on the current.

A schematic representation of the equivalent constant current load model is shown in Figure 4.37. Depending on the on/off voltage-controlled block output the load current is calculated using equation (4.32) or is equal to zero. The transition is again filtered through a first order filter given by equation (4.27).

The complete load model is validated using the same successive voltage steps as for the constant power load (Figure 4.38). For a constant current load (P_{CCL}) of 1 pu at a nominal voltage (V_n) of 1 pu and using a filter time-constant (τ_f) of 2 ms, the load current (I_L) should also be equal to 1 pu when the voltage is inside the normal operating envelope and zero otherwise.

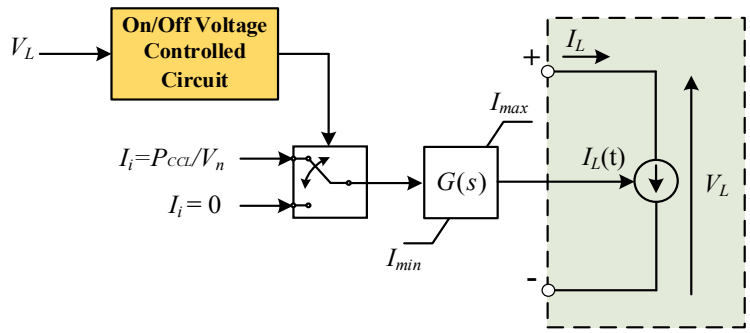

Figure 4.37 Constant Current Load Model Schematic Representation

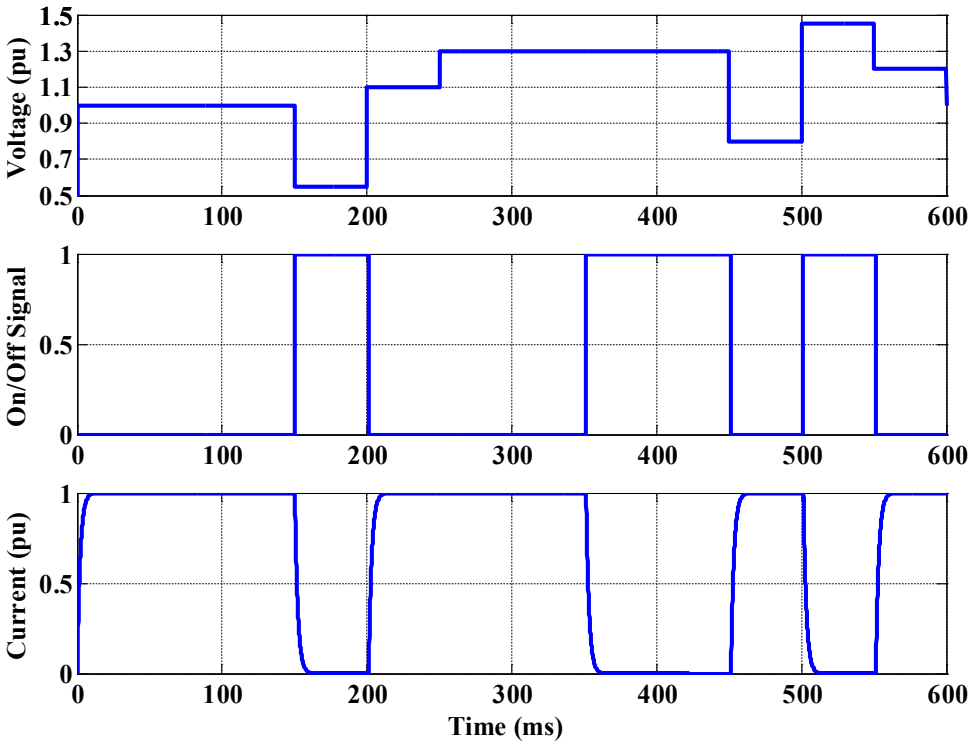

Figure 4.38 Complete Constant Current Load Model Simulation Validation

4.7 Complete Train DC Auxiliary System Model

A typical 5-car complete train DC auxiliary system model is implemented in EMTP-RV based on past and current projects data (Figure 4.1). The complete train DC auxiliary system architecture is presented in Appendix B. The models developed in section 4.2 to 4.6 are used to develop the A-, B-, and C-car models. The complete train model is built by connecting the vehicle models as in Figure 4.1.

The nominal voltage of the Low Voltage Bus (LVB) is 110 V and the nominal voltage of the Intermediate Voltage Bus (IVB) is 380 V.

4.7.1 Low Voltage Bus (LVB) – 110 V

In normal operation, two (2) Low Voltage Power Supply (LVPS) and (2) backup batteries are connected on the 110 V bus located inside the two (2) B-car. The negative of the 110 V system is grounded through high resistances and a Ground Fault Detector (GFD) inside the two (2) B-car. Transient overvoltage devices (MOV) are used on the 110 V bus in the two (2) B-car. The DC loads are modeled with equivalent constant power, constant current and resistive load models. Constant power and constant current load models are voltage-controlled and disconnected outside the IEC 60571 voltage envelope. Equivalent filter models are implemented because of the large number of filters typically distributed over the entire LVB in each vehicle. The equivalent filters are isolated from the 110 V bus using equivalent non-linear diodes. Bus Circuit Breaker (BCB) are 2 poles bidirectional ABB Tmax T5 400A with detailed detection ("hot" curve) and opening mechanisms models. The circuit breaker Time Current Curve (TCC) is given in Figure 4.16. Main Circuit Breaker (MCB) are modeled using ideal switches.

The complete model parameters on the 110 V bus are given in Appendix C. Otherwise mentioned, these parameters are considered fixed for all the simulation cases.

4.7.2 Intermediate Voltage Bus (IVB) – 380 V

In normal operation, two (2) Intermediate Voltage Power Supply (IVPS) located inside the two (2) B-car are supplying the 380 V bus load demand. The negative of the 380 V system is solidly grounded in the C-car. The combination of each AC motor and its inverter are modeled with an equivalent constant power load model and a front-end equivalent filter (Figure 4.39). The

equivalent filters are all isolated from the 380 V bus using equivalent non-linear diodes. Loads are disconnected outside the IEC 60571 voltage envelope. There is two (2) 440 VDC fuses at the output of each IVPS. Fuse current rating can be selected to be 100 A, 125 A, or 160 A through the model mask. Each fuse has a series switch for physical isolation of the IVPS from the IVB. The individual load circuit breakers (CB38X) are modeled by ideal switches. The complete model IVB parameters are given in Appendix D. Similarly to the 110 V bus, these parameters are considered fixed for all the simulation cases otherwise mentioned.

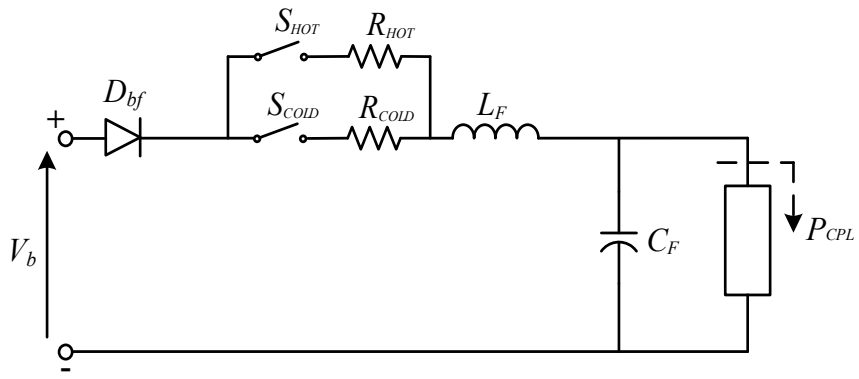

Figure 4.39 IVB (380 V) Constant Power Load Model Schematic Representation

CHAPTER 5 CASE STUDY

5.1 110 V Bus Case Study

During the design of DC power systems, many analysis can be performed using simulation models to reduce the cost and the time associated with field testing. It also allows to study multiple scenarios which cannot always be tested in practice.

In this section, an example of complete overcurrent protection study on the 110 V bus is first presented. Then a ground fault analysis is performed and an example of ground fault detector design validation is presented. An example of transient overvoltage study is also presented with an analysis of the impact of overvoltage protective devices. The design and implementation of a transient overvoltage filter is also presented using the simulation model. Finally a complete battery sizing case is demonstrated on a typical train emergency scenario.

5.1.1 Overcurrent Protection

A line-to-line fault located in (F1) in the train power system of Appendix B is applied at t=25 ms. All the car auxiliary systems are running initially at their full power set-point and both LVPS and both backup battery are present when the fault occurs. The MOV in each B-car are not connected. The fault current and the sources (LVPS and Battery) contribution to the total fault current are shown in Figure 5.1. The total load current in each car and the protective devices thermal and magnetic trip travel are shown in Figure 5.2. The simulation time step Δt is equal to 2 μs. The first 20 ms of simulation are hidden because the simulation initialization is performed in the time-domain.

For the fault in F1, the total fault current in steady-state is 4350 A. Since the total current contribution of the B4-car is high enough (Battery≈2100 A, LVPS=197 A, Total=2297 A) to reach the magnetic region of the circuit breaker (2200 A), the circuit breaker (BCB1) in the B4-car trips approximatively after its instantaneous delay (16 ms). However, because the fault is located closer from the B4-car than the B2-car, the current contribution from the B2-car is smaller and also not high enough (Battery≈1850 A, LVPS=195 A, Total=2045 A) to reach the magnetic region of the circuit breaker. The BCB2 in the B2-car then operates in its thermal region following its TCC of Figure 4.16 (hot region) which leads to a trip time around 425 ms.

Figure 5.2 also shows that the loads are rapidly disconnected after the fault occurred since the voltage in each car drops under the minimum voltage limit of 66 V (0.6 pu). When the fault is isolated from the B4-car by the BCB1 circuit breaker in the B4-car, the voltage goes back to normal in the B4- and A5-car such that the loads can run again in these two (2) cars. Then, when the fault is finally cleared by the circuit breaker BCB2 in the B2-car, the loads in the A1- and B2-car are also able to run again. The C3-car is at this point isolated from both sides.

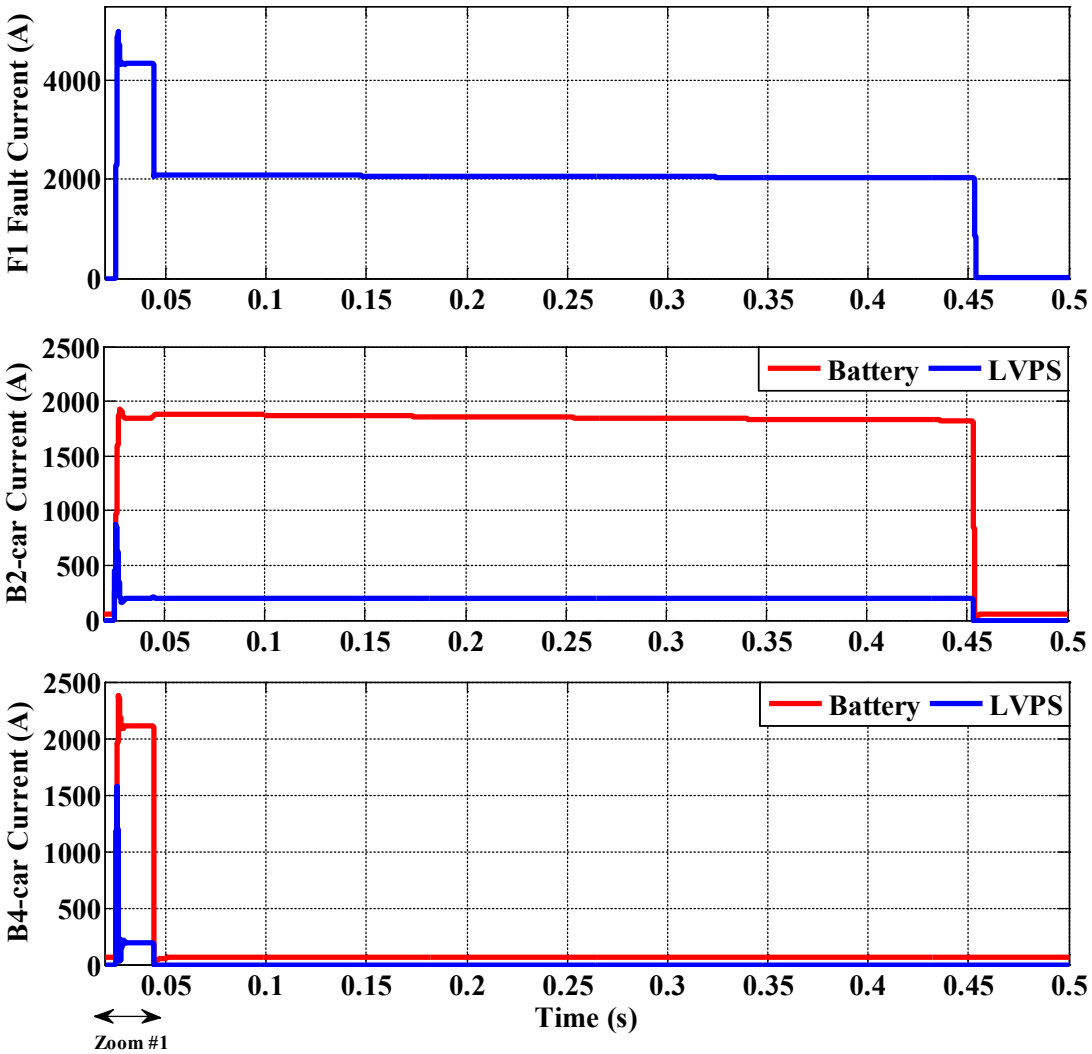

Figure 5.1 Total Fault Current and Sources Contribution (F1-Fault)

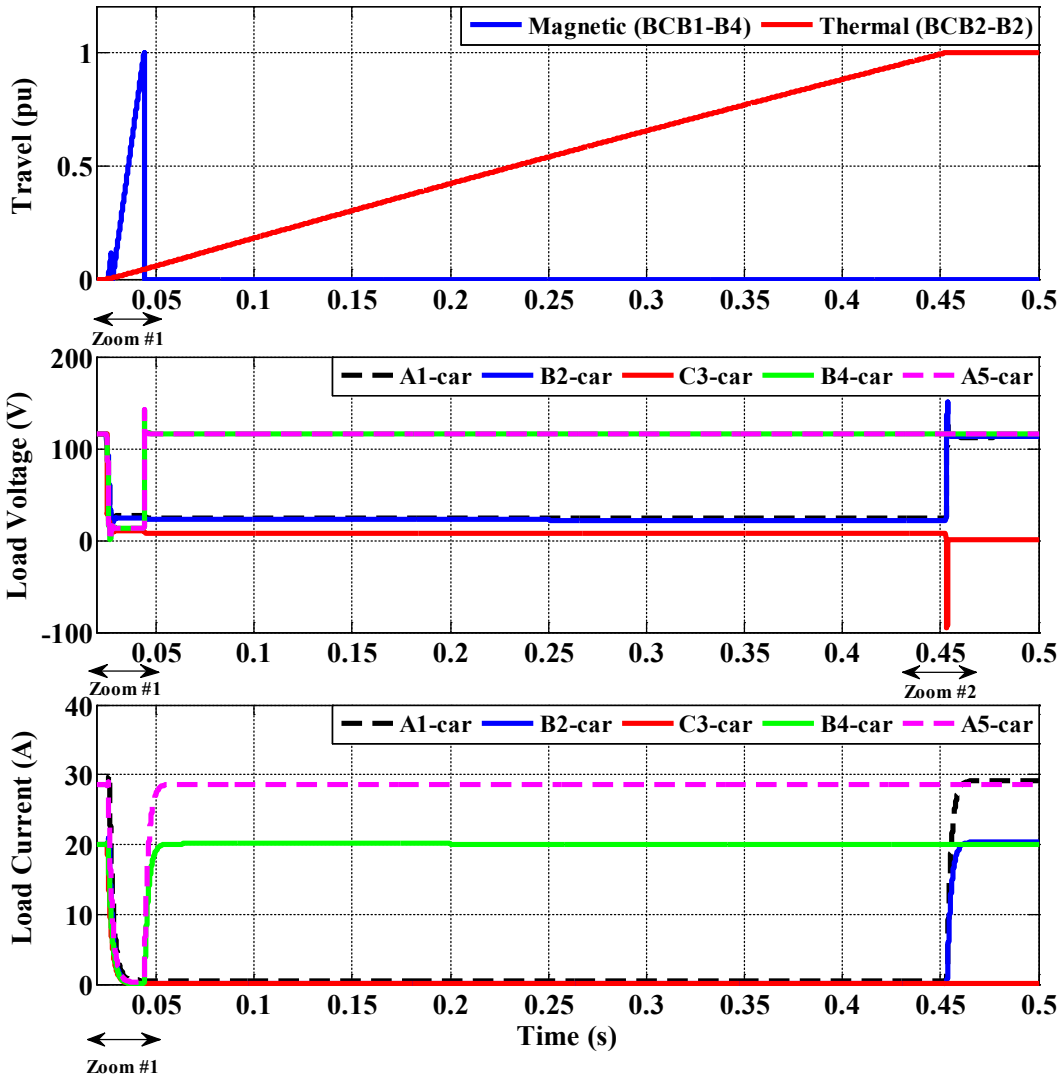

Figure 5.2 Circuit Breaker Travel, Load Voltage and Load Current (F1-Fault)

Up to now, the analysis has been performed considering steady-state values. By looking closer to the transient regions (Figure 5.3, Figure 5.4, and Figure 5.5), the transient behavior of the system can be studied. First, the peak current and the oscillatory behavior in the battery current at fault ignition is due to the LVPS capacitor discharge which leads to a large voltage drop on the DC bus and to oscillation with system inductances. The battery internal voltage can be considered constant during fast transient such that the battery current follows the voltage oscillation of the DC bus.

Also, it is observed in Figure 5.4 that the magnetic trip travel of the BCB1 circuit breaker in the B4-car is initiated twice but the first travel calculation is reset because the current circulating

through the circuit breaker is not over the instantaneous current setting (2200 A) for a long enough duration (< 16 ms). However, when the current goes beyond 2200 A for the second time, the current duration is now long enough for the BCB1 circuit breaker in the B4-car to trip in the magnetic region.

The transient overvoltages seen by the loads in Figure 5.4 and Figure 5.5 are also realistic when compared to experimental results that have been obtained during field testing. In this case, the maximum overvoltage is 151 V (Figure 5.5). The voltage is also momentarily negative in the C3-car when the BCB2 circuit breaker in the B2-car opens because both poles are breaking the fault current and no other source is connected on the DC bus to provide a counter reaction.

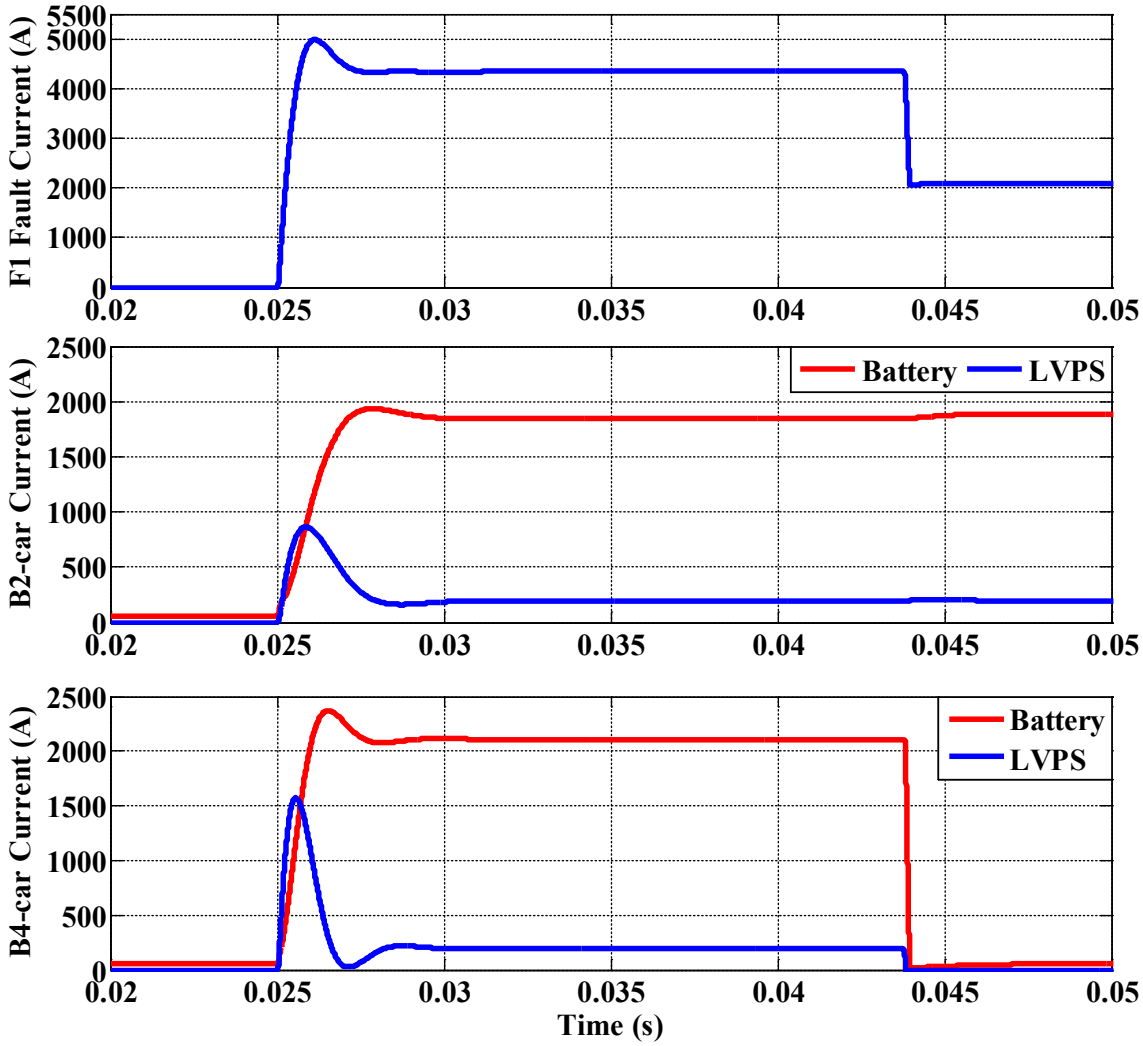

Figure 5.3 Total Fault Current and Sources Contribution (Zoom #1)

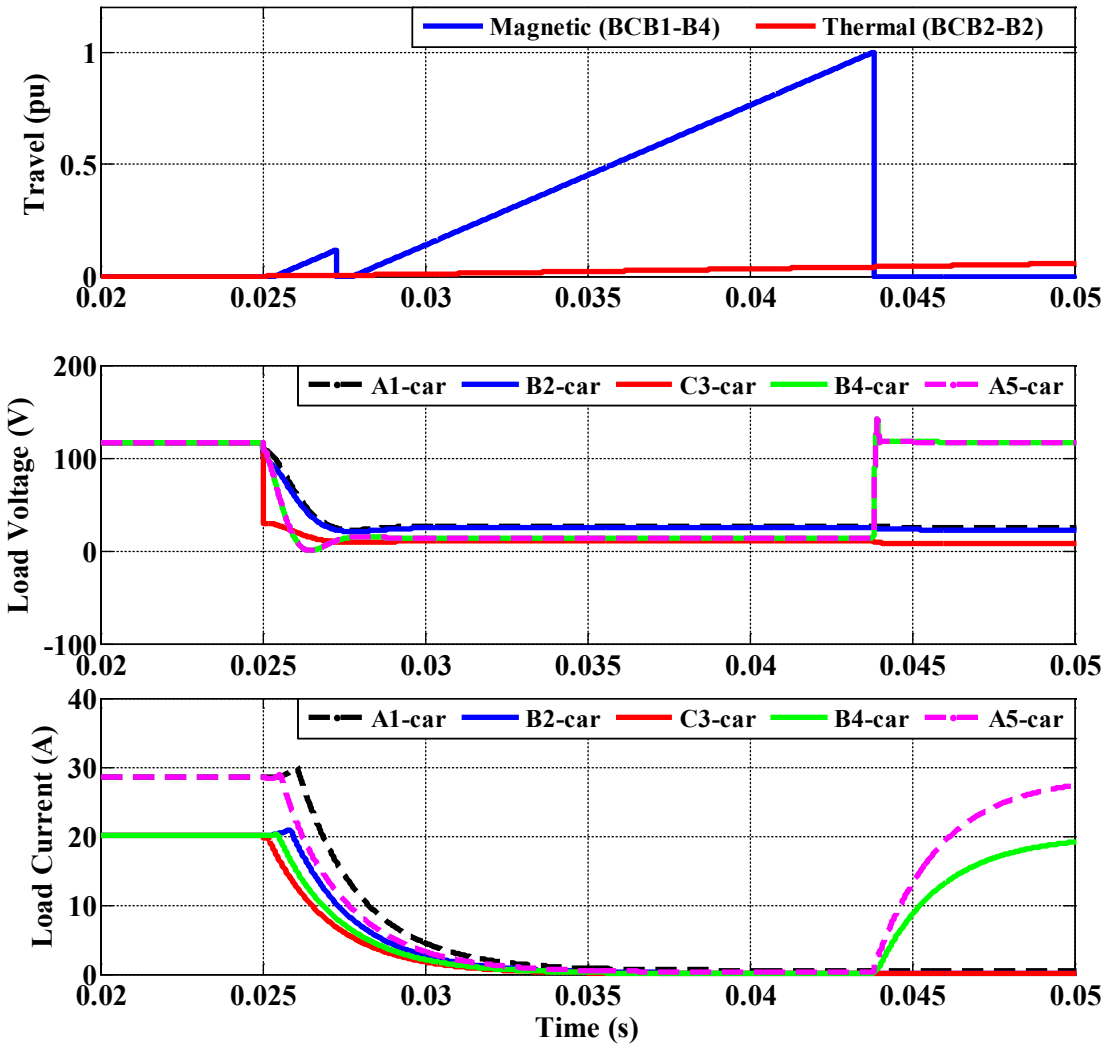

Figure 5.4 Circuit Breaker Travel, Load Voltage and Load Current (Zoom #1)

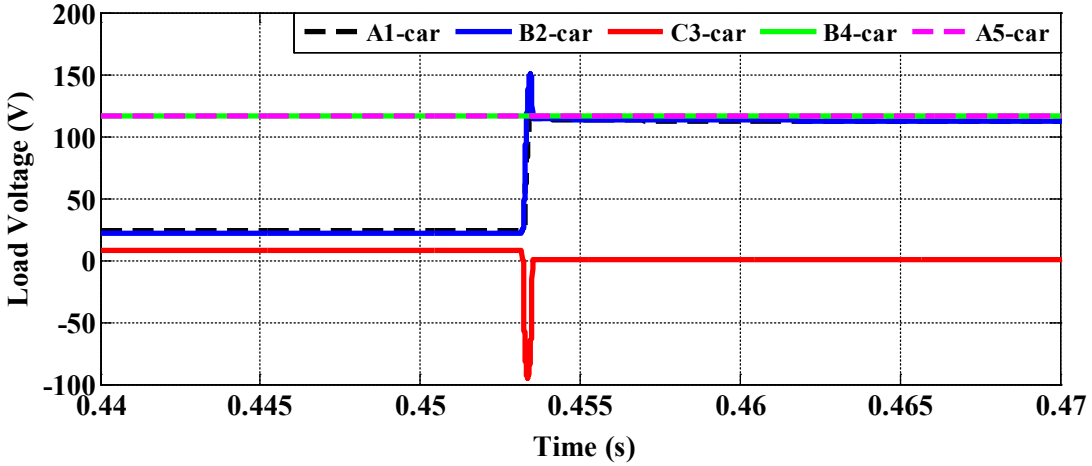

Figure 5.5 Overvoltage at Opening of BCB2-B2 (Zoom #2)

5.1.2 Ground Fault Detection

In section 2.4, an important discussion on system grounding and bonding has been presented. The importance of detecting a first ground fault in a high impedance system has been discussed and the single-pole interruption problem briefly presented. In this section, the simulation model is used to design a simple ground fault detector and to reproduce the single-pole interruption problem.

The 110 V system grounding is done through a Ground Fault Detector (GFD). The GFD schematic representation is shown in Figure 5.6. The value of the resistances R_{G1} and R_{G2} is 10 kΩ and the value of R_{G3} is 2 kΩ. Under normal conditions the current in R_{G3} is nil. When a ground fault occurs, a small current will flow in R_{G3}. A simple trip detection scheme based on the filtered voltage value across R_{G3} (noted V_{G3}) is implemented in EMTP-RV. Based on multiple simulation, it has been possible to determine that beyond a value of V_{G3} of 16 V, a ground fault is certainly present.

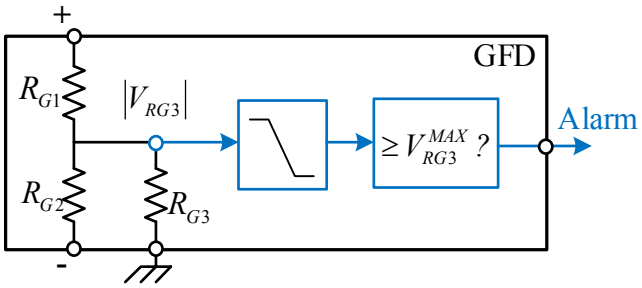

Figure 5.6 Ground Fault Detector (GFD) Schematic Representation

The problem of single-pole interruption is discussed in detail in [67]. A single pole interruption will happen if: two (2) simultaneous line-to-ground faults occur, one of the fault is on the load side, the other fault is on the source side of the circuit breaker, each fault are located on a different polarity, and the fault current is high enough to trip one of the circuit breaker. If all these conditions are met, one (1) pole of the circuit breaker will be required to interrupt the entire fault current. In this case, it is important to ensure that the fault current does not exceed the circuit breaker tested one-pole interrupting capability [67]. Figure 5.7 shows the two (2) cases of single-pole interruption in DC systems (negative pole (a) and positive pole (b)). Even if the conditions are unlikely to happen, it is considered here to show the capability of the developed train model to study advanced grounding fault with a high level of details in a MTDC system.

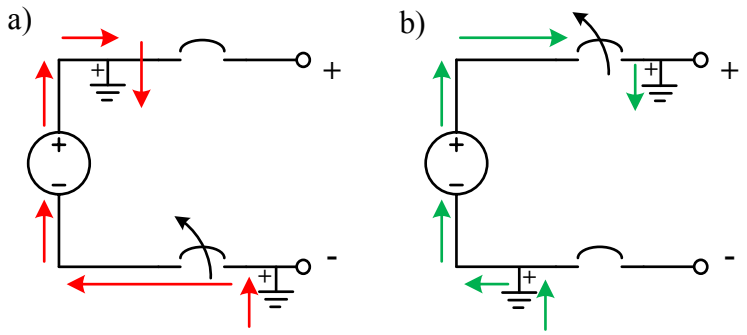

Figure 5.7 Single-Pole Interruption with Double-Fault-to-Ground

As an example, a first ground fault located at F2 (B4-car) is applied at t=25 ms in the train power system of Appendix B. A second ground fault located at F3 (A5-car) is applied at t=50 ms. The circuit breaker BCB2 in the B4-car will be required to break the fault current by the mean of only its positive pole as depicted in Figure 5.7 b). The simulation results are presented in Figure 5.8, Figure 5.9, and Figure 5.10. The simulation time step Δt is equal to 0.5 µs.

The GFD signals in the B2-car are shown in Figure 5.8. A similar analysis can be performed for the GFD signals in the B4-car. Initially, the current and the voltage of the resistance R_{G3} is zero as required. When the first ground fault (F2) occurs at t=25 ms, the current in the resistance R_{G3} rises up to 8.3 mA, leading to an increase in the voltage across R_{G3} up to 16.6 V. Thus, after a certain amount of time determined by the GFD filter cut-off frequency (here 1 kHz), the filtered voltage across R_{G3} exceeds 16 V and an alarm signal is sent at the output of the GFD. In this case, no corrective action is taken such that when the second ground fault (F3) occurs at t=50 ms, the system falls under a double-fault-to-ground condition. The GFD no longer detect a ground fault because it is bypassed by the fault path which offers a smaller resistance.

However, the steady-fault current is now near 4000 A (Figure 5.9). The fault current is negative in the fault switch F2 (negative pole fault) and positive in the fault switch F3 (positive pole fault) assuming the ground polarity shown in Figure 5.7 b). The fault current only flows in the positive pole of the BCB2 circuit breaker in the B4-car (Figure 5.10). Since the fault current exceeds the instantaneous current setting of the circuit breaker (2200 A), the circuit breaker trips after 16 ms with only the positive pole breaking the entire fault current leading to a large arc voltage requirement. Once the fault is cleared, since the ground fault in F2 is not removed, the GFD is still detecting a ground fault (Figure 5.8).

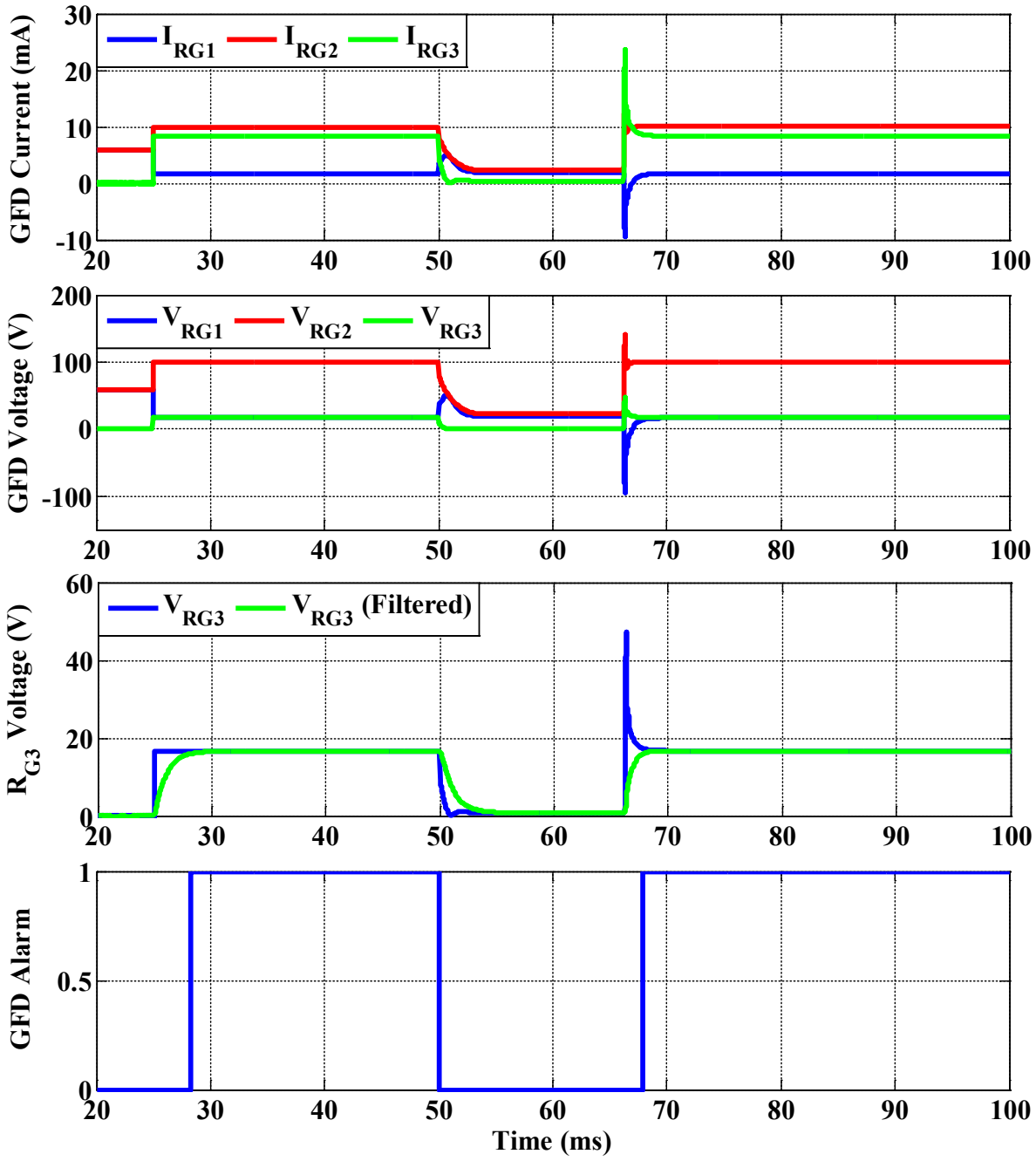

Figure 5.8 Double-Fault-to-Ground (F2-F3) GFD Signals

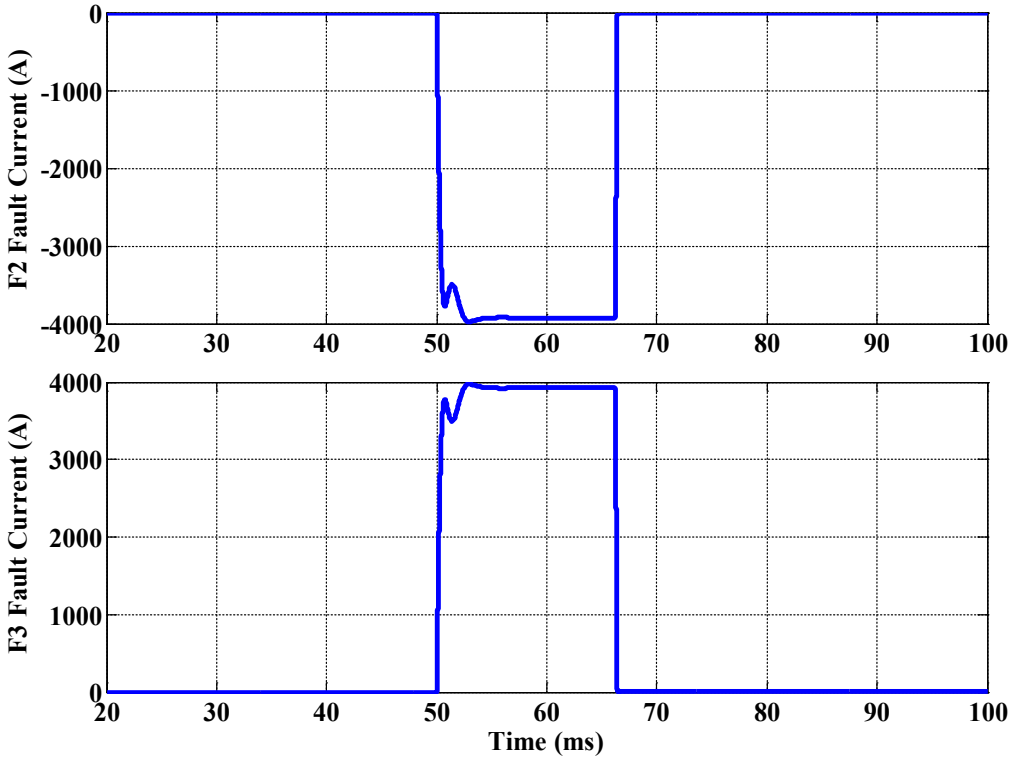

Figure 5.9 Double-Fault-to-Ground (F2-F3) Fault Current

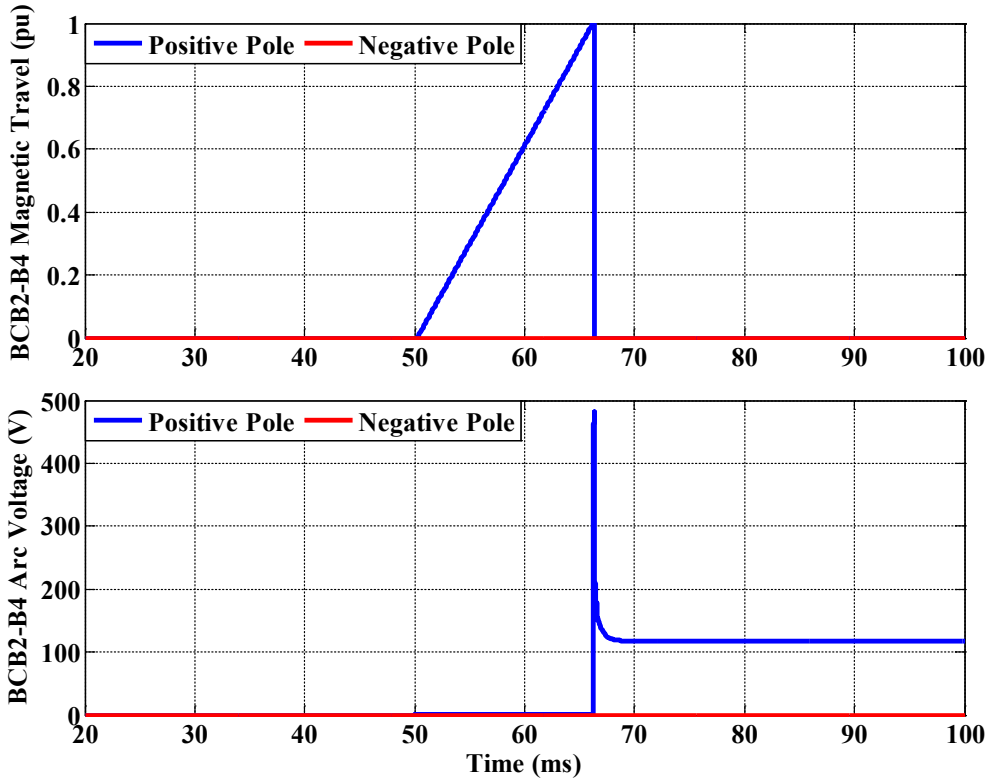

Figure 5.10 Double-Fault-to-Ground (F2-F3) Circuit Breaker Single-Pole Interruption

5.1.3 Transient Overvoltage (TOV)

In this section, transient overvoltage (TOV) at circuit breaker opening is studied. A TOV Bus Filter (BF) is also designed for the train simulation model and the performance of the selected MOV are compared to the designed filter. It should be kept in mind that the circuit breaker model is not developed at first to study circuit breaker transient overvoltage but it can be used to reproduce realistic transient overvoltage conditions during circuit breaker fault interruption.

A schematic representation of the proposed transient overvoltage filter is shown in Figure 5.11. It should be mentioned that S_{pc} and S_{bf} are ideal switches for the purpose of the simulation. In practice, contactors or semiconductors should be used. If the capacitor inrush level is allowed by the system, the switches (S_{pc} and S_{bf}) are not necessary. It has been seen in section 3.3.1 that adding capacitance on the DC bus can reduce transient overvoltage at circuit opening. Installing capacitor on the DC bus must be done by considering inrush current and high discharge of current during fault. Initially, the bus filter capacitor (C_{bf}) is pre-charged through the resistance (R_{pc}) by closing the switch (S_{pc}). Once the capacitor is charged, the switch (S_{pc}) is opened and the switch (S_{bf}) is closed. If the capacitor voltage (V_{Cbf}) is equal to the bus voltage (V_b) the transfer is smooth. When an overvoltage condition occurs, the bus voltage (V_b) becomes greater than the capacitor voltage (V_{Cbf}) and the diode (D_{bf}) is conducting such that extra capacitance (C_{bf}) is added on the DC bus. If a fault occurs on the bus side, the capacitor (C_{bf}) is isolated by the diode (D_{bf}). The resistance (R_{dis}) is added to discharge the capacitor if the switches (S_{pc} and S_{bf}) are left opened. Low capacitor ESR is also necessary to enhance filter performance.

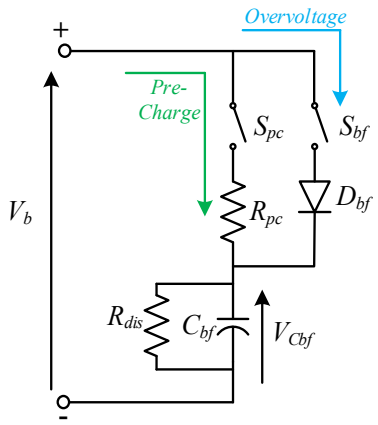

Figure 5.11 Transient Overvoltage Bus Filter (BF) Schematic Representation

The TOV bus filter parameters are presented in Table 5.1. The diode (D_{bf}) is modeled using a non-linear VI-curve approximation. The value of the pre-charge resistance (R_{pc}) is selected to be small to reduce the capacitor charging time (simulation time). In practice the value should be larger (around 10 Ω).

A line-to-line fault located at (F4) is applied at t=25 ms. For the sake of simplicity, the loads and the load filters are excluded from the simulation. The fault current is shown in Figure 5.12. Again the fault current exceeds the instantaneous current setting of the circuit breaker (2200 A) and the circuit breaker trips rapidly after approximately 16 ms. The simulation time step Δt is equal to 0.5 μs.

The circuit breaker BCB2 in the B4 car must interrupt a high fault current resulting into a large transient overvoltage of 255 V on the 110 V nominal bus (Figure 5.13). This overvoltage condition is not acceptable considering the maximum voltage defined in the IEC 60571 standard (1.4 pu = 154 V). By adding a MOV on the 110 V bus in the B2- and B4-car, the transient overvoltage is reduced to 230 V which is still not enough to meet the IEC 60571 requirement. In fact, only the closest MOV from the opening point (B4-car) is absorbing energy from the surge (Figure 5.14). Replacing the MOV by the designed filter, the TOV is reduced to 152 V which is now acceptable. From this, it can be concluded that the designed filter provides better clipping performance than the selected MOV. Going with a MOV from the same manufacturer [105] having a voltage rating smaller than the MOV selected is also not possible for a 110 V nominal bus because the leakage current through the MOV would not be acceptable.

Table 5.1: Transient Overvoltage Bus Filter Parameters

Description	**Symbol**	**Value**
Pre-Charge Resistance	R_{pc}	0.5 (Ω)
Discharge Resistance	R_{dis}	10 (kΩ)
Bus Filter Capacitor	C_{bf}	12 (mF)
Bus Filter Capacitor ESR	R_{Cbf}	10 (mΩ)

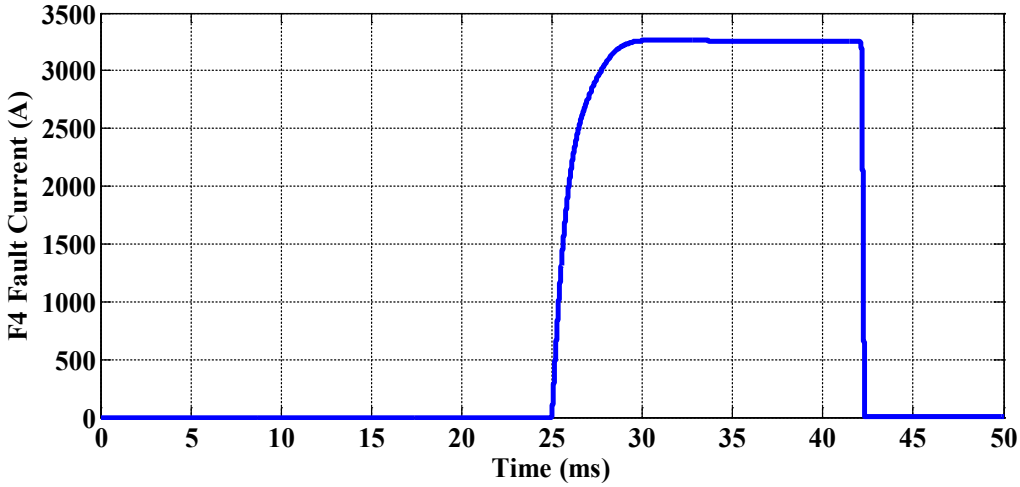

Figure 5.12 Fault Current for a Fault in F4

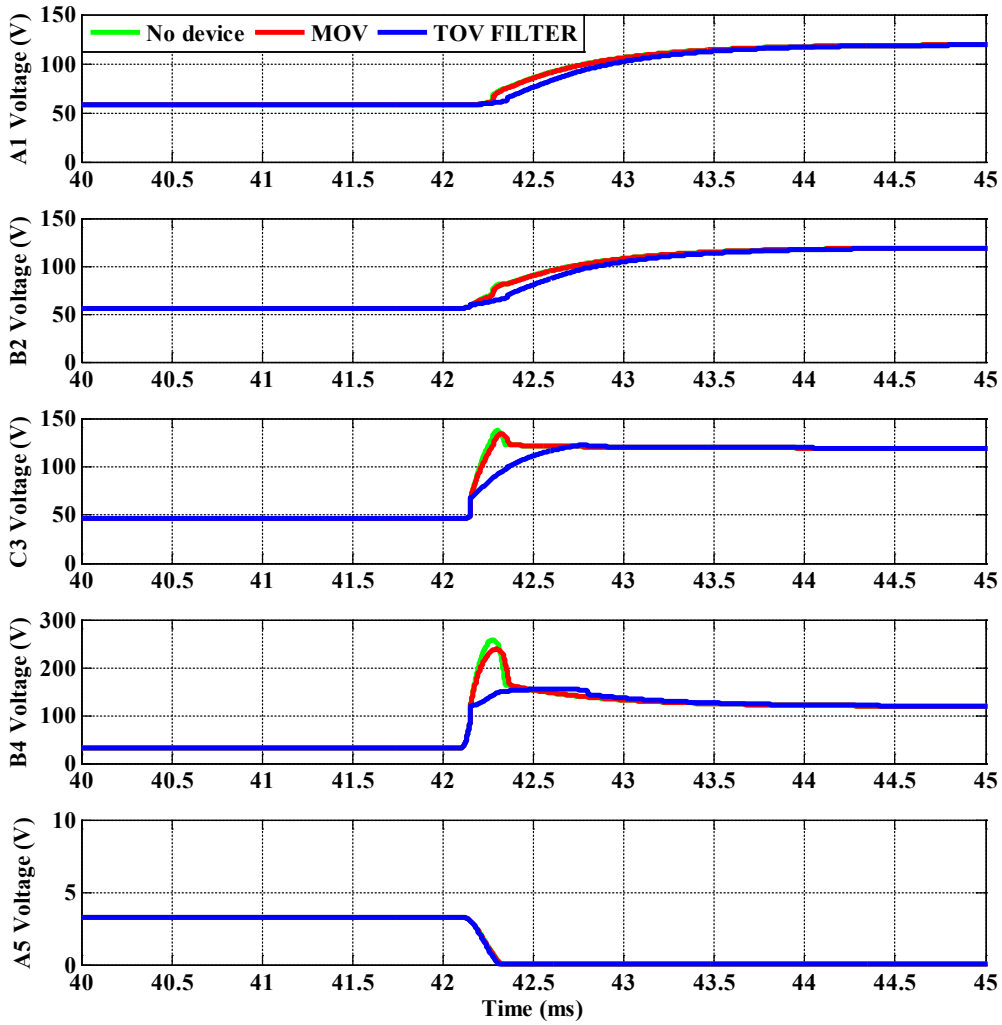

Figure 5.13 Impact of Surge Protective Devices on Transient Overvoltage

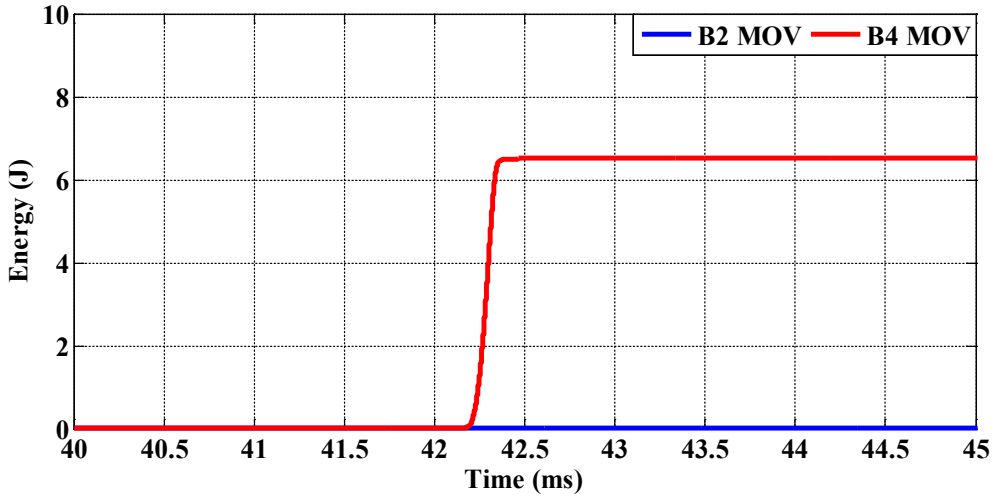

Figure 5.14 MOV Energy Absorbed from the Surge

5.1.4 Emergency Battery Sizing

Battery sizing in train DC auxiliary power systems is generally performed following IEEE Std 1476 with concurring responsibilities between the transit authority, the car manufacturer and the battery manufacturer. The following steps are a summary of the IEEE Std 1476 general approach [9] and they are presented in order to introduce the role of the simulation model throughout the battery sizing process:

1. Transit authority specify emergency condition requirements (duration, essential and nonessential loads, operating temperature and other particularities).
2. Car manufacturer compiles DC loads with information from subsystem suppliers.
3. Car manufacturer defines the minimum acceptable voltage at the load (with margin) and the distribution voltage drops.
4. Car manufacturer quantifies the load set-points under emergency conditions.
5. Car manufacturer defines the load current profile during emergency condition.
6. Battery manufacturer specifies the nominal battery capacity (Ah) considering available state-of-charge, aging and temperature factors, and based on other information provided by the car manufacturer (load profile, equipment minimum voltage, voltage margin, and voltage drop). This step can be done by following the IEEE Std 1568 calculation method [106].

The simulation model can play a major role starting from step 5. Once the load set-point profile in each car during emergency condition is known, these data can be introduced in each load model to reproduce the emergency scenario (Figure 5.15).

The parameters used in the battery model should then be selected and implemented by working closely with the battery manufacturer. With a detailed simulation model of the train power system, the distribution voltage drops (step 3.) can be evaluated accurately by taking into account the location of the loads. Also, using constant power, constant current and resistive load models the effect of the load behavior under voltage variation on the load current profile can be considered in the battery sizing process. This whole process can require multiple simulations to determine the appropriate battery capacity considering the available state-of-charge, aging and temperature factors as well as the voltage drop, the equipment minimum voltage and the safety voltage margin. Even if using a simulation model still requires some design assumptions, it reduces considerably the number of assumptions compared to the IEEE Std 1568 approach especially regarding the voltage profile and the load behavior.

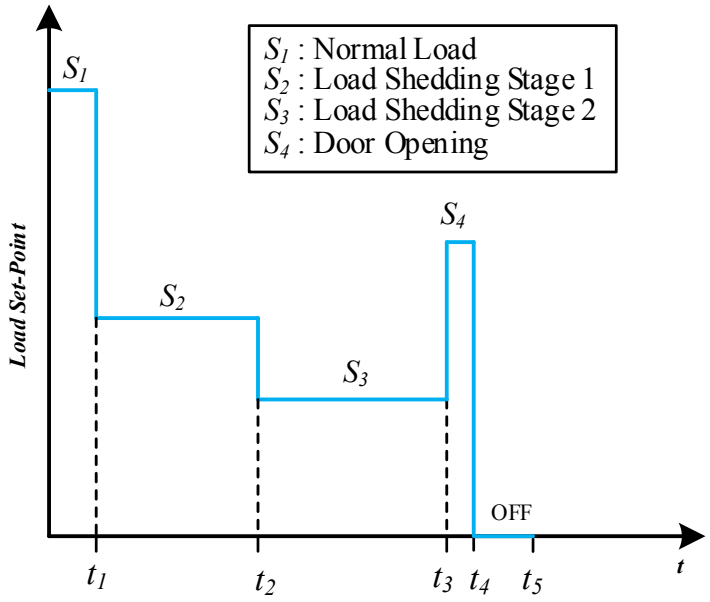

Figure 5.15 Load Set-Point Profile in Emergency Condition

An example of battery sizing analysis is performed using the developed train model in EMTP-RV. A single battery is used in this case in the B2-car to power the whole train under emergency condition. The load set-point profile is entered in percentage of the normal load for

constant current and constant power loads. Resistive loads are never shed in the simulation model. The design factors used for this example are presented in Table 5.2 and are based on [106]. Based on these design factors the overall design margin (F_o) is obtained. The simulation time step Δt is equal to 10 ms and the load model filter time-constant (τ_f) is increased to 20 ms.

Table 5.2: Battery Sizing - Design Factors, Margins and Limits

Description	Symbol	Value
Temperature Derating Factor	F_T	1.0
State-of-Charge Factor	F_{SOC}	0.9
Aging Factor	F_A	0.9
Design Margin	F_M	0.95
Overall Design Margin	F_o	**0.77**
Voltage Limit + Margin	V_{LIM}	**96 V**

The complete battery sizing analysis include the battery and load current profiles (Figure 5.16), the battery and load terminal voltage profiles (Figure 5.17), the available capacity (Q_a), and the battery state-of-charge (SOC) profiles (Figure 5.18). The battery available capacity (Q_a) is calculated using (4.13) and the battery SOC is calculated based on the nominal battery capacity with (4.15).

From these results, even if the load voltage is kept beyond the acceptable voltage limit of 96 V (Figure 5.17), the battery nominal capacity (Q_5=65 Ah) is too small for this application.

In fact, the battery capacity is derated due to the overall design margin (F_o) and the loss of available battery capacity (Q_a) caused by the Peukert effect. It results into a variable minimum total SOC limit throughout the emergency discharge time (Figure 5.18). The two (2) limits depicted on Figure 5.18 can be calculated using (5.1) and (5.2):

The minimum SOC limit due to the design margin (F_o) is given by:

$$SOC_{MIN} = \left(1 - F_o\right) \cdot 100 \tag{5.1}$$

The total minimum SOC limit due to both design margin (F_o) and the Peukert effect (Q_a) is calculated by:

$$SOC_{MIN} = \left(1 - \frac{F_o Q_a}{Q_n}\right) \cdot 100 \tag{5.2}$$

The SOC of the battery should never be at any time under the total minimum SOC limit calculated by (5.2). If it does, it means that at a given instant, the battery is not guaranteed to have enough remaining charge to perform the required function imposed by the emergency load profile. In this case, the battery capacity is not properly sized to sustain the emergency discharge profile after t=52 min. Under the same design consideration, a battery with an increased nominal capacity (Q_5) of 85 Ah can meet both the voltage and capacity requirements over the entire emergency discharge profile (Figure 5.19 and Figure 5.20).

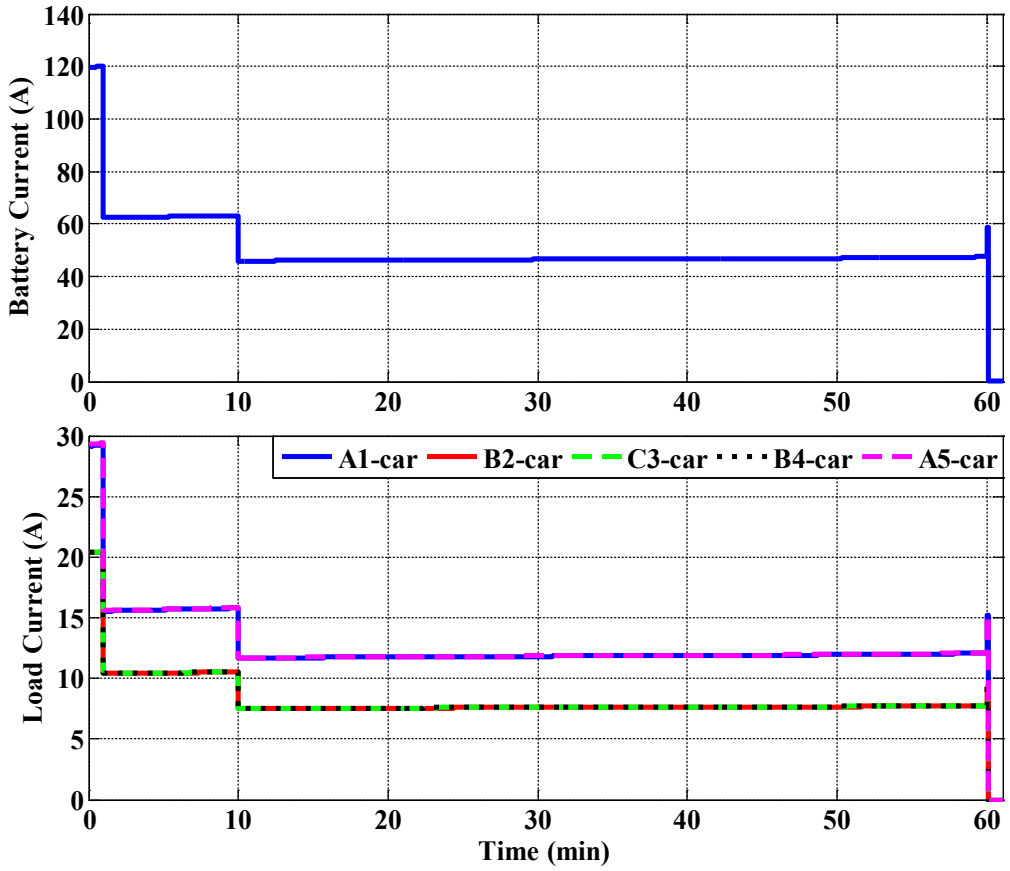

Figure 5.16 Battery and Load Current Profiles (Q_5=65 Ah)

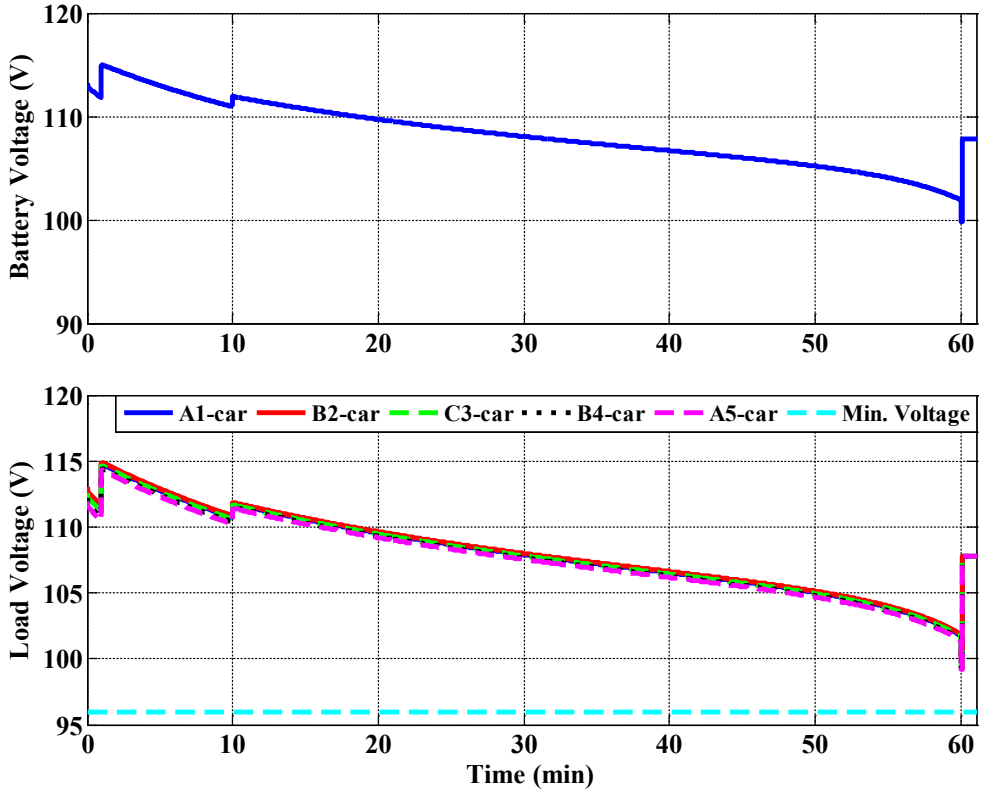

Figure 5.17 Battery and Load Voltage Profiles (Q_5=65 Ah)

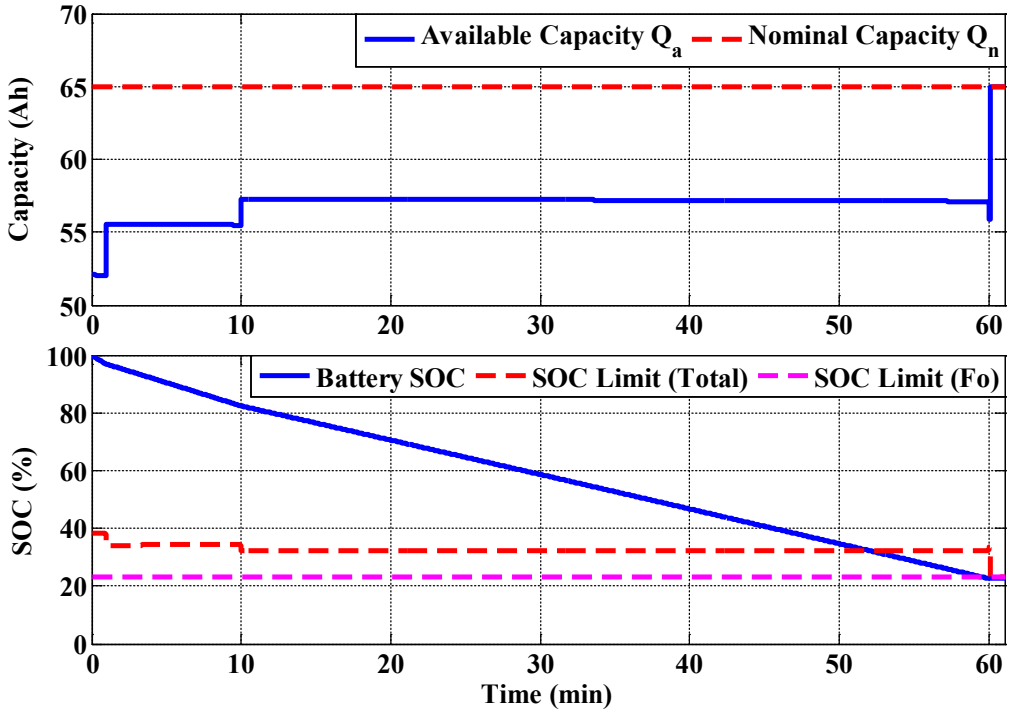

Figure 5.18 Available Battery Capacity and State-of-Charge (Q_5=65 Ah)

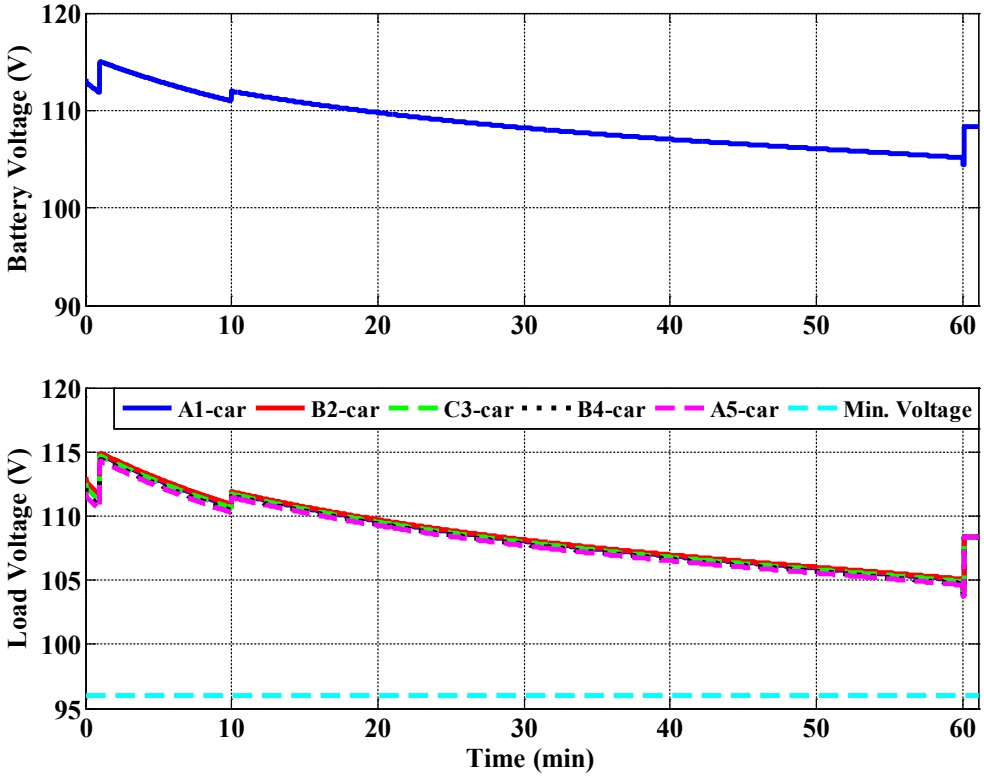

Figure 5.19 Battery and Load Voltage Profiles (Q_5=85 Ah)

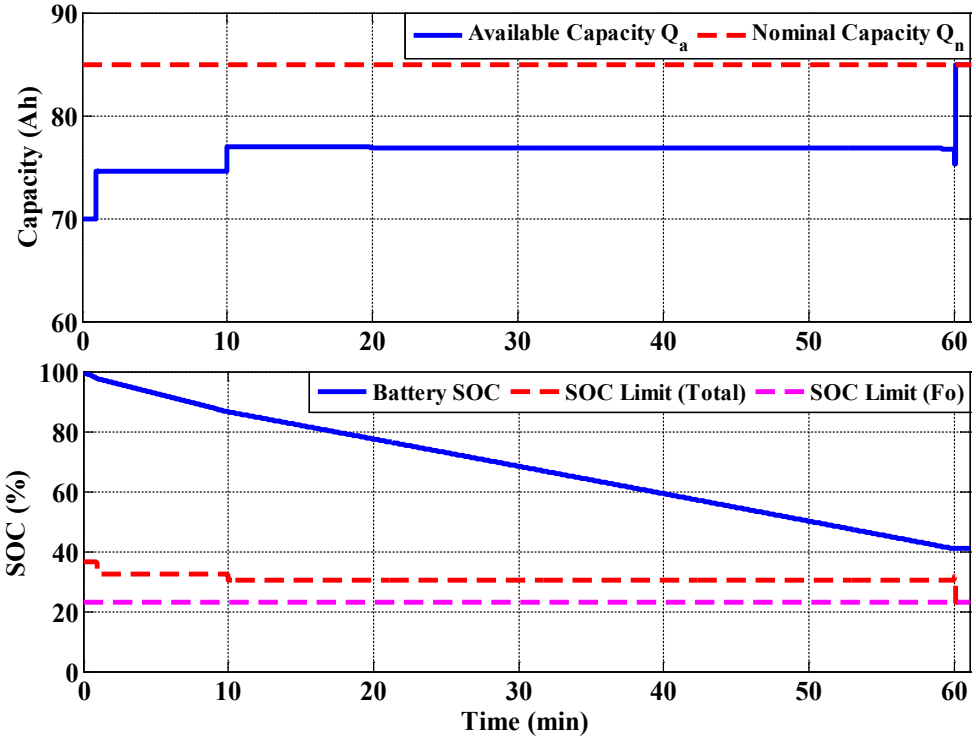

Figure 5.20 Available Battery Capacity and State-of-Charge (Q_5=85 Ah)

5.2 380 V Bus Case Study

5.2.1 Stability

Stability has been discussed in section 3.1 and simple criteria have been established. These criteria were developed for simple equivalent circuits.

However, simulation on the train auxiliary system model have shown that the application of these criteria is not as straightforward as it may appear. In fact, non-linear element such as diodes and the converter VI-characteristic must be considered in stability assessment because they both act as non-linear resistances. Because of the non-linear effect of these elements, the complete power system must be considered throughout the stability analysis. For example, the converter output equivalent VI resistance (R_{VI}) depends on where the converter is operated on its VI-characteristic (Figure 3.9) and the forward resistance of the filter diode is a highly non-linear function of its quiescent point. For the stability simulation performed, the simulation time step Δt is equal to 25 μs.

5.2.1.1 Large Constant Power Load (CPL) and Filter Inductance Effect

Large Constant Power Loads (CPL) must be integrated carefully to avoid instability resulting into voltage oscillations on the DC bus. In Appendix D, the 380 V load power set-points and their input filter parameters from Figure 4.39 are tabulated. The M7-load (P_{CPL} =12 kW) is a large constant power load compared to the other loads.

By neglecting the capacitor internal resistance (R_{ceq}) and the resistive load term (P_R), from section 3.1 stability should be guaranteed if:

$$P_{CPL} < P_{MAX} \tag{5.3}$$

With:

$$P_{MAX} = \frac{V_o^2 R_{EQ} C_F}{L_F} \tag{5.4}$$

$$R_{EQ} = R_{conv} + R_{diode} + R_{cable} + R_F \tag{5.5}$$

For the simple case where only the IVPS in the B2-car is ON, we can say by neglecting the non-linear resistance of the diodes, and by assuming that the IVPS is running in zone (1) that:

$$R_{EQ} = \frac{V_{MAX} - V_{NOM}}{I_{NOM}} + R'_x l_x + R_F \approx 22\ \text{m}\Omega \tag{5.6}$$

Thus, the system voltage is expected to be stable at the M7-load because (5.3) is met:

$$P_{MAX} = \frac{(380\ \text{V})^2 (22\ \text{m}\Omega)(4000\ \mu\text{F})}{(250\ \mu\text{H})} = 50.8\ \text{kW} > 12\ \text{kW} \tag{5.7}$$

To assess stability, simulations are performed using the complete 380 V bus model developed in EMTP-RV. The IVPS are initially running, the filter capacitors are pre-charged through the "cold" resistance and the "hot" resistance is introduced after.

When the loads are turned ON at t=500 ms, if no oscillation occurs or the oscillations are damped, it means that the system is stable. Otherwise the system is considered unstable. Assessment of stability can done by observing the load filter capacitor voltage in the B2 and B4-car after t=500 ms (Figure 5.21). Even if the voltage is oscillatory for a short instant after the loads are turned ON, the oscillations are damped and the voltage is stable in steady-state as expected.

By varying the filter inductance, it is possible to study different scenarios and reach system instability (Figure 5.22). Keeping P_{CPL} constant and increasing the M7-load filter inductance (L_F) to 500 µH, the system is still stable as expected (P_{MAX}=25.4 kW). Increasing the filter inductance (L_F) to 1 mH, the system would have been expected to be stable (P_{MAX}=12.7 kW) but it is not the case because of the interaction between the two (2) large M7-loads in the two (2) B-car.

The impact of the M7-load in the B4-car on stability can be shown by keeping the value of the filter inductance (L_F) to 1 mH and by removing the M7 load in the B4-car. The results show the system is stable as expected even if very oscillatory (Figure 5.23). This is explained by the fact that the M7 constant power load (P_{CPL}=12 kW) is near the maximum acceptable power (P_{MAX}=12.7 kW).

Finally, using the ScopeView tool in EMTP-RV, it is possible to perform signal processing on the waveforms for L_F=1 mH. By calculating the Fast Fourier Transform (FFT) of the M7 load capacitor voltage in the B2-car, we see that the frequency of the oscillation is at 80 Hz (Figure 5.24).

In fact, it was easy to predict because it is no other than the cut-off frequency of the M7-Load input filter:

$$f_o = \frac{1}{2\pi\sqrt{L_F C_F}} = \frac{1}{2\pi\sqrt{(1\text{ mH})(4000\ \mu\text{F})}} = 80\text{ Hz} \tag{5.8}$$

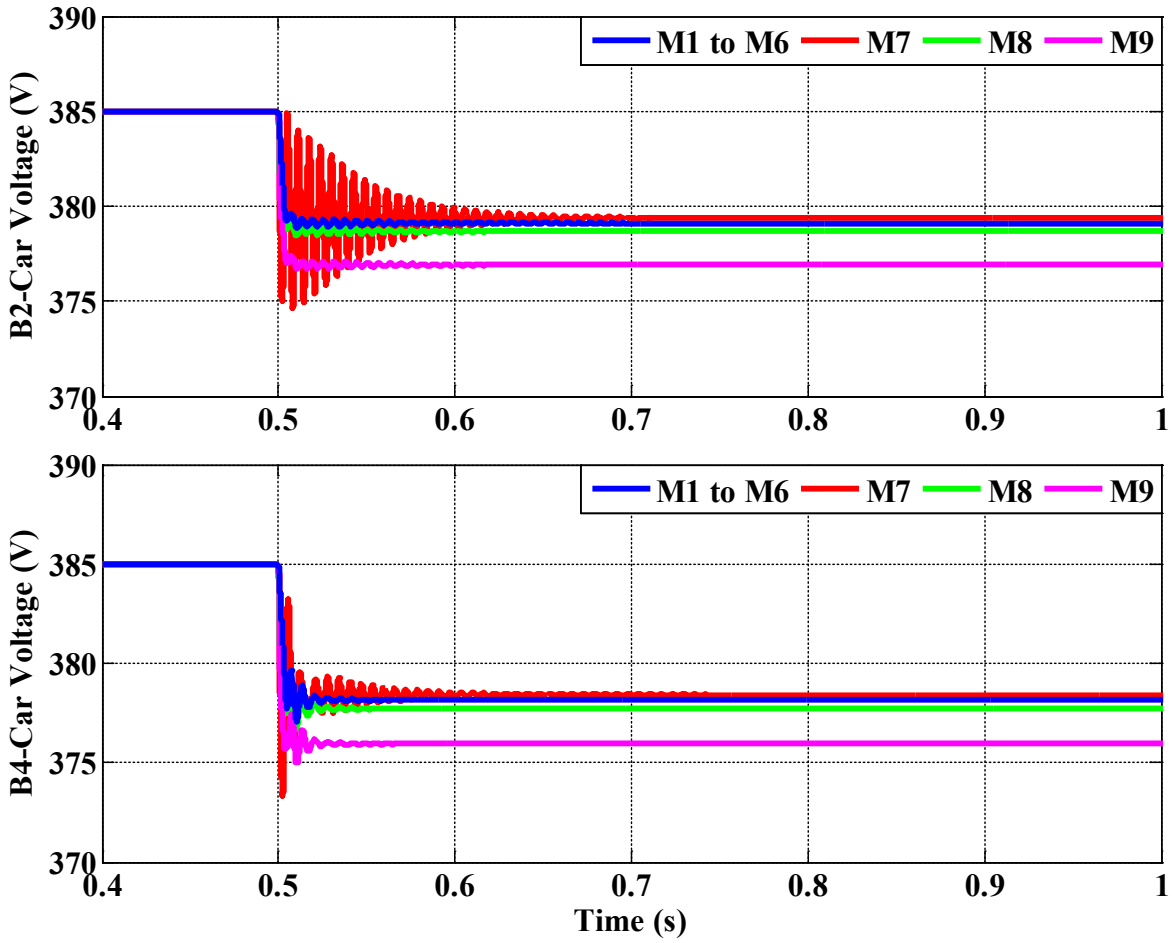

Figure 5.21 Load Filter Capacitor Voltage in the B2- and B4-car

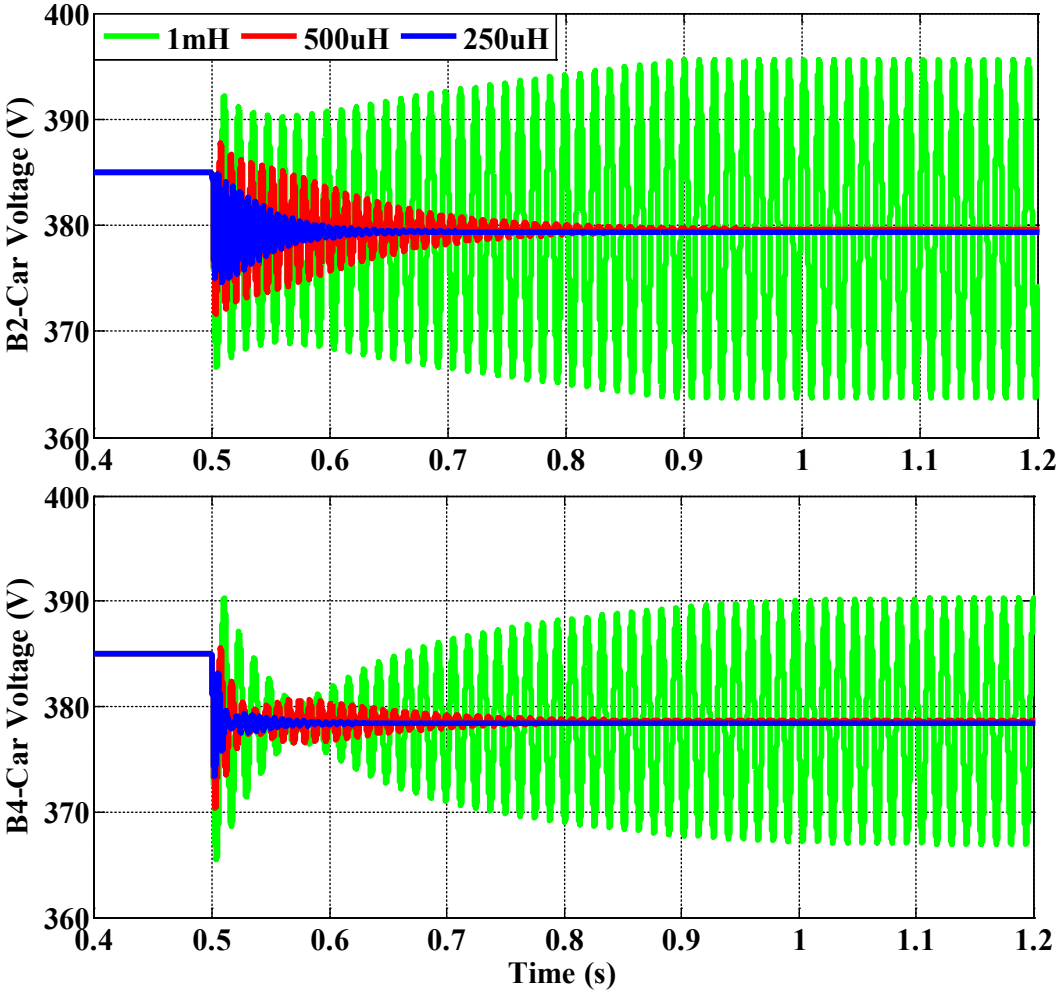

Figure 5.22 M7-Load Filter Capacitor Voltage for Different Filter Inductance (L_F)

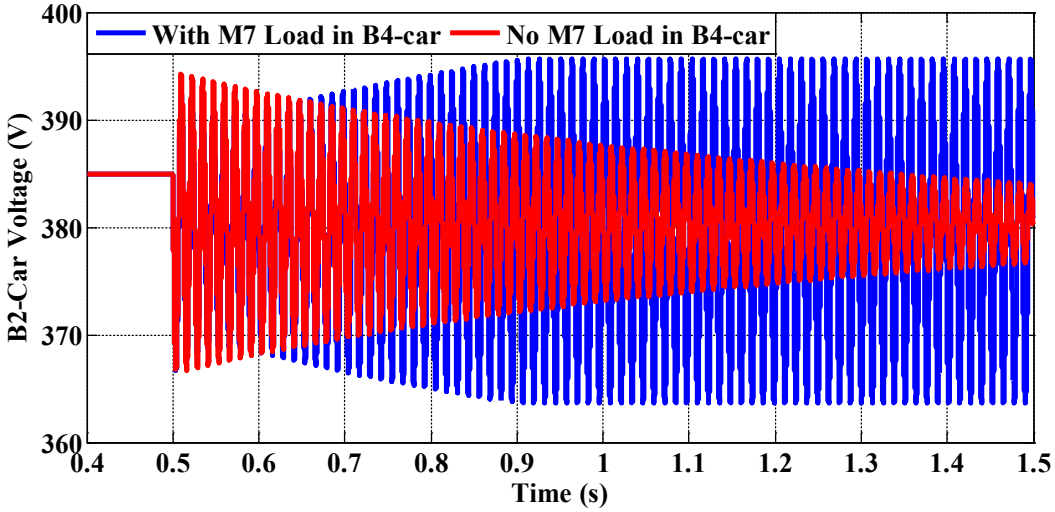

Figure 5.23 Loads Impact on M7-Load Filter Capacitor Voltage Stability (L_F=1 mH)

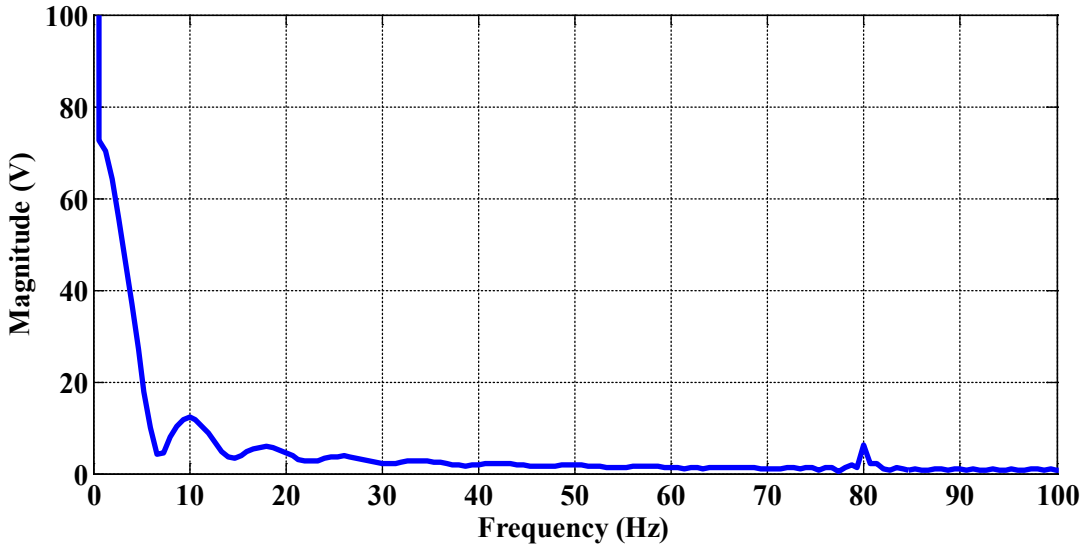

Figure 5.24 FFT of M7-Load Filter Capacitor Voltage (L_F=1 mH)

5.2.1.2 Capacitor ESR Effect

In the previous section, it has been observed that the system is unstable when the two (2) large M7-loads are turned ON simultaneously with a filter inductance (L_F) of 1 mH and a filter capacitance (C_F) of 4000 µF. The capacitor ESR was assumed to be nil. Let's now increase the capacitor ESR to 10 mΩ, the system becomes stable (Figure 5.25). Reducing the capacitor ESR to 2 mΩ and the system is back unstable. This case is used to reproduce the possible stability issue when changing an old electrolytic capacitor having a high ESR by a new film capacitor having a low ESR.

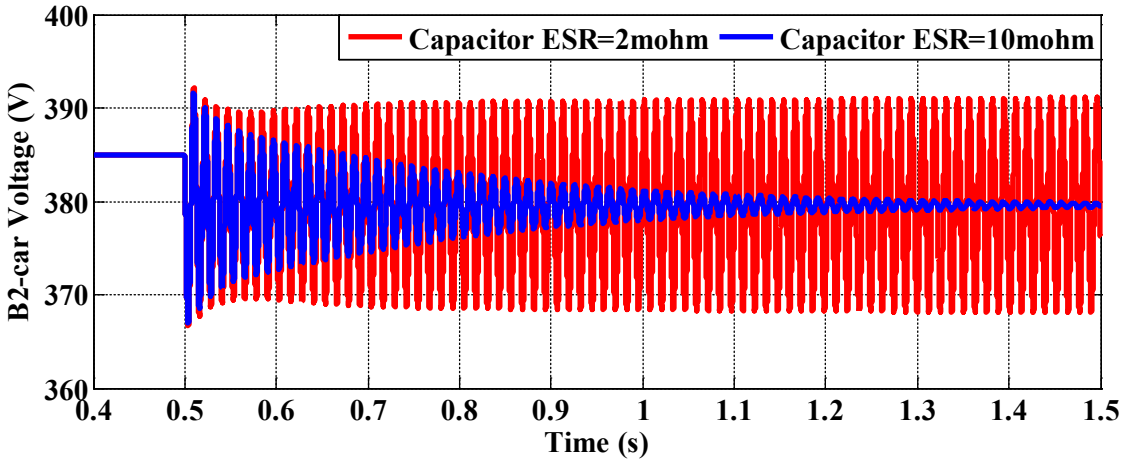

Figure 5.25 Impact of M7-Load Filter Capacitor ESR on Voltage Stability

5.2.1.3 Constant Power Load Model Effect

Again, in section 5.2.1.1, the system was unstable when the two (2) large M7 loads were turned ON simultaneously with a filter inductance (L_F) of 1 mH and a filter capacitance (C_F) of 4000 µF. The M7-load model filter time-constant has been selected very small (τ_f=0.1 ms) to ensure that the load was acting as a tightly controlled constant power load. By increasing the M7-load model filter time-constant by a factor of 10 (τ_f=1 ms), the system becomes stable (Figure 5.26). This is because the two (2) M7-load are less behaving as constant power loads during transient. As a matter of fact, changing the load behavior has been in the past the preferred solution to avoid constant power load instability.

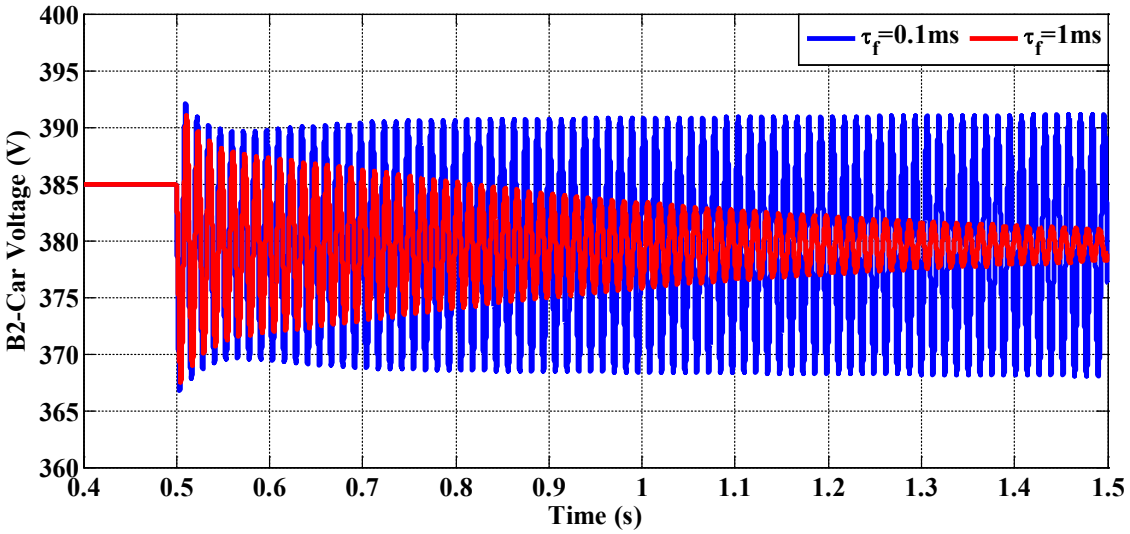

Figure 5.26 Impact of M7-Load Behavior on Voltage Stability

5.2.2 Inrush

Inrush current can also be studied using the developed train auxiliary system model in EMTP-RV. The Intermediate Voltage Bus (IVB) is particularly interesting because of the large number of filters connected along the 380 V bus. For the inrush simulation performed, the simulation time step Δt is equal to 10 µs.

Inrush current studies must be done for normal operating scenario and degraded mode conditions. For example, under the loss of one (1) IVPS, the other IVPS must be capable of supporting the total bus inrush current. Also, the fuses (F380) should not melt or even start to melt under the worst inrush current conditions. The fuses are rated 160 A in this case.

Two (2) cases are presented. The first case is a normal operating scenario with both IVPS running while the second case is a degraded mode scenario with only the B2-car IVPS running.

For the first case both IVPS are initially running, all MCBs are initially closed, all the loads are initially OFF and the two (2) S380 switches are simultaneously closed at t=500 ms. The load voltage in both A-car (the farthest), the inrush current contribution from each car and the total current seen by both IVPS are shown in Figure 5.27.

For the second case, only the IVPS in the B2-car is initially running. All MCBs are also initially closed, all the loads are initially OFF and the S380 switch in the B2-car is closed at t=500 ms. The load voltage in both A-car, the inrush current contribution from each car and the total current seen by the IVPS are shown in Figure 5.28.

In both case, the 160 A fuses (S180) are adequate because they do not melt. The maximum current seen by a single IVPS is 1200 A (Figure 5.28). Also mention that the undervoltage in the A1- and A5-car is lower when a single IVPS must support the entire inrush current.

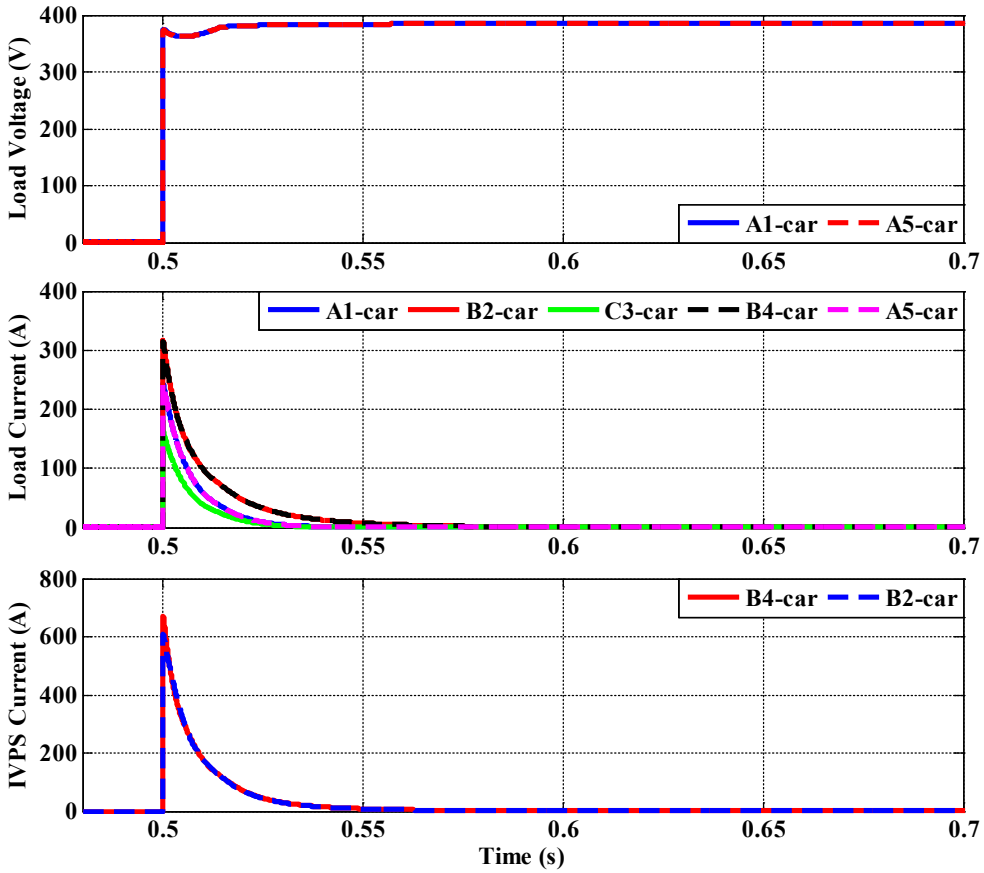

Figure 5.27 Inrush Current Analysis in Normal Operating Mode (2 IVPS)

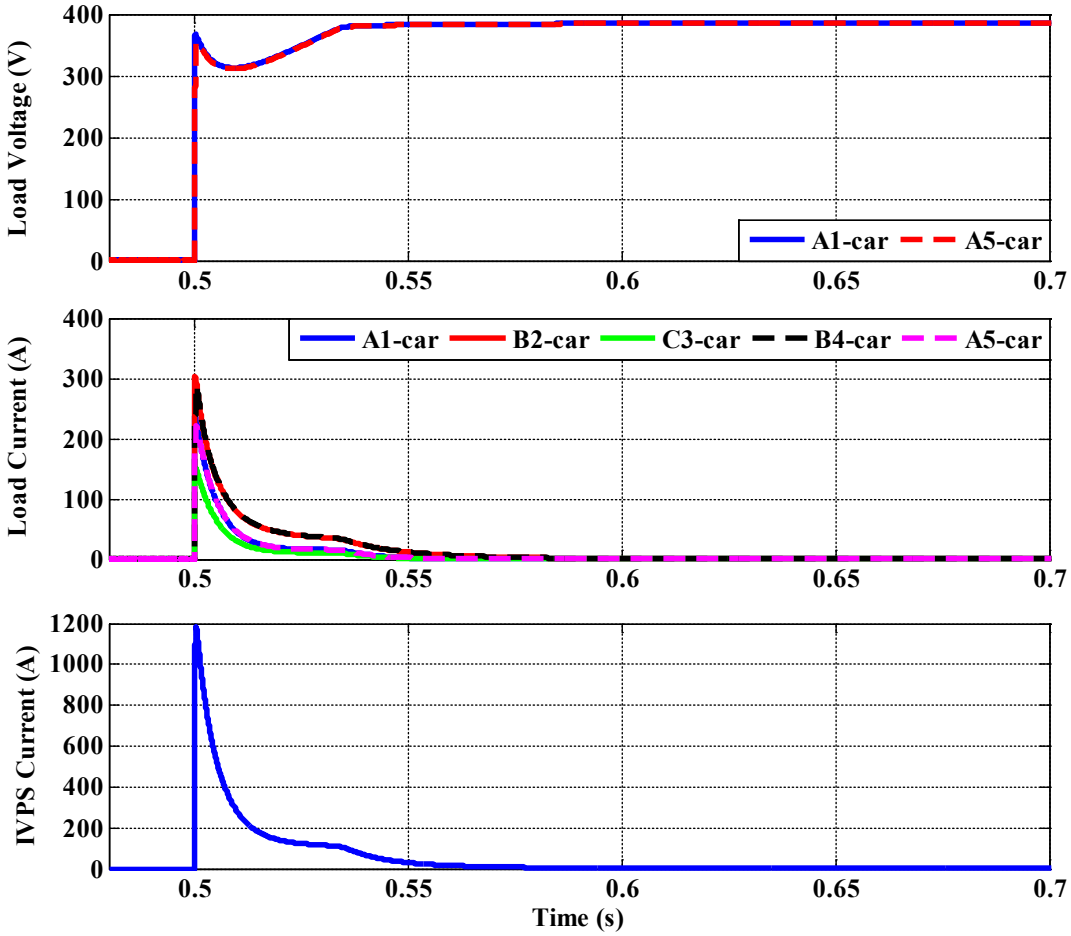

Figure 5.28 Inrush Current Analysis in Degraded Operating Mode (1 IVPS in the B2-car)

CHAPTER 6 CONCLUSION AND RECOMMENDATIONS

One of the main objective in railway vehicle manufacturing business is to provide vehicles with optimal operational performance. It requires innovative solutions. At the end, the main goals are to increase the efficiency and reduce the weight and the cost of the manufactured vehicles while keeping high levels of reliability, availability, maintainability, and safety.

The new developments in 380 V DC systems are interesting for improvement and standardization of on-board DC auxiliary distribution. DC auxiliary systems were and are typically at voltage levels ranging between 24 V to 110 V. The shift toward higher voltage DC auxiliary systems leads to new technical challenges and safety concerns because of the high level of energy implicated.

The development of new architectures and the integration of new technologies must be done with an appropriate understanding of the rail environment and the actual standards. Analysis using simulation models combined with established industry practices, industry past experiences, and standards can greatly reduce the risks.

In this project, a complete train DC auxiliary system model has been successfully developed in EMTP-RV. It has been divided into two (2) decoupled bus having very different characteristics in order to present very different power system analysis. Models of the network components have been developed and validated individually based on the available information. For each component, a literature review has been performed to determine the model assumptions. Depending on the available information, the models were validated based on the expected theoretical behavior, applicable standards, manufacturer's data, or field measurements. The models were finally used to develop different vehicle models and a complete train model has been built by assembling multiple vehicles together.

The developed train model is highly oriented toward the industry specific needs and provides sufficient level of details for design purpose, architecture development, and standardization of railway car DC auxiliary systems. In fact, at the beginning of this project, multiple integration analysis were identified and the model has been developed to meet these simulation objectives. In addition, a literature survey highlighted other design considerations, multiple integration and operational issues which may arise when developing and operating DC systems.

The capabilities of the simulation model have been demonstrated for different power system studies such as: overcurrent protection, ground fault analysis, transient overvoltage, insulation coordination, battery sizing, voltage stability, and inrush current. Prior to perform these analysis, a complete review of power system transients in DC systems has been performed to understand the influence of the network parameters.

Complete overcurrent protection studies can be performed. It includes fault current calculation, protective devices detection time evaluation, and protective devices arcing characteristics replication. Simulation results have been successfully validated by field experiments. Due to proprietary information, it was not possible to show all these results but section 4.2.2.3 has introduced through the battery model validation some of the fault experimental results.

The simulation model has also been used to design a simple ground fault detector and to reproduce the single-pole interruption problem which may occurs during double-fault-to-ground condition in a high resistance DC grounding system. This case is particularly interesting because it shows that the complete model can be used for the purpose of engineering understanding to reproduce scenarios with multiple conditions and to observe various signals. The fault and ground fault detector currents, the current in each pole of the circuit breaker, and the detection and opening evolution of the circuit breaker were necessary signals for a complete understanding of this problem. The results have demonstrated the importance of detection and mitigation of a first fault-to-ground condition in a high resistance DC grounding system.

Transient overvoltage at circuit breaker opening has also been investigated. To reproduce transient overvoltage at circuit breaker opening, a detailed model based on the Schwarz arc model is implemented. It is in fact impossible to reproduce accurately transient overvoltage at circuit breaker opening in DC system without a detailed model of the circuit breaker arcing behavior. A transient overvoltage filter has also been designed and the performance of a selected MOV were compared to the designed filter. Results have demonstrated that the transient overvoltage devices location is important to improve their protection capability during circuit breaker opening. The results have shown that they should be located near the switching devices; the cable resistance and inductance reducing their effectiveness. Finally, the results have demonstrated that protecting DC bus using low voltage MOV is not the most effective method. MOV are of a limited use to

meet IEC 60571 requirements. The developed capacitor-based filter circuit is in fact much more effective.

A complete battery sizing analysis has also been performed including the battery and load current profiles, the battery and load terminal voltage profiles, the available capacity and the battery state-of-charge evolution. Battery sizing analysis requires detailed model of the battery including the Peukert effect as well as detailed models of the loads taking into account their reaction to voltage fluctuation. Experimental measurements have shown that the battery simulation model is accurate enough for battery sizing (Section 4.2.2.3).

Moreover, stability analysis based on criteria found in the literature were performed. The impacts of network parameters and load behavior on voltage stability have been studied based on their theoretical behavior. Voltage stability analysis requires high level of details and non-linear modelling capabilities. For example, the load input filters need to be modeled with many details taking into account parameters such as inductance and capacitor ESR and diode non-linear VI-characteristic. Large constant power loads need also to be accurately modeled because they are the main cause of voltage instability in DC systems.

Finally, inrush current has been investigated when multiple input filter capacitors are energized simultaneously. Normal and degraded operating scenarios were considered. The simulation model allows in fact to study multiple scenarios and provides an easy way to compare the different scenarios. For accurate inrush current analysis, it is important to model accurately the inrush current limitation circuits of each load front-end. Experimental results have shown that using the nominal (cold) resistance value of NTC resistor limitation circuit in the simulation model is accurate enough to evaluate the peak inrush current (Section 4.5.6).

The main limits of the developed models are especially related to the constraints in data availability. All the models were in fact developed with the mindset of being easily filled with typical available data from manufacturers but also of being easily reused. However, available data from manufacturers are not always complete to perform advanced analysis. Sometimes assumptions must be made for certain parameters. For example, data on circuit breaker arcing characteristic are never provided by low voltage circuit breaker manufacturers. The parameters were selected to reproduce approximatively the transient overvoltage based on what have been

observed in the field to be realistic. Converter dynamic and control structure is also something generally unknown that may be necessary to integrate in the future for more advanced analysis.

For complex power systems, simulation requires the formulation of a large number of detailed models to develop a power system model that represents the expected behavior of the real system. Models should be developed and simulation should be performed during the design phase of every project and the results from the testing phases should be used to validate the developed models and increase model reliability for future use in power system analysis.

The developed DC auxiliary system model is also initialized in the time-domain. A transient analysis tool such as EMTP-RV can perform the initialization process based on the AC load-flow solution before the time-domain computation. This means that the system can be already initialized in steady-state at the beginning of the time-domain simulation at t=0. It reduces the simulation time required to initialize the system in the time-domain. In DC systems, the initialization must be performed manually or during the time-domain solution. The control blocks must be initialized as well. The initialization process has been partially implemented in EMTP-RV to ensure stability during time-domain initialization. However, further work should include the development of a fully-integrated method to find the steady-state solution with detailed models in MTDC systems.

To conclude, the complete train DC auxiliary system model developed in EMTP-RV does meet the initial objectives. It can be used to perform various power system studies with high level of sophistication which could not be done before. Moreover, sequential accidents analysis models (FTA, FMEA, FMECA) are generally used in the railway industry because they are easy to represent graphically. However, they are of a limited use for complex dynamic systems. Detailed simulation models can be used as an efficient complementary tool to investigate safety hazards at an early design stage such as it reduces the cost of the mitigation process.

BIBLIOGRAPHY

[1] American Public Transportation Association (APTA) [online], "Ridership Report – First Quarter 2015 Ridership – Definitions of terms and abbreviations used". Available: http://www.apta.com/resources/statistics/Pages/ridershipreport.aspx.

[2] P. Pozzobon, "Transient and steady-state short-circuit currents in rectifiers for DC traction supply," *Vehicular Technology, IEEE Transactions on*, Vol. 47, no. 4, pp.1390-1404, Nov. 1998.

[3] IEEE Guide for Rail Transit Traction Power Systems Modeling, *IEEE Std 1653.3-2012*, Jan. 18, 2013.

[4] Bombardier Transportation [online], www.bombardier.com/en/transportation.

[5] J.S. Morton, "Circuit Breaker and Protection Requirements for DC Switchgear Used in Rapid Transit Systems," *Industry Applications, IEEE Transactions on*, vol.IA-21, no.5, pp.1268-1273, Sept.-Oct. 1985.

[6] D. Paul, "DC Traction Power System Grounding," *Industry Applications, IEEE Transactions on*, vol.38, no.3,pp.818-824, May-June 2002.

[7] M. Berger, C. Lavertu, I. Kocar, and J. Mahseredjian, "Performance Analysis of DC Primary Power Protection in Railway Cars using a Transient Analysis Tool," *Vehicle Power and Propulsion Conference (VPPC), 2015 IEEE*, Oct. 2015 [accepted].

[8] R.R. Pecharroman, A. Lopez-Lopez, A.P. Cucala, and A. Fernandez-Cardador, "Riding the Rails to DC Power Efficiency: Energy efficiency in dc-electrified metropolitan railways," *Electrification Magazine, IEEE* , vol.2, no.3, pp.32-38, Sept. 2014.

[9] IEEE Standard for Passenger Train Auxiliary Power Systems Interfaces, *IEEE Std 1476-2000*, March 30, 2000.

[10] IEC Railway applications – Electric Equipment for Rolling Stock, Part 1: General Service Conditions and General Rules, *IEC 60077-1*, 1999.

[11] R. Cuzner, D. MacFarlin, D. Clinger, M. Rumney, and G. Castles, "Circuit Breaker Protection Consideration in Power Converter-Fed DC Systems," *IEEE Electric Ship Technologies Symposium,* pp.360-367, April 2009.

[12] B. Laska, P. Steimer, M. Debruyne, L. Cecchi, R. Klein, M. Kunz, C. Laurencin, and M. Weytens, "Standardization of system architectures for onboard auxiliary power supply systems," *Power Electronics and Motion Control Conference (EPE/PEMC), 14th International*, pp.S8-5,S8-9, Sept. 2010.

[13] Y. Khersonsky, "Advancing New Technologies in Electrical Ships: IEEE standards are the risk mitigation tool," *Electrification Magazine, IEEE* , vol.3, no.2, pp.34-39, June 2015.

[14] M.-A. Lemaire, "Développement d'un premier modèle intégral d'un réseau électrique d'avion sous EMTP-RV," M.S. thesis, École Polytechnique de Montréal, Montréal, QC, Canada, 2011.

[15] L. Montealegre Lobo, "First Simulink Benchmark for Off-Line and Real-Time Simulation of More-Electric Aircraft (MEA) Electrical Power System," M.S. thesis, École Polytechnique de Montréal, Montréal, QC, Canada, 2011.

[16] S. R. Rudraraju, "Small signal and transient stability analysis of MVDC shipboard power system," M.S. thesis, Mississippi State University, MS, 2009.

[17] J. M. Candelaria, "Fault detection and isoloation in low-voltage DC-bus microgrid systems," M.S. thesis, University of Colorado at Denver, CO, 2012.

[18] J. Mahseredjian, V. Dinavahi, and J. A. Martinez, "Simulation Tools for Electromagnetic Transients in Power Systems: Overview and Challenges," *Power Delivery, IEEE Transactions on,* vol. 24, pp. 1657-1669, July 2009.

[19] N. Mohan, T.M. Undeland, and W.P. Robbins, *Power Electronics: Converters, Applications and Design*, Third Edition, John Wiley & Sons, Inc., 824 p., 2002.

[20] J. Mahseredjian, S. Dennetière, L. Dubé, B. Khodabakhchian, and L. Gérin-Lajoie, "On a new approach for the simulation of transients in power systems," Electric Power Systems Research, Vol. 77, Issue 11, pp. 1514-1520, Sept. 2007.

[21] Electrical Safety in Low Voltage Distribution Systems up to 1000V a.c and 1500 V d.c – Equipment for testing, measuring or monitoring of protective measures - Part 1: General Requirements, *IEC 61557-1*, 2007.

[22] IEEE Recommended Practice for 1 kV to 35 kV Medium-Voltage DC Power Systems on Ships, *IEEE Std 1709-2010* , Nov. 2010.

[23] Peng Wang, L. Goel, L, Xiong Liu, and Fook Hoong Choo, "Harmonizing AC and DC: A Hybrid AC/DC Future Grid Solution," *Power and Energy Magazine, IEEE* , vol.11, no.3, pp.76-83, May-June 2013.

[24] R.E.J Quigley, "More Electric Aircraft," in *Applied Power Electronics Conference and Exposition, APEC '93. Conference Proceedings, Eighth Annual*, pp. 906-911, March 1993.

[25] J.A. Rosero, J.A. Ortega, E. Aldabas, and L. Romeral "Moving towards a more electric aircraft," *Aerospace and Electronic Systems Magazine, IEEE*, vol.22, no.3, pp.3-9, March 2007.

[26] S.D.A. Fletcher, P.J. Norman, S.J. Galloway, and G.M. Burt, "Determination of protection system requirements for DC unmanned aerial vehicle electrical power networks for enhanced capability and survivability," in *Electrical Systems in Transportation, IET*, Vol. 1, Iss. 4, pp.137-147, June 2011.

[27] J.G. Ciezki, and R.W. Ashton, "Selection and stability issues associated with a navy shipboard DC zonal electric distribution system," *Power Delivery, IEEE Transactions on*, vol.15, no.2, pp.665-669, April 2000.

[28] P. Cairoli, and R.A. Dougal, "New Horizon in DC Shipboard Power Systems: New Fault protection strategies are essential to the adoption of dc power systems.," *Electrification Magazine, IEEE*, vol.1, no.2, pp.38-45, Dec. 2013.

[29] A. Sannino, G. Postiglione, and M.H.J. Bollen, "Feasibility of a DC network for commercial facilities," *Industry Applications, IEEE Transactions on*, vol. 39, no.5, pp.1499-1507, Sept.-Oct. 2003.

[30] D. Salomonsson, and A. Sannino, "Low-Voltage DC distribution System for Commercial Power Systems With Sensitive Elecronic Loads," *Power Delivery, IEEE Transactions on*, vol.22, no.3, pp.1620-1627, July 2007.

[31] M.E. Baran, and N.R. Mahajan, "DC distribution for industrial systems: opportunities and challenges," *Industry Applications, IEEE Transactions on*, vol.39, no.6, pp.1596-1601, Nov.-Dec. 2003.

[32] G. AlLee, and W. Tschudi, "Edison Redux: 380 Vdc Brings Reliability and Efficiency to Sustainable Data Centers," Power and Energy Magazine, IEEE, vol.10, no.6, pp.50-59, Nov.-Dec. 2012.

[33] D.J. Becker, and B.J. Sonnenberg, "DC microgrids in buildings and data centers," *Telecommunications Energy Conference (INTELEC), IEEE 33rd International*, pp.1-7, Oct. 2011.

[34] R. Cuzner, and G. Venkataramanan, "The status of DC micro-grid protection" *IEEE Industry Applications Society Annual Meeting,* pp.1-8, Oct. 2008.

[35] Jae-Do Park, J. Candelaria, Liuyan Ma, and K. Dunn, "DC Ring-Bus Microgrid Fault Protection and Identification of Fault Location," *Power Delivery, IEEE Transactions on*, vol.28, no.4, pp.2574-2584, Oct. 2013.

[36] Lianxiang Tang, and Boon Teck Ooi, "Locating and Isolating DC Faults in Multi-Terminal DC Systems," *Power Delivery, IEEE Transactions on*, vol.22, no.3, pp.1877-1884, July 2007.

[37] D. Salomonsson, L. Soder, and A. Sannino, "Protection of Low-Voltage DC Microgrids," *Power Delivery, IEEE transactions on*, vol.24, no.3, pp.1045-1053, July 2009.

[38] P.G. Cardinal, "Grounding: Bonding to Earth - We Leave Out Something Big When We Just Say "Bonding"," *Industry Applications Magazine, IEEE*, vol.21, no.3, pp.40-47, May-June 2015.

[39] E. Rappaport, "Does Grounding Make a System Safe?: Analyzing the Factors That Contribute to Electrical Safety," *Industry Applications Magazine, IEEE*, vol.21, no.3, pp.48-57, May-June 2015.

[40] Nailen, R.L., "Battery protection - where do we stand?," *Industry Applications, IEEE Transactions on*, vol.27, no.4, pp.658-667, Jul.-Aug., 1991.

[41] S.D.A. Fletcher, P.J. Norman, S.J. Galloway, and G.M. Burt, "Mitigation against overvoltages on a DC marine electrical system," *Electric Ship Technologies Symposium, ESTS 2009. IEEE*, pp.420-427, April 2009.

[42] R. Morel, "Schneider Cahier technique no154 - LV circuit breaker breaking technique," pp.1-29, 2000.

[43] T. Gammon, Wei-Jen Lee, Zhenyuan Zhang, and B.C. Johnson, "A Review of Commonly Used DC Arc Models," *Industry Applications, IEEE Transactions on*, vol.51, no.2, pp.1398-1407, March-April 2015.

[44] C.H. Cline, "Fuse Protection of DC System", in *Annual meeting of the American Power Conference*, pp. 1-6, April 1995.

[45] G.D. Gregory, "Applying low-voltage circuit breakers in direct current systems," *Industry Applications, IEEE Transactions on*, vol.31, no.4, pp.650-657, Jul.-Aug. 1995.

[46] D.R. Doan, "Arc Flash Calculations for Exposures to DC Systems," *Industry Applications, IEEE Transactions on*, vol.46, no.6, pp.2299-2302, Nov.-Dec. 2010.

[47] M.E. Valdes, C. Cline, S. Hansen, and T. Papallo, "Selectivity Analysis in Low-Voltage Power Distribution Systems with Fuses and Circuit Breakers," in *Industry Applications, IEEE Transactions on*, Vol. 46, no. 2, pp. 593-602, March-April 2010.

[48] B. DiMarco, and S.R. Hansen, "Interplay of energies in circuit breaker and fuse combinations," *Industry Applications, IEEE Transactions on*, vol.29, no.3, pp.557-561, May-June 1993.

[49] E. Belbel, and M. Lauraire, "Behavior of Switching Arc in Low-Voltage Limiter Circuit Breakers," in *Components, Hybrids, and Manufacturing Technology, IEEE Transactions on*, Vol. 8, no. 1, pp.3-12, March 1985.

[50] L. Kojovic, and S. Hassler, "Application of current limiting fuses in distribution systems for improved power quality and protection," *Power Delivery, IEEE Transactions on*, vol.12, no.2, pp.791-800, April 1997.

[51] S. Krstic, E.L. Wellner, A.R. Bendre, and B. Semenov, "Circuit Breaker Technologies for Advanced Ship Power Systems," *Electric Ship Technologies Symposium, 2007. ESTS '07. IEEE*, pp.201-208, May 2007.

[52] IEEE Recommended Practice for Industrial and Commercial Power Systems Analysis, *IEEE Std 399-1997*, April 1997.

[53] IEC Railway applications – Electronic Equipment used on Rolling Stock, *IEC 60571*, 2012.

[54] P. Kundur, J. Paserba, V. Ajjarapu, G. Andersson, A. Bose, C. Canizares, N. Hatziargyriou, D. Hill, A. Stankovic, C. Taylor, T. Van Cutsem, and V. Vittal, "Definition and classification of power system stability IEEE/CIGRE joint task force on stability terms and definitions," *Power Systems, IEEE Transactions on*, vol.19, no.3, pp.1387-1401, Aug. 2004.

[55] R.T. Pinto, "Multi-Terminal DC Networks: System Integration, Dynamics and Control," Ph.D Thesis, Delft University of Technology, Netherlands, 2014.

[56] P. Karlsson, and J. Svensson, "DC bus voltage control for a distributed power system," *Power Electronics, IEEE Transactions on*, vol.18, no.6, pp.1405-1412, Nov. 2003.

[57] J.M. Guerrero, J.C Vasquez, J. Matas, L.G de Vicuña, and M. Castilla, "Hierarchical Control of Droop-Controlled AC and DC Microgrids - A General Approach Toward Standardization," *Industrial Electronics, IEEE Transactions on*, vol.58, no.1, pp.158-172, Jan. 2011.

[58] A.B Jusoh, "The instability effect of constant power loads," *Power and Energy Conference, PECon 2004. Proceedings. National*, pp.175-179, Nov. 2004.

[59] A. Emadi, A. Khaligh, C.H. Rivetta, and G.A. Williamson, "Constant power loads and negative impedance instability in automotive systems: definition, modeling, stability, and control of power electronic converters and motor drives," *Vehicular Technology, IEEE Transactions on*, vol.55, no.4, pp.1112-1125, July 2006.

[60] N.O. Sokal, "System oscillations from negative input resistance at power input port of switching-mode regulator, amplifier, DC/DC converter, or DC/DC inverter," *Power Electronics Specialists Conference, 1973 IEEE*, pp.138-140, June 1973.

[61] M. Belkhayat, R. Cooley, and A. Witulski, "Large signal stability criteria for distributed systems with constant power loads," *Power Electronics Specialists Conference, PESC '95 Record., 26th Annual IEEE* , vol.2, pp.1333-1338, June 1995.

[62] M. Bollen, *Understanding Power Quality Problems: Voltage Sags and Interruptions,* Wiley-IEEE Press, 2000.

[63] K. Hirose, T. Tanaka, T. Babasaki, S. Person, O. Foucault, B.J. Sonnenberg, and M. Szpek, "Grounding concept considerations and recommendations for 400VDC distribution system," *Telecommunications Energy Conference (INTELEC), 2011 IEEE 33rd International*, pp.1-8, Oct. 2011.

[64] Lulu Li, Jing Yong, Liqiang Zeng, and Xiaoyu Wang, "Investigation on the system grounding types for low voltage direct current systems," *Electrical Power & Energy Conference (EPEC), 2013 IEEE*, pp.1-5, Aug. 2013.

[65] Low Voltage Electrical Installations – Part 1: Fundamental principles, assessment of general characteristics, definitions, *IEC 60364-1*, 2005.

[66] IEEE Recommended Practice for the Design of DC Auxiliary Power Systems for Generating Systems, *IEEE Std 946-2004*, June 2005.

[67] G.D. Gregory, "Single-pole short-circuit interruption of molded-case circuit breakers," *Industry Applications, IEEE Transactions on*, vol.35, no.6, pp.1265-1270, Nov./Dec. 1999.

[68] Effects of Current on Human Beings and Livestock – Part 1: General aspects, *IEC 60479-1*, 2005.

[69] Federal Transit Administration (FTA) [online], Handbook for Transit Safety and Security Certification, Nov. 2012, Available: http://www.fta.dot.gov/documents/SSC.pdf.

[70] Federal Transit Administration (FTA) [online], Rail Safety Statistics Report – An analysis of safety data reported by state safety oversight agencies and rail transit agencies for the years 2003- 2008,
Available: http://transit-safety.volpe.dot.gov/publications/RailSafety/Rail_Safety_Statistics_Report_2009-FINAL.pdf.

[71] C.L. Brooks, "Integrating Arc-Flash Analysis: A Look at Protective Device Coordination," *Industry Applications Magazine, IEEE*, vol.20, no.3, pp.14-23, May-June 2014.

[72] P. Underwood, and P. Waterson, "Systems thinking, the Swiss Cheese Model and accident analysis: A comparative systemic analysis of the Grayrigg train derailment using the ATSB, AcciMap and STAMP models," in *Accident Analysis & Prevention*, vol. 68, pp.75-94, 2014.

[73] E. Hollnagel, "Understanding accidents – from root causes to performance variability," *Human Factors and Power Plants, 2002, Proceedings of the 2002 IEEE 7th Conference on*, pp.1-6, 2002.

[74] A. Emadi, M. Ehsani, and J.M. Miller, *Vehicular Electric Power Systems: Land, Sea, Air, and Space Vehicles, New York, NY, Marcel Dekker,* 2003.

[75] S.D. Sudhoff, K.A. Corzine, S.F. Glover, H.J. Hegner, and H.N. Robey Jr., "DC link stabilized field oriented control of electric propulsion systems," *Energy Conversion, IEEE Transactions on* , vol.13, no.1, pp.27-33, March 1998.

[76] Short-circuit currents in d.c. auxiliary installations in power plants and substations – Part 1: Calculation of short-circuit currents, *IEC 61660-1*, 1997.

[77] A. Berizzi, A. Silvestri, D. Zaninelli, and S. Massucco, "Short-circuit current calculations for DC systems," *Industry Applications, IEEE Transactions on*, vol.32, no.5, pp.990-997, Sept./Oct. 1996.

[78] C.E. Restrepo, "Arc Fault Detection and Discrimination Methods," *Electrical contacts - 2007, the 53rd ieee holm conference on*, pp.115-122, Sept. 2007.

[79] J.L. Kohler, and Jingcheng Li, "DC trolley fires-a new solution to an old problem," *Industry Applications, IEEE Transactions on* , vol.31, no.4, pp.726-732, Jul./Aug. 1995.

[80] Texas Instruments [online], White Paper - Implementing Arc Detection on Solar Applications: Achieving Compliance with the new UL 1699B Standard, Available: http://www.ti.com/lit/wp/spry209/spry209.pdf.

[81] Jincheng Li, and J.L. Kohler, "New insight into the detection of high-impedance arcing faults on DC trolley systems," *Industry Applications, IEEE Transactions on*, vol.35, no.5, pp.1169-1173, Sept./Oct. 1999.

[82] IEEE Guide for Performing Arc-Flash Hazard Calculations, *IEEE Std 1584-2002*, Sept. 2002.

[83] Standard for Electrical Safety in the Workplace, *NFPA 70E*, 2015.

[84] A.B. Thompson, G. Richardson, P. Dellar, M. McGuinness, and C. Budd [online], "Arc Phenomena in low-voltage current limiting circuit breaker". Available: http://www.maths-in-industry.org/miis/300/1/arc.pdf.

[85] P.J. Norman, S.J. Galloway, and J.R. McDonald, "Simulating electrical faults within future aircraft networks," in *Aerospace and Electronic Systems, IEEE Transactions on*, vol.44, no.1, pp.99-110, 2008.

[86] N. Mohan, T.M. Undeland, and W.P. Robbins, *Power Electronics: A First Course*, First Edition, John Wiley & Sons, Inc., 270 p., 2012.

[87] J. H. Kim, S. J. Lee, E. S. Kim, S. K. Kim, C. H. Kim, and L. Prikler, "Modeling of Battery for EV using EMTP/ATPDraw," *Journal of Electrical Engineering and Technology*, *9*(1), pp.98-105, 2014.

[88] O. Tremblay, and L.-A. Dessaint "Experimental validation of a battery dynamic model for EV applications," *World Electric Vehicle Journal*, *3*(1), pp.1-10, 2009.

[89] O. Tremblay, L.-A. Dessaint, and A.-I. Dekkiche, "A Generic Battery Model for the Dynamic Simulation of Hybrid Electric Vehicles," *IEEE Vehicle Power and Propulsion Conference (VPPC)*, pp.284-289, Sept. 2007.

[90] X. Feng, and Z. Sun, "A battery model including hysteresis for State-of-Charge estimation in Ni-MH battery," *IEEE Vehicle Power and Propulsion Conference (VPPC)*, pp.1-5, Sept. 2008.

[91] D. Doerffel, and S.A. Sharkh "A critical review of using the Peukert equation for determining the remaining capacity of a lead-acid and lithium-ion batteries," Journal of Power Sources, vol. 155, no.2, pp.395-400, 2006.

[92] I. Buchmann, "Memory: Myth or Fact?", Available: www.buchmann.ca/article10-page1.asp, April 2001.

[93] J.D. Glover, M.S. Sarma, and T.J. Overbye, *Power System Analysis, Analysis and Design*, 5th Edition, Cengage Learning, 828 p., 2012.

[94] R.M.M. Mohd, S.A.A. Huzainie, and B.A.G. Ahmad, "Study of cable crimping factors affecting contact resistance of medium voltage cable ferrule and lug," in *Electricity Distribution (CIRED 2013), 22nd International Conference and Exhibition on*, pp.1-4, June 2013.

[95] ABB SACE, "Working with the Trip Characteristic Curves of ABB SACE Low Voltage Circuit-Breakers," White Paper, 36p., Sept. 2007.

[96] ABB, "Application Guide – Miniature circuit breakers," 10p., April 2009.

[97] Ferraz Shamut, "Power Semiconductor Fuse Applications Guide," 50p., Oct. 2006.

[98] Huaren Wu, Ling Yuan, Lin Sun, and Xiaohui Li, "Modeling of Current-Limiting Circuit Breakers for the Calculation of Short-Circuit Current," in *Power Delivery, IEEE Transactions on*, vol.30, no.2, pp.652-656, April 2015.

[99] ABB, "ABB Molded Case Circuit Breakers – UL 482 and CSA C22.2 Standard," *Technical Catalog* , 280p., Sept. 2007.

[100] ABB, "ABB Circuit-Breakers for Direct Current Applications," *Technical Application Papers*, 56p., Sept. 2007.

[101] Ferraz Shawmut [online], "440VDC - Special Purpose Fuse - Type gLB ", Available: http://www.ferrazshawmutsales.com/pdfs/CC4142227.pdf.

[102] S.J. Goldman [online], *"*Selecting Protection Devices : TVS Diodes vs. Metal-Oxide Varistors*",* Available: http://powerelectronics.com/regulators/selecting-protection-devices-tvs-diodes-vs-metal-oxide-varistors.

[103] Littelfuse [online] *"*Transient Voltage Suppression Diodes-SMCJ Series Datasheet*",* 2012, Available: http://www.littelfuse.com/~/media/electronics/datasheets/tvs_diodes/littelfuse_tvs_diode_smcj_datasheet.pdf.pdf.

[104] EPCOS [online], "SIOV Metal Oxide Varistor – General Technical Information"*,* 2011, Available: http://en.tdk.eu/blob/531268/download/2/siov-general.pdf.

[105] BOURNS [online], "MOV-20D121K Metal Oxide Varistor Datasheet", Available: https://www.bourns.com/data/global/pdfs/MOV20D.pdf.

[106] IEEE Recommended Practice for Electrical Sizing of Nickel-Cadmium Batteries for Rail Passenger Vehicles, *IEEE Std 1568-2003*, Dec. 2003.

APPENDIX A – PROOF OF AMEDI ET AL. STABILITY CRITERION

In this appendix, the proof of the Amedi et al. stability criterion [74] is presented with the inclusion of constant current load. By writing Kirchhoff's voltage law (KVL) and Kirchhoff's current law (KCL) in the circuit of Figure 3.3, a set of differential equations can be written [74]:

$$v_s = R_{eq} i_{in} + L_{eq} \frac{di_{in}}{dt} + v_o \tag{A.1}$$

$$i_{in} = C_{eq} \frac{dv_o}{dt} + \frac{P_{CPL}}{v_o} + \frac{v_o}{R_L} + I_{CCL} \tag{A.2}$$

To evaluate small-signal stability, the equivalent transfer function between the source voltage (v_s) and the load voltage (v_o) must be defined around the circuit operating point.

By linear approximation of the non-linear term in (A.2) and by transforming into a deviation model equation around the operating point, this set of differential equations becomes:

$$\Delta v_s = R_{eq} \Delta i_{in} + L_{eq} \frac{d\Delta i_{in}}{dt} + \Delta v_o \tag{A.3}$$

$$\Delta i_{in} = C_{eq} \frac{d\Delta v_o}{dt} - \frac{P_{CPL}}{\overline{v}_o^2} \Delta v_o + \frac{\Delta v_o}{R_L} \tag{A.4}$$

It should be noted that the I_{CCL} vanishes in (A.4) because it is only seen as a shift on I_{in} such as it does not impact the deviation model equations.

By inserting (A.4) in (A.3) and rearranging, it leads to:

$$\Delta v_s = L_{eq} C_{eq} \frac{d\Delta v_o}{dt^2} + \left(R_{eq} C_{eq} + \frac{L_{eq}}{R_L} - \frac{L_{eq} P_{CPL}}{\overline{v}_o^2} \right) \frac{d\Delta v_o}{dt} + \left(1 - \frac{R_{eq} P_{CPL}}{\overline{v}_o^2} + \frac{R_{eq}}{R_L} \right) \Delta v_o \tag{A.5}$$

By applying Laplace's Transform, the deviation model transfer function is obtained:

$$\frac{\Delta v_o(s)}{\Delta v_s(s)} = \frac{1 \big/ L_{eq} C_{eq}}{s^2 + \left(\frac{R_{eq}}{L_{eq}} + \frac{1}{C_{eq}} \left(\frac{1}{R_L} - \frac{P_{CPL}}{\overline{v}_o^2} \right) \right) s + \frac{\left(1 + R_{eq} (1/R_L - P_{CPL}/\overline{v}_o^2) \right)}{L_{eq} C_{eq}}} \tag{A.6}$$

Unstable condition is obtained when the damping coefficient is negative:

$$\frac{R_{eq}}{L_{eq}} + \frac{1}{C_{eq}}\left(\frac{1}{R_L} - \frac{P_{CPL}}{\overline{v}_o^2}\right) < 0 \tag{A.7}$$

Rearranging, the following stability criterion is obtained:

$$P_{CPL} < \frac{\overline{v}_o^2}{R_L} + \frac{R_{eq}C_{eq}}{L_{eq}}\overline{v}_o^2 \tag{A.8}$$

Or simply:

$$P_{CPL} < P_R + \frac{R_{eq}C_{eq}}{L_{eq}}\overline{v}_o^2 \tag{A.9}$$

The operating point can be obtained by solving the following equation:

$$\overline{i}_{in} = \frac{P_R}{\overline{v}_o} + \frac{\overline{v}_o}{R_L} + I_{CCL} \tag{A.10}$$

APPENDIX B – COMPLETE TRAIN POWER SYSTEM FOR CASE STUDY

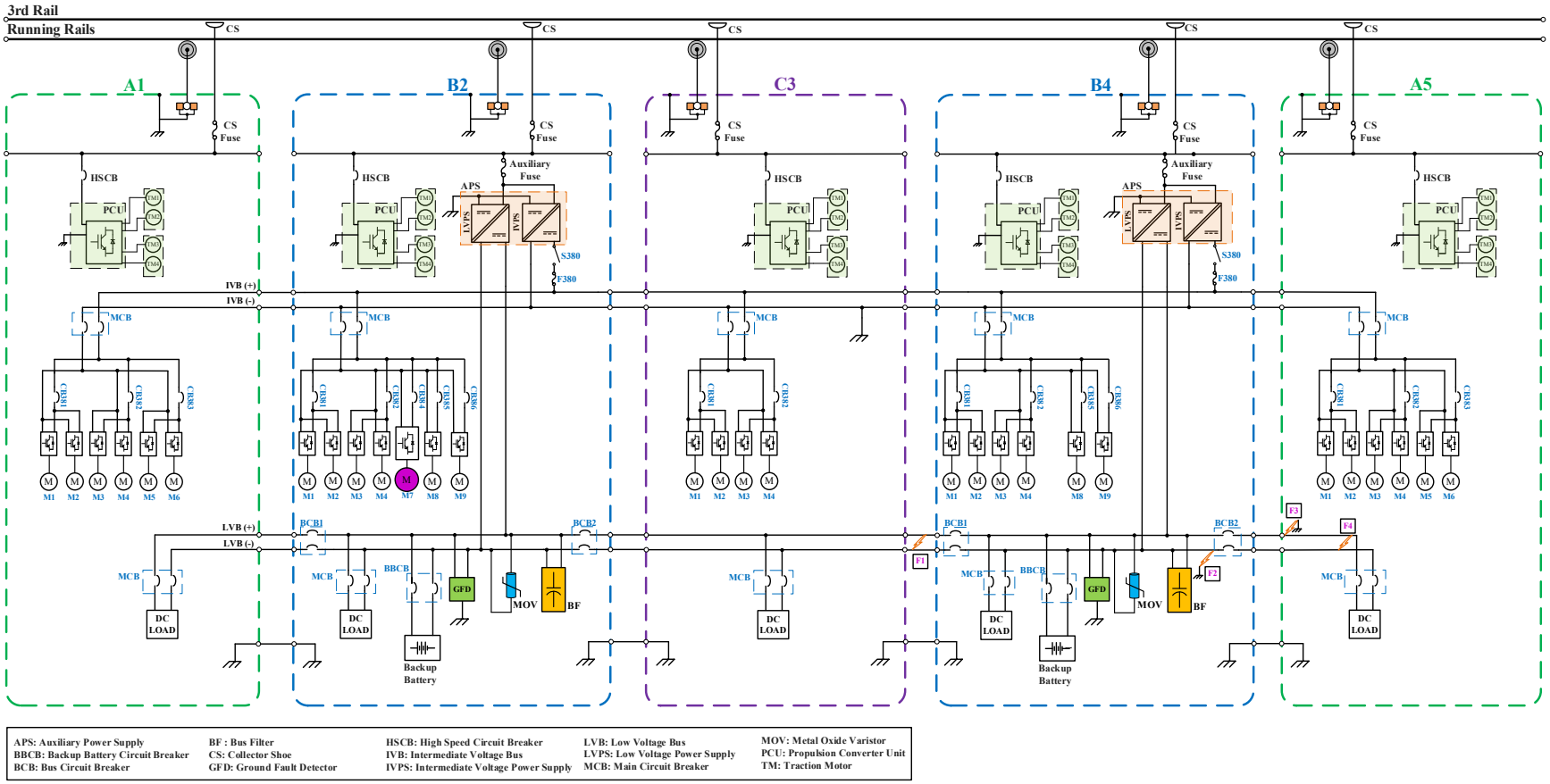

APS: Auxiliary Power Supply
BBCB: Backup Battery Circuit Breaker
BCB: Bus Circuit Breaker
BF : Bus Filter
CS: Collector Shoe
GFD: Ground Fault Detector
HSCB: High Speed Circuit Breaker
IVB: Intermediate Voltage Bus
IVPS: Intermediate Voltage Power Supply
LVB: Low Voltage Bus
LVPS: Low Voltage Power Supply
MCB: Main Circuit Breaker
MOV: Metal Oxide Varistor
PCU: Propulsion Converter Unit
TM: Traction Motor

APPENDIX C – 110 V BUS SIMULATION PARAMETERS

Model	Description	Symbol	Value	Units
LVPS	Nominal Voltage	V_{NOM}	110	V
	Minimum Voltage	V_{MIN}	108.9	V
	Maximum Voltage	V_{MAX}	111.1	V
	Nominal Current	I_{NOM}	150	A
	Current Limit	I_{LIM}	180	A
	Maximum Current	I_{MAX}	200	A
	Filter Capacitor	C_F	11.6	mF
	Filter Inductance	L_F	0	H
Battery	Exponential Zone Amplitude	A	11.4	V
	Inverse Exponential Zone Time-Constant	B	0.05	Ah^{-1}
	Polarization Constant	K	0.005859	V/Ah
	Battery Constant Voltage	E_0	108.2	V
	Battery Nominal Capacity	Q_n	65	Ah
	Peukert Coefficient	α	1.1	n/a
	Discharge Time to obtain Q_n	n	5	h
	Battery Internal Resistance	R	49.5	mΩ
	Initial State-of-Charge	SOC_0	100	%
	Filter Time-Constant	T_r	1	s
Conductor	Single Conductor Resistance per unit length	R'_x	0.177	mΩ/m
	Single Conductor Inductance per unit length	L'_x	0.649	µH/m
	Overall Bus Length (A-Car)	l_A	17.7	m
	Overall Bus Length (B-Car)	l_B	21.0	m
	Overall Bus Length (C-Car)	l_C	21.0	m
	Distance between the bus and the battery	l_{batt}	1.8	m
	Inter-Car Jumper	l_J	1.46	m

Model	Description	Symbol	Value	Units
Connection	Connection Resistance	R_1	0	Ω
BCB (Detection)	Pickup Current Setting	I_{pickup}	280	A
	Instantaneous Current Setting	I_{inst}	2200	A
	Thermal Time-Constant	T_{ther}	100	s
	Instantaneous Delay	T_{inst}	16	ms
BCB (Opening)	Contact Resistance	R_c	0.12	mΩ
	Anode-Cathode Voltage Drop	U_0	20 (V)	V
	Arc Length Equation Parameters	c	0.01	n/a
		d	0.05	n/a
	Schwarz Arc Model Parameters	P_0	1000	n/a
		a	0.06	n/a
		b	1.3	n/a
		τ_s	0.00001	n/a
MOV	MOV-20D121K (see below)	n/a	n/a	n/a
Constant Power Load	Power Set-Point (A-Car)	P_{CPL}	2	kW
	Power Set-Point (B-Car)		1	kW
	Power Set-Point (C-Car)		1	kW
	Filter time-constant	τ_f	2	ms
Constant Current Load	Current Set-Point (A-Car)	I_{CCL}	9.1	A
	Current Set-Point (B-Car)		10.9	A
	Current Set-Point (C-Car)		10.9	A
	Filter time-constant	τ_f	2	ms
Resistive Load	Nominal Resistance (A-Car)	R_L	50	Ω
	Nominal Resistance (B-Car)		200	Ω
	Nominal Resistance (C-Car)		200	Ω

Metal Oxide Varistor (MOV-20D121K) VI-Characteristic [105]:

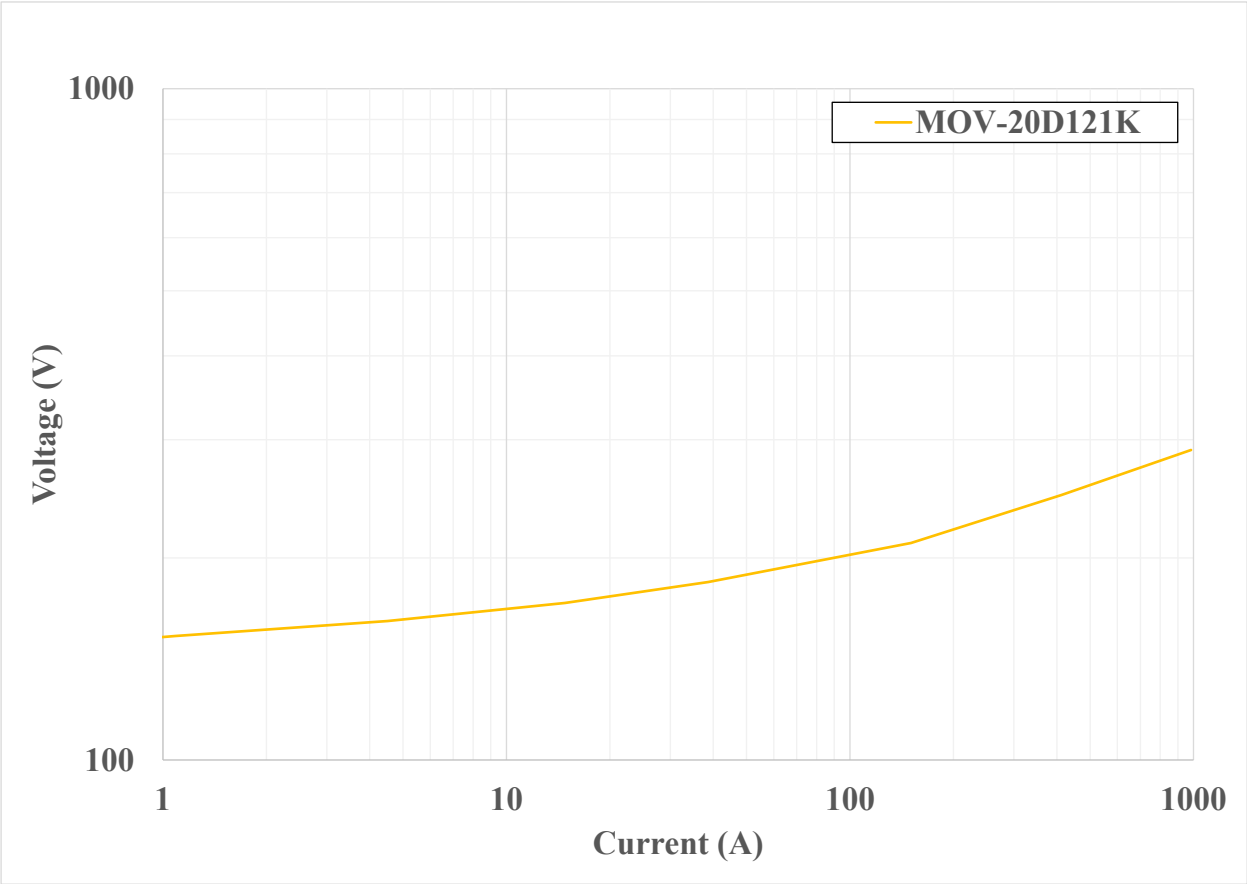

APPENDIX D – 380 V BUS SIMULATION PARAMETERS

Model	Description	Symbol	Value	Units
IVPS	Nominal Voltage	V_{NOM}	380	V
	Minimum Voltage	V_{MIN}	365	V
	Maximum Voltage	V_{MAX}	385	V
	Nominal Current	I_{NOM}	250	A
	Current Limit	I_{LIM}	275	A
	Maximum Current	I_{MAX}	300	A
	Filter Capacitor	C_F	48	mF
	Filter Inductance	L_F	0	H
Conductor	Single Conductor Resistance per unit length	R'_x	0.177	mΩ/m
	Single Conductor Inductance per unit length	L'_x	0.649	µH/m
	Overall Bus Length (A-Car)	l_A	16.5	m
	Overall Bus Length (B-Car)	l_B	21.0	m
	Overall Bus Length (C-Car)	l_C	21.0	m
	Distance between the IVPS and the bus	l_{IVPS}	0.9	m
	Inter-Car Jumper	l_J	1.5	m
Connection	Connection Resistance	R_1	0	Ω
Fuse	Time-Current Curve - Figure 4.20 (160A)	n/a	n/a	n/a
	Nominal Resistance	R_0	1	mΩ
	First Corner Resistance	R_1	5	Ω
	Second Corner Resistance	R_2	100	Ω
	First Slope Duration	T_1	10	ms
	Second Slope Duration	T_2	20	ms

Model	Description	Symbol	Value	Units
Constant Power Load	M1 to M6 Power Set-Point	P_{CPL}	0.5	kW
	M7 Power Set-Point		12	kW
	M8 Power Set-Point		1	kW
	M9 Power Set-Point		3	kW
	Filter time-constant	τ_f	0.1	ms
	M1 to M6 Filter Capacitor	C_F	780	µF
	M1 to M6 Filter Inductance	L_F	150	µH
	M1 to M6 Filter Hot Resistance	R_{HOT}	0.325	Ω
	M1 to M6 Filter Cold Resistance	R_{COLD}	9	Ω
	M7 Filter Capacitor	C_F	4000	µF
	M7 Filter Inductance	L_F	250	µH
	M7 Filter Hot Resistance	R_{HOT}	0.001	Ω
	M7 Filter Cold Resistance	R_{COLD}	5	Ω
	M8 Filter Capacitor	C_F	220	µF
	M8 Filter Inductance	L_F	150	µH
	M8 Filter Hot Resistance	R_{HOT}	0.325	Ω
	M8 Filter Cold Resistance	R_{COLD}	9	Ω
	M9 Filter Capacitor	C_F	1100	µF
	M9 Filter Inductance	L_F	120	µH
	M9 Filter Hot Resistance	R_{HOT}	0.325	Ω
	M9 Filter Cold Resistance	R_{COLD}	9	Ω